CELLULAR, HISTOLOGICAL AND BEHAVIORAL CHANGES IN THE PATHOGENESIS OF HYDROCEPHALUS IN THE RO1 MOUSE MODEL

Allison Beth McMullen

A dissertation submitted to the faculty of the University of North Carolina at Chapel Hill in partial fulfillment of the requirements for the degree of Doctor of Philosophy in the Department of Pharmacology.

Chapel Hill
2011

Approved by:

Ken D. McCarthy, Ph.D.

T. Kendall Harden, Ph.D.

Gary L. Johnson, Ph.D.

Lee M. Graves, Ph.D.

Patricia F. Maness, Ph.D.

ABSTRACT

ALLISON BETH MCMULLEN: Cellular, histological and behavioral changes in the pathogenesis of hydrocephalus in the Ro1 model
(Under the direction of Ken D. McCarthy)

Hydrocephalus is a highly prevalent neurological disorder characterized by elevated levels of cerebrospinal fluid (CSF) in the brain and subsequent enlargement of the lateral ventricles. Currently, the only treatment for this disorder is recurrent neurosurgery to insert and revise shunts that drain the CSF. To develop better treatments for hydrocephalus, an understanding of the cellular, histological and behavioral changes that occur in the pathogenesis of hydrocephalus is required. To this end, we have developed a novel model of hydrocephalus, called the Ro1 model, which was created using the tetracycline inducible system to direct Ro1 expression to cells expressing glial fibrillary acidic protein. This model is unique in that hydrocephalus can be induced at any age with complete penetrance and without interfering pathologies, enabling the investigation of the earliest pathological changes that lead to hydrocephalus. Also, the specific activation of a G-protein coupled receptor (the Ro1 receptor) in a specific subset of cells makes investigating signaling pathways involved in hydrocephalus tractable.

We discovered that the earliest pathological changes in this model were ventriculomegaly and disorganization of the ependymal lining of the aqueduct of Sylvius. Thinning and eventual denudation of the ependymal lining was subsequent to ventriculomegaly. Additionally, following severe ventriculomegaly, periventricular

edema and areas of the ventricular walls void of microvilli were observed. Stenosis of the aqueduct of Sylvius was not present even with severe ventriculomegaly, suggesting that the Ro1 model represents a model of communicating hydrocephalus. Interestingly, even with severe ventriculomegaly, there were no behavioral changes, possibly due to compensation of the brain tissue due to the slow progression of hydrocephalus in this model. These data provide insight into the earliest cellular, histological and behavioral changes in the pathogenesis of hydrocephalus, which may lead to the development of therapeutic treatments for this disorder.

ACKNOWLEDGEMENTS

The completion of this dissertation would not have been possible without support and help from others. I am deeply grateful to my mentor, Ken D. McCarthy, and my fellow lab members, Sarah Taves, Suzanne Minton, Kristen Boyt, Cendra Agulhon, Molly Cook, Daniel Bonder, Elizabeth Sweger, Dibs Almonte and Jeremy Petravicz, for their unfailing support and encouragement. I am also indebted to numerous other scientists for their help and advice, including, but not limited to, Eric Zimmerman, Deborah Granger, Amy Abell, Sheryl Moy, Richard Weinberg, Susan Burette, Harold Mekeel, Mark Ellisman and Eric Bushong. I have also been strongly motivated by the support and belief in my abilities provided by my family, especially my parents, Susan and John, who have always encouraged me to try my best and never give up. Lastly, I would like to thank my husband, Matthew Berginski, who has been by my side throughout the entire process—from application to graduation—and who has been an unwavering source of support, advice and encouragement.

TABLE OF CONTENTS

LIST OF TABLES

Table

LIST OF FIGURES

Figure

ABBREVIATIONS

CMV	Cytomegalovirus
CNS	Central nervous system
CP	Choroid plexus
CRASH	Corpus callosum hypoplasia, retardation, adducted thumbs, spastic paraparesis and hydrocephalus
CSF	Cerebrospinal fluid
DCX	Doublecortin
dox	Doxycycline
DWM	Dandy-Walker malformation
EL2	Extracellular loop 2
ETV	Endoscopic third ventriculostomy
FGF	Fibroblast growth factor
GFAP	Glial fibrillary acidic protein
GPCR	G-protein coupled receptor
H&E	Hematoxylin and eosin
H-Tx	Hydrocephalus Texas rat
ICP	Intracranial pressure
IVH	Intraventricular hemorrhage
KOR	Kappa opioid receptor
LV	Lateral ventricle
MBP	Myelin basic protein
MRI	Magnetic resonance imaging
NeuN	Neuronal nuclei

norBNI	Norbinaltorphamine
NPH	Normal pressure hydrocephalus
NSC	Neural stem cell
PFA	Paraformaldehyde
PTX	Pertussis toxin
RASSL	Receptor activated solely by a synthetic ligand
RMS	Rostral migratory stream
SCO	Subcommissural organ
SVZ	Subventricular zone
TGFβ	Transforming growth factor beta
tTA	Tetracycline transactivator
US	Ultrasonography
VZ	Ventricular zone

Chapter I

Overview of hydrocephalus

Hydrocephalus is a highly prevalent neurological disorder characterized by elevated levels of cerebrospinal fluid (CSF) in the brain and subsequent enlargement of the ventricles. If left untreated, the buildup of CSF often causes increased intracranial pressure (ICP), resulting in the disruption and compression of cerebral structures. In the United States, approximately 1 in 1000 children are born with hydrocephalus, and approximately 69,000 to 80,000 new cases of hydrocephalus are diagnosed each year in both adults and children (Bondurant and Jimenez, 1995; Patwardhan and Nanda, 2005). Additionally, health care costs related to hydrocephalus cost the United States over a billion dollars annually (Patwardhan and Nanda, 2005). Over 50% of children with untreated hydrocephalus die within 10 years, and more than 60% of surviving children have neurological impairments (McCullough and Balzer-Martin, 1982; Persson et al., 2007). Currently, there is no cure for hydrocephalus, and the only treatment involves either redirecting CSF flow by shunt placement or creating a new pathway for CSF flow. Shunts, first developed in 1952, are the predominant treatment for hydrocephalus; however, shunt placement surgery has a mortality of 2.7% and two-thirds of shunts fail within 10 years following surgery (Patwardhan and Nanda, 2005). As a result, there is a critical need for the development of better treatments for hydrocephalus.

The lack of pharmacological therapy for hydrocephalus stems, in large part, from the multifactorial causes of this disease and the lack of good animal models in which to study hydrocephalus. In existing animal models, penetrance is often low and hydrocephalus appears to be one of a spectrum of diseases, making it difficult to sort out the cellular mechanisms that are specifically contributing to hydrocephalus. Our lab has developed a novel model of hydrocephalus that gives us the unique ability to control the onset of the disease and thereby study early cellular and morphological changes that lead to the development of hydrocephalus.

This model was created using the tetracycline-inducible system to drive the expression of a mutated Gi-coupled G protein-coupled receptor (GPCR; Ro1 receptor) to cells expressing glial fibrillary acidic protein (GFAP) (Coward et al., 1998a; Redfern et al., 1999; Scearce-Levie et al., 2001a; Sweger et al., 2007). When mice are taken off doxycycline (a tetracycline derivative), allowing for Ro1 expression in GFAP+ cells, 100% of mice develop hydrocephalus (Sweger et al., 2007). Unlike other models, hydrocephalus also appears to be the primary pathology. Due to the inducibility, complete penetrance and activation of a specific signaling cascade in a specific population of cells, the Ro1 model provides us with the unique ability to study the morphological, cellular and behavioral changes that play a role in the pathogenesis of this disorder. It is our hope that a better understanding of hydrocephalus obtained through the use of the Ro1 model will increase the early diagnosis of this disorder and lead to the development of novel therapeutics to treat this disorder.

Chapter II

The Ventricular System

a. Anatomy of the ventricular system

The ventricular system. Before the pathological changes to the brain and ventricular system found in hydrocephalus can be discussed, an understanding of the ventricular system is necessary. The ventricular system is composed of four ventricles—two lateral ventricles, a third ventricle and a fourth ventricle—through which the cerebrospinal fluid (CSF) flows. CSF, which is produced primarily by the choroid plexus found in each of the four ventricles, flows from the lateral ventricles through the foramen of Monroe to the third ventricle and travels from the third ventricle through the aqueduct of Sylvius to the fourth ventricle. Each lateral ventricle can be divided into five regions: the anterior horn, the body, the posterior horn, the temporal horn and the collateral trigone (Di Terlizzi and Platt, 2006; Johanson, 2003). The third ventricle lies below the lateral ventricles and is irregularly shaped with four recesses known as the optic, infundibular, pineal and supra-pineal recesses (Johanson, 2003). The aqueduct of Sylvius also has multiple regions, narrowing after exiting the third ventricle and subsequently dilating into the ampulla before narrowing into the pars posterior, which dilates as it opens into the lateral apertures of the fourth ventricle (Di Terlizzi and Platt, 2006). The fourth ventricle is the most caudally located portion of the ventricular system, lying far below the lateral and third ventricles and bound by the pons, the medulla oblongata and the cerebellum (Johanson, 2003). The CSF flows out of the fourth ventricle through the midline foramen of Magendie and two lateral foramina of Lushka, which are located in the roof of the fourth ventricle, into the cisterna magna and the basal cisterns of the subarachnoid space, respectively (Brodbelt and Stoodley, 2007; McLone, 2004). The cavity of the fourth ventricle also extends into the central canal of the spinal cord (Di Terlizzi and Platt, 2006). After exiting into the cisterna magna, the CSF then traverses the subarachnoid space over the surface of the cortex and drains back into the blood via the

arachnoid granulations (described below), spinal nerve roots and the olfactory tracts (Brodbelt and Stoodley, 2007). The aqueduct of Sylvius, which is the narrowest part of the ventricular system, and the foramen of Monroe are the most common sites of blockage in human non-communicating hydrocephalus (McLone, 2004). The anatomy of the ventricular system is shown in Figure 1.

Meningeal structures. The meninges are composed of dura, arachnoid and pia mater, and a fluid-containing compartment called the subarachnoid space is present between the pia and arachnoid layers (Brodbelt and Stoodley, 2007; Haines et al., 1993). The dura mater is the outermost layer and is attached to the skull (Haines et al., 1993; Vandenabeele et al., 1996). It is composed of fibroblasts, extracellular collagen, elastic fibers and glycoproteins (Brodbelt and Stoodley, 2007; Haines et al., 1993; Vandenabeele et al., 1996). The external dura is attached to the inner surface of the skull. This layer contains fewer fibroblasts and more extracellular collagen due to the network of nerves and blood vessels in the region (Frederickson, 1991; Haines et al., 1993). This is in contrast to the inner part of the dura, which has more fibroblasts and proportionally less collagen (Frederickson, 1991; Haines et al., 1993). The fibroblasts of this region show an elongated and flattened morphology and form a layer that is several cell processes thick and is continuous with the arachnoid mater (Alcolado et al., 1988; Haines et al., 1993).

The arachnoid mater, located immediately internal to the inner dura mater, is a densely packed region of cells, called the arachnoid barrier cells, with little extracellular space (Haines et al., 1993). These cells are connected by desmosomes, tight and gap junctions, hemidesmoses and intermediate junctions, which provide strength for this layer and prevent the movement of fluids, large molecular weight substances and ions (Frederickson, 1991; Haines et al., 1993). The

arachnoid trabeculae, specialized fibroblasts that bridge the subarachnoid space and attach to and surround traversing blood vessels, exits immediately internal to the arachnoid barrier cells (Brodbelt and Stoodley, 2007; Frederickson, 1991; Haines et al., 1993). These cells are attached to each other by cell junctions and reinforced by collagen (Brodbelt and Stoodley, 2007; Haines et al., 1993). Arachnoid villi are invaginations of the arachnoid into a venous region (Brodbelt and Stoodley, 2007; Weed, 1914). These villi penetrate the dura and surround CSF drainage veins (Brodbelt and Stoodley, 2007; Tripathi and Tripathi, 1974; Weed, 1914). A large dilation of the subarachnoid space within a villus forms an arachnoid granulation, which is found in humans older than 18 months (Brodbelt and Stoodley, 2007). Vacuolar, transcellular channels found on the arachnoid villi are thought to be a drainage site for CSF, although recently this has become controversial (Brodbelt and Stoodley, 2007; Tripathi and Tripathi, 1974).

The pia mater is formed by a single, continuous layer of flattened fibroblasts lying on the surface of the brain, which are attached to the external glial limiting membrane (Alcolado et al., 1988; Brodbelt and Stoodley, 2007; Haines et al., 1993; Hutchings and Weller, 1986). These cells have few cell junctions and surround vessels in the subarachnoid space (Brodbelt and Stoodley, 2007; Haines et al., 1993). Figure 2 shows the structure of the meninges.

The choroid plexus. The choroid plexi (CP) are composed of modified ependymal cells and are found in each of the four ventricles, extending from the walls of the lateral ventricles and the roof of the third and fourth ventricles (Brodbelt and Stoodley, 2007; Redzic and Segal, 2004). In each of these ventricles, the CP forms fine leaf-like projections, with a large surface area of 200 cm^2 (Brodbelt and Stoodley, 2007; Redzic and Segal, 2004). The ependymal lining of the ventricles is attached to the CP by a thin stalk and is continuous with the outer covering of the

CP (Redzic and Segal, 2004). The CP is composed by a choroidal epithelium joined by tight junctions that form a water-impermeable barrier separating the CSF from the choroidal interstitial fluid (Brodbelt and Stoodley, 2007; Redzic and Segal, 2004). The CSF-facing side of this epithelium is covered in a dense coat of microvilli, and in some species, long cilia are present (Brodbelt and Stoodley, 2007; Kimelberg, 2004; Redzic and Segal, 2004).The CP is highly vascularized. In the lateral ventricles, the CP is fed by the anterior choroidal and lateral posterior choroidal arteries, while the paired medial posterior choroidal arteries and the posterior inferior cerebellar artery supply the CP of the third and fourth ventricles, respectively (Brodbelt and Stoodley, 2007; Redzic and Segal, 2004). Within the center of the CP, a complex vascular network of large, fenestrated capillaries exists, allowing the flow of small hydrophilic molecules into the interstitial fluid of the CP (Redzic and Segal, 2004). The role of the choroid plexus in the production of CSF will be discussed below.

Ependymal cells and tanycytes. The ventricles of the brain and the central canal of the spinal cord are lined by a continuous layer of ependymal cells with the occasional tanycyte (Brodbelt and Stoodley, 2007). Ependymal cells are ciliated cuboidal or columnar epithelial cells, and unlike the tight junctions that connect the epithelial cells of the choroid plexus, these cells are connected by zonula adherens in the brain and have extensive gap junctions (Brightman and Reese, 1969; Brodbelt and Stoodley, 2007; Bruni and Reddy, 1987; Redzic and Segal, 2004). Electrophysiologically, ependymal cells are similar to glial cells, possessing high negative resting membrane potentials, responsiveness to extracellular potassium levels and low input resistances (Bruni, 1998; Jarvis and Andrew, 1988).

Mature ependymal cells have been shown to play a number of roles in the adult brain. For example, the coordinated beating of ependymal cilia has been shown to create a current of CSF along the walls of the lateral ventricle, and disturbances to the beating of ependymal cilia leads to disturbances in CSF flow and hydrocephalus (Banizs et al., 2005; Kobayashi et al., 2002; Sawamoto et al., 2006). Interestingly, the beating of ependymal cilia and the CSF currents subsequently generated appear to direct the migration of neuroblasts born within the subventricular zone from the lateral ventricles to the olfactory bulb in the mouse (Sawamoto et al., 2006). Ependymal cells have also been suggested to regulate the transport of ions, small molecules and water between the CSF and neuropil (Bruni, 1998), protect the brain from harmful substances in the CSF (Kuchler et al., 1994) move cellular debris with bulk CSF flow and disperse neural messengers throughout the CSF (Bruni, 1998; Roth et al., 1985). Fetal ependymal cells have been suggested to serve a primarily secretory function (Bruni, 1998; Sarnat, 1992). Other roles for fetal ependymal cells have also been suggested, including the arrest of neurogenesis, axonal guidance, maintenance and transformation of radial glia and the transport of nutrients prior to the development of capillary networks (Gould et al., 1990; Sarnat, 1992).

Tanycytes, which are specialized ependymal cells primarily found in the third ventricle, are interspersed among the ependymal cells (Bruni, 1998). These cells have radially directed basal processes that extend into the neuropil and often enwrap blood vessels or terminate on neurons, glia or the external glial limitans (Bruni, 1998; Wittkowski, 1998). In the third ventricle, tanycytes extend from the floor of the ventricle, where they contact the CSF, to the median eminence of the hypothalamus, which suggests a neuroendocrine role for these cells (Wittkowski, 1998).

During brain development, the ventricular zone of the brain consists of a psuedostratified neuroepithelium that contains multipotent radial stem cells (Jimenez et al., 2009; Spassky et al., 2005). These radial glia give rise to ependymal cells, which develop along a caudal to rostral gradient (Bruni, 1998; Sarnat, 1992; Spassky et al., 2005). In the third ventricle, ependymal cells undergo their final division between embryonic days 11 (E11) and E13, and in the lateral ventricles, the majority of the ependymal cells are generated between E14 and E16 (Rakic and Sidman, 1968; Spassky et al., 2005). Ependyma and cilia formation do not occur until the first postnatal week; these events progress caudorostrally and ventrodorsaly along the lateral wall of the lateral ventricles of the rodent brain (Spassky et al., 2005). Additionally, differentiated ependymal cells are postmitotic, suggesting that these cells are exclusively produced during development (Spassky et al., 2005). This finding also explains why the ependymal layer in the mammalian brain does not regenerate when injured, as found in severe cases of hydrocephalus (Sarnat, 1995). Tanycytes also appear to only acquire their adult form postnatally, maturing as late as P34 in rats (Bruni, 1998; Card and Rafols, 1978).

In humans, ependymal cells begin to differentiate in the floor plate of the neural tube at four weeks following gestation. Ependymal differentiation is complete in the lateral and third ventricles by 22 weeks following gestation (Bruni, 1998; Sarnat, 1992). Some studies have suggested that tanycytes represent a transitional cell type during human fetal development (Bruni, 1998; Gould et al., 1990). As these cells differentiate, their processes retract, and they eventually become indistinguishable from ependymal cells as they mature (Bruni, 1998; Gould et al., 1990).

The subventricular zone. Underneath the ependymal cell layer in the lateral ventricles lies the subventricular zone (SVZ). The SVZ is comprised of three major cell classes: "A" cells, or neuroblasts, astrocyte-like "B" cells, and undifferentiated "C" cells (Doetsch et al., 1997). "B" cells are the neural stem cells (NSCs) of the SVZ, giving rise to the intermediary C cell population, which then differentiates into the migratory neuroblast, or "A" cell, population (Doetsch et al., 1999a). "A" cells migrate in the rostral migratory stream (RMS) to the olfactory bulb, where they form new inhibitory interneurons. "B" cells ensheathe the "A" cells in the RMS, secrete factors that promote mitotic phases in "A" cells and aid in their migration to the olfactory bulb (Lim and Alvarez-Buylla, 1999; Mason et al., 2001). Additionally, "B" cells extend processes that integrate into the ependymal layer and contact the ventricular surface as well as form connections with the vasculature (Mirzadeh et al., 2008). As a result, "B" cell astrocytes are central to the maintenance of the VZ/SVZ due to their close relationship with the ependymal layer, their role as the NSC of the SVZ and their role in guiding "A" cell neuroblasts to the olfactory bulb.

b. Cerebrospinal fluid function, production, composition and absorption

Cerebrospinal fluid function. The CSF primarily plays a protective role in the central nervous system, providing a stable and specialized extracellular fluid environment for neurons and protecting the brain from the fluctuations in arterial and central venous pressure that occur with changes in posture, respiration and physical exertion (Bergsneider, 2001; Di Terlizzi and Platt, 2006; Johanson, 2003). More specifically, the CSF and cerebral blood flow regulate intracranial pressure (ICP) by varying inversely to maintain ICP within normal levels despite variations in cardiac function and respiration (Di Terlizzi and Platt, 2006). Under physiological conditions,

pressure fluctuations of 1 – 2 mm H_2O are associated with the arterial pulse, and fluctuations of 2 – 5 mm H_2O are associated with normal breathing, likely due to the changes in intracranial venous pressure associated with breathing (Di Terlizzi and Platt, 2006). In pathological conditions in which ICP is elevated, such as hydrocephalus, the CSF pressure fluctuates considerably (Di Terlizzi and Platt, 2006). Sudden increases in intracranial blood volume result in uptake of CSF into the subarachnoid space, whereas chronic changes are compensated by increased absorption of decreased formation of CSF. Rises in ICP due to impairment of these compensatory changes result in reduced cerebral blood flow (Di Terlizzi and Platt, 2006).

Additionally, the buoyancy of CSF, which is approximately 99% water, protects the brain against shearing forces caused by acceleration or deceleration (Johanson, 2003; Redzic and Segal, 2004). The CSF reduces the momentum of the brain in response to stresses on strains inflicted on the head, thereby reducing injury (Bergsneider, 2001; Johanson, 2003). By reducing the brain's weight to 25% of its total mass, the CSF also reduces the tension on the nerve roots (Redzic and Segal, 2004).

The CSF also transports nutrients and biologically active substances, such as hormone-releasing factors, growth factors, neurotransmitters and neuropeptides, the concentrations of which may be altered in pathological states (Bergsneider, 2001; Di Terlizzi and Platt, 2006; Johanson, 2003; Podell and Hadjiconstantinou, 1997; Vaughn et al., 1988). Micronutrients that are transported in the CSF include vitamins C and B_6, folates and deoxyribonucleotides, which are actively transported across the CP epithelium and subsequently distributed across the ventricular wall and in the subarachnoid space by bulk flow (Johanson, 2003). The large volume of CSF also acts as a source of osmolytes for brain volume regulation and a buffer of ions

(Bergsneider, 2001). Neurons, in particular, require a consistent ionic composition in the extracellular space (Davson and Oldendorf, 1967; Di Terlizzi and Platt, 2006).

The CSF also plays an important role in the removal of toxic byproducts of cerebral metabolism, thereby regulating the chemical composition of the fluids that bathe brain cells (Bergsneider, 2001; Di Terlizzi and Platt, 2006; Johanson, 2003). Because the brain lacks a lymphatic system, proteins and other substances, such as cells and bacteria, are primarily removed via the perivascular spaces and are absorbed through the arachnoid villi into the cerebral veins and the lymphatic vessels (Di Terlizzi and Platt, 2006). For example, catabolites of serotonin and dopamine, such as 5-OH-indolic acetic acid and homovanillic acid, are actively reabsorbed by the CP and cleared by the arachnoid villi, preventing the buildup of metabolic waste products in the CSF (Bergsneider, 2001; Johanson, 2003). The CSF also acts to filter substances by allowing the movement of water-soluble substances from the parenchyma into the CSF (Di Terlizzi and Platt, 2006).

Cerebrospinal fluid production. The CSF is primarily produced by the choroid plexus, the main function of which is to secrete CSF, within the lateral, third and fourth ventricles (Brodbelt and Stoodley, 2007; Brodbelt and Stoodley, 2007; Redzic and Segal, 2004). The choroid plexi produce approximately 60% of the total CSF at a rate of approximately 0.4 ml/min in people and 3.3×10^{-4} ml/min in mice, and the turnover rate of CSF is approximately 4 and 11 volumes of CSF per 24 hours in humans and rats, respectively (Bergsneider, 2001; Di Terlizzi and Platt, 2006; Johanson et al., 2008). This rate is related to the weight of the CP and the rate of sodium and bicarbonate ion exchange (Di Terlizzi and Platt, 2006). The remainder of the CSF is produced by the ependymal cells lining the ventricular system, the external pial-glial membrane

of the brain surface and blood vessels in the pia-arachnoid space (Di Terlizzi and Platt, 2006; Speake et al., 2001). CSF is formed in the CP by both the passive ultrafiltration of plasma across the fenestrated choroidal capillary endothelial wall due to the high degree of vascularization of the CP as well as by active secretion by choroidal epithelial cells, which depends on the active transport of sodium ions into the ventricles (Bergsneider, 2001; Di Terlizzi and Platt, 2006). CSF formation begins by the filtration of plasma across the choroidal capillaries, which is proportional to the hydrostatic pressure gradient between the blood and choroid interstitial fluid. Thus, the elevated ventricular CSF pressure found in hydrocephalus is transmitted to the choroidal ISF, reducing plasma transport into the ISF and thereby decreasing CSF formation (Johanson et al., 2008). Fluid and solute exchange is controlled by the barriers of the CP at the epithelial cell level (Redzic and Segal, 2004). The zonula occludens that connect the choroidal endothelial and epithelial cells permit the passage of most small hydrophilic molecules but limit pericellular movement, forming the blood-CSF barrier (Bergsneider, 2001). Additionally, peptidases on the apical brush border of the CP provide a metabolic barrier that degrades unwanted proteins. Lastly, specific membrane and transport proteins provide a cellular barrier that regulates the transcellular movement of fluid and ions to and from the CSF (Brodbelt and Stoodley, 2007; Kimelberg, 2004; Redzic and Segal, 2004). Many of these transporters are ATP-dependent and act to create a gradient of sodium, chloride and bicarbonate ions across the epithelial layer of the CP, which drives the unidirectional, transcellular movement of water by osmosis through water channels, especially aquaporin 1 (Brodbelt and Stoodley, 2007; Gunnarson et al., 2004; Redzic and Segal, 2004). Interestingly, AQP1 knockout mice have normal CSF production, suggesting that other transmembrane mechanisms of water transport exist (Gunnarson et al., 2004). The production of CSF by the CP is very constant and

independent of CSF pressure and blood pressure; as ICP rises, the arachnoid villi allow increased flow of CSF into the blood (Di Terlizzi and Platt, 2006). However, in hydrocephalus, in which there is chronic increase in ICP, CSF formation may be reduced, possibly due to atrophy of the CP (Di Terlizzi and Platt, 2006).

Cerebrospinal fluid composition. The CSF is a clear, nearly acellular liquid, which is 99% water (Di Terlizzi and Platt, 2006; Johanson et al., 2008). The composition of the CSF is highly regulated by an array of transporters in the CP epithelium. When this regulation fails, normal neuronal function is interrupted (Johanson et al., 2008). The CSF contains glucose to supply energy to neural cells, and the CSF glucose concentration is generally 60 – 80% of the blood glucose concentration. The concentration of glucose in the CSF is dependent on the blood glucose concentration, the rate of glucose transport into the CSF and the metabolic rate of the central nervous system (CNS) (Di Terlizzi and Platt, 2006). Sodium is the most abundant ion in the CSF with a concentration of approximately 158 mmol/L and is important in ion and water transport and osmoregulation (Di Terlizzi and Platt, 2006; Johanson, 2003). The potassium concentration in the CSF is also critical because it is involved in neuronal function and the release of neurotransmitters. It is lower in the CSF than in plasma and is maintained within a narrow margin of approximately 3 mmol/L (Di Terlizzi and Platt, 2006). The permeability of the epithelium of the CP is greater for sodium than potassium, and the CP regulates the sodium and potassium ion concentrations in the CSF through Na^+, K^+-ATPase pumps (Di Terlizzi and Platt, 2006). The calcium in the CSF is also lower than in the plasma and ranges from 1 – 1.5 mmol/L, and the stability of the calcium ion concentration is also critical for maintaining normal levels of neuronal excitability (Di Terlizzi and Platt, 2006; Johanson, 2003). In contrast, magnesium and

chloride are found at slightly higher concentration in the CSF than in plasma (1.5 and 138 mmol/L, respectively) (Di Terlizzi and Platt, 2006; Johanson, 2003). Magnesium and chloride play important roles in neuronal conduction (Di Terlizzi and Platt, 2006).

To provide support to neural cells, the CSF also contains a full complement of vitamins, peptides, nucleosides and growth factors (Johanson et al., 2008). For example, vitamins B and C are specifically transported across the CP into the CSF and adjacent neural tissue (Johanson et al., 2008). Protein concentrations in the CSF are low and range from 10 – 40 mg/dL in dogs and cats as compared to 5 – 7 g/dL in the serum (Di Terlizzi and Platt, 2006). Albumin makes up 50 – 70% of the protein concentration in the CSF (Di Terlizzi and Platt, 2006). Some enzymes are also found in the CSF, and changes in their concentrations are often indicative of neurobiological disease (Di Terlizzi and Platt, 2006). Cells, such as lymphocytes and sloughed choroidal epithelial, ependymal or arachnoid cells, are rarely found in the CSF in healthy individuals (Johanson, 2003). The appearance of ependymal and choroidal cells in the CSF, in addition to an increased white blood cell count, is often a sign of disease (Johanson, 2003). Neurotransmitters, such as gamma-aminobutyric acid and glutamate, are also found in the CSF. Elevated glutamate concentrations are found in several diseases due to the role of glutamate in mediating secondary tissue damage (Di Terlizzi and Platt, 2006).

Homeostasis of CSF solute composition is critical because even small changes in the ion concentrations in the CSF can have a considerable affect on respiration, blood pressure, heart rate, muscle tone and emotional state (Di Terlizzi and Platt, 2006; Johanson, 2003). The choroid plexus plays a major role in maintaining the stability of these solute concentrations (Brodbelt and Stoodley, 2007; Johanson, 2003). The tight junctions between the epithelial cells of the CP act as a permeability barrier, blocking bidirectional diffusion of substances between the blood and CSF.

Additionally, the presence of numerous transporters on the CP epithelium allows it to tightly regulate the transport of substances across this barrier (Brodbelt and Stoodley, 2007; Johanson, 2003). Neuropeptides and neurotransmitters can also regulate the secretion of ions, water and proteins from the CP. The CP contains a wide variety of receptors, including those for norepinephrine, serotonin, angiotensin II and vasopressin (Chodobski and Szmydynger-Chodobska, 2001; Johanson, 2003; Nilsson et al., 1992). For example, serotonin, vasopressin and angiotensin have all been found to inhibit the release of chloride ions from the epithelial cells of the CP into the CSF, thereby reducing the formation rate of CSF (Chodobski and Szmydynger-Chodobska, 2001; Johanson, 2003; Nilsson et al., 1992). Additionally, the superior cervical ganglia send adrenergic fibers to the CP, providing an inhibitory tone on CSF formation. When sympathetic signals are blocked, there is enhanced CSF production by the CSF; in contrast, when α and β adrenergic agonists are administered, CSF production is reduced (Boassa and Yool, 2005; Cardinali et al., 1981; Johanson, 2003; Lindvall and Owman, 1981). Thus, the CP tightly regulates the solute concentration of the CSF by a combination of active transport, facilitated diffusion and regulation of neurotransmitter receptors on the CP epithelium (Johanson, 2003).

Cerebrospinal fluid flow. Bulk flow of the CSF occurs from the lateral to third ventricle via the foramen of Monro, to the fourth ventricle via the aqueduct of Sylvius and out of the fourth ventricle through the midline foramen of Magendie and the lateral foramina of Lushka into the cisterna magna (Brodbelt and Stoodley, 2007; Di Terlizzi and Platt, 2006). Pressure gradients between the subarachnoid space, venous sinuses and lymphatic spaces as well as movements of the brain and spinal cord with changes in blood pressure and respiration contribute to direction and pulsatile nature of bulk flow (Bergsneider, 2001; Brodbelt and Stoodley, 2007).

Additionally, ependymal cilia appear to help direct CSF flow through the ventricles (Brodbelt and Stoodley, 2007). However, there is no net bulk flow down the spinal canal; bulk flow of CSF only exists in the ventricular system (Bergsneider, 2001). Maintenance of this flow of CSF is important for cerebral metabolism because the CSF supplies micronutrients and peptides to neuronal networks and removes catabolites (Johanson et al., 2008). When CSF flow is blocked during fetal life, brain development is severely inhibited, partly due to compromised transport of growth factors (Miyan et al., 2003). Additionally, reduced CSF flow due to reduced production of CSF by the CP during aging and disease results in the buildup of toxic peptides and metabolites in the CSF (Johanson et al., 2008; Pratico et al., 2004; Rubenstein, 1998).

Cerebrospinal fluid absorption. CSF is reabsorbed into the systemic circulation by the venous system of the arachnoid villi in the superior sagittal sinus, the lymphatic system of the cribiform plate above the nose, the nasal submucosa and the olfactory, optic and cranial nerves (VII and VIII) (Brodbelt and Stoodley, 2007; Johanson et al., 2008). In recent years, it was demonstrated that the arachnoid villi are not the primary site of CSF reabsorption in most mammals, but may increase their CSF clearance under pathological conditions that raise ICP, such as hydrocephalus (Johanson et al., 2008). However, the arachnoid villi are thought to be the primary site of absorption of protein and cells (Bergsneider, 2001). When the ICP is high, brain capillaries may also upregulate aquaporin channels, specifically aquaporins 1 and 4, at the CP and brain microvessels to absorb interstitial fluid under high pressure (Johanson et al., 2008). In the H-Tx and kaolin-induced models of hydrocephalus, aquaporin 4 is significantly upregulated (Bloch et al., 2006; Mao et al., 2006; Shen et al., 2006). Reabsorbed CSF drains into the venous blood, and hydrocephalus has been associated with impaired extracranial venous obstruction (Johanson et

al., 2008; Papaiconomou et al., 2002). Disrupted CSF reabsorption is common in patients with communicating hydrocephalus; however, an imbalance between the rates of CSF formation and absorption cannot be the only cause of hydrocephalus because the CSF absorptive capacity exceeds that of formation even in patients with severe hydrocephalus (Bergsneider, 2001; Johanson et al., 2008). Recently, two theories have emerged to explain the pathology of communicating hydrocephalus: the bulk flow theory in which extraventricular obstruction of CSF flow occurs and the pulsation theory, which posits that decreased intracranial compliance causes ventriculomegaly via increased pulsatile stress on the ventricular walls (Egnor et al., 2002; Greitz, 2004).

Chapter III

Hydrocephalus: Classification, causes, pathology, treatment and animal models

a. Classification

Congenital vs. acquired. Hydrocephalus can either be congenital, in which the patient is born with hydrocephalus, or acquired, where the patient develops hydrocephalus after birth. Both congenital and acquired hydrocephalus can be either acute or chronic. In acute hydrocephalus, the ventricles are enlarging and intracranial pressure is high or unstable. In contrast, in chronic hydrocephalus, the ventricles are enlarged but intracranial pressure is normal or only slightly elevated but stable (Bret and Chazal, 1995; Larsson et al., 1999). Both acute and chronic hydrocephalus are multifactorial diseases and share a similar pathology; however, chronic hydrocephalus progresses more slowly because the adult brain tissue appears to better compensate in response to ventricular enlargement than the immature or developing brain (Edwards et al., 2004). Congenital hydrocephalus comprises approximately 50% of all cases of hydrocephalus and is commonly associated with other genetic diseases, such as spina bifida (Schrander-Stumpel and Fryns, 1998; Vintzileos et al., 1983; Zhang et al., 2006). In contrast, acquired hydrocephalus develops after birth and is due to brain damage that can be caused by a variety of insults, including acute trauma, hemorrhage, stroke, infection or tumors (Jensen and Jensen, 1979; Jensen, 1979). However, in both congenital and acquired hydrocephalus, the etiology is largely unknown.

Communicating vs. non-communicating. Hydrocephalus can be divided into two broad categories: communicating and non-communicating. Non-communicating hydrocephalus results from physical obstruction of the ventricular system, which prevents normal CSF flow. A common cause of non-communicating hydrocephalus is obstruction of the aqueduct of Sylvius, which is the narrowest part of the ventricular system and connects the third and fourth ventricles

of the brain. Congenital abnormalities, tumors, genetic defects, meningitis and hemorrhage are common sources of obstruction of the ventricular system in non-communicating hydrocephalus (Vertinsky and Barnes, 2007). In contrast, in communicating hydrocephalus, the passages of the ventricular system remain patent. While the mechanisms leading to communicating hydrocephalus remain unclear, excess CSF production by the choroid plexus or abnormal reabsorption of CSF by the arachnoid villi has traditionally been thought to be the cause (Egnor et al., 2002). However, the development of hydrocephalus due to the overproduction of CSF is thought to be extremely rare (McAllister and Chovan, 1998; Mori, 1995).

Recently, two theories have emerged to explain the pathology of communicating hydrocephalus: the bulk flow theory in which extraventricular obstruction of CSF flow occurs and the pulsation theory, which posits that decreased intracranial compliance causes ventriculomegaly via increased pulsatile stress on the ventricular walls (Egnor et al., 2002; Greitz, 2004). In the bulk flow model of communicating hydrocephalus, dilation of all four ventricles is thought to be caused by obstruction of CSF distal to the fourth ventricle but proximal to the subarachnoid spaces, resulting in an imbalance between CSF formation and absorption (Greitz, 2004; Rahme and Bojanowski, 2010). In contrast, the pulsation model is based on the idea that nearly all CSF motion is pulsatile, resulting from changes in vascular and CSF flow during systole and diastole (Egnor et al., 2002). During presystole, there are no pressure gradients in the brain. During early systole, the systolic pulse wave causes a large expansion of the arteries with a concomitant and significant decrease of the arterial pulse pressure, which is transmitted to the entire subarachnoid space. This arterial expansion causes a large volume conduction of CSF that compresses the outlets of the cortical veins and increases systolic blood flow in the venous sinus. At the same time, this arterial expansion pushes CSF into

the compliant spinal canal. After a brief delay (60 ms), the pulse wave is transmitted to the brain capillaries (Greitz, 2004). In contrast, in hydrocephalus, the intracranial capacitance vessels are thought to be narrow, resulting in decreased intracranial compliance. During early systole, the decreased intracranial compliance restricts arterial expansion, preventing damping of the pulse pressure in the arteries. Due to the decreased volume conduction of the CSF, the systolic CSF flow in the dural sinus and in the subarachnoid space is decreased. Thus, due to the decrease in arterial expansion, the volume of CSF conduction is also decreased, resulting in increased vascular resistance. Subsequently, the high pulse pressure in the arteries is transmitted into the brain capillaries, increasing CSF pulse pressure and systolic flow in the aqueduct of Sylvius. These changes are thought to result in increased transmantle stress and ventricular dilation (Egnor et al., 2002; Greitz, 2004). In sum, the pulsatile model suggests that ventricular dilation is caused by the transmission of pulsatile stress through the choroidal arteries and ventricular walls due to decreased intracranial compliance, possibly due to scarring in the subarachnoid spaces (Egnor et al., 2002; Greitz, 2004; Rahme and Bojanowski, 2010).

Normal pressure hydrocephalus. Normal pressure hydrocephalus (NPH) is a type of chronic, communicating hydrocephalus in which ventricular enlargement occurs in the absence of large increases in intracranial pressure (Kondziella et al., 2008; Siraj, 2011). Although NPH remains underdiagnosed, it is estimated that up to 10% of all dementia patients suffer from NPH (Hakim and Adams, 1965; Vale and Miranda, 2002). NPH is characterized by a triad of clinical symptoms that include gait ataxia, dementia and urinary incontinence and occurs most commonly in patients in their 60s or 70s (Kondziella et al., 2008; Shprecher et al., 2008; Siraj, 2011). NPH can be either classified as idiopathic, when there is no known cause, or secondary,

when there is a clear cause (Kondziella et al., 2008; Siraj, 2011). Secondary NPH can be caused by subarachnoid or intraventricular hemorrhage caused by trauma or aneurysms, infections such as meningitis and inflammatory conditions (Siraj, 2011). One leading theory for idiopathic NPH suggests that poor venous compliance, particularly in the superior sagittal sinus, impairs CSF pulsations, which reduces CSF flow through the aqueduct, and CSF absorption through the arachnoid villi (Bateman, 2000; Shprecher et al., 2008). Additionally, 83% of patients with idiopathic NPH also have hypertension, which may contribute to the disturbances in CSF flow found in NPH (Krauss et al., 1996). Cytokines, such as tumor necrosis factor-α (TNFα) and transforming growth factor-β (TGFβ), may also play a role in idiopathic NPH (Li et al., 2007; Shprecher et al., 2008; Tarkowski et al., 2003). Both TNFα, which is known to regulate CSF production, and TGFβ are elevated in idiopathic NPH (Li et al., 2007; Tarkowski et al., 2003); however, it is unclear whether these cytokines accumulate secondary to impaired CSF flow and thereby regulate the symptoms of NPH or whether overproduction of these cytokines is an adaptive response to hydrocephalus (Shprecher et al., 2008). The placement of shunts to drain the excess CSF, as discussed in section IIId, remains the only treatment for NPH (Siraj, 2011).

Hydrocephalus ex vacuo. Hydrocephalus ex vacuo is defined as the enlargement of the ventricles due to atrophy of the brain parenchyma (Bradley, 2001; LeMay and Hochberg, 1979). Hydrocephalus ex vacuo is commonly present in patients with Alzheimer's disease and other neurodegenerative disorders (LeMay and Hochberg, 1979; Silverberg, 2004). In hydrocephalus ex vacuo, the dilation of the ventricular system is often highly asymmetrical, which is in contrast to the more symmetrical dilation of the ventricles seen in other types of hydrocephalus, such as NPH (Sjaastad et al., 1969). Hydrocephalus is not considered to be related to CSF

hydrodynamics, but this conclusion is controversial; it is possible that hydrocephalus ex vacuo may be related to the loss of proper CSF flow (Silverberg, 2004).

b. Causes

Physical malformations. Chiari II and Dandy-Walker malformations as well as aqueductal stenosis often lead to hydrocephalus. Chiari II malformations are a prominent cause of hydrocephalus, accounting for approximately one-third of infantile hydrocephalus cases (Stevenson, 2004; Vertinsky and Barnes, 2007). Chiari II malformations result from failure of neural tube closure, and its cardinal signs include myelomeningocele in the thoraco-lumbar spine, herniation of the hindbrain into the cervical spinal canal and compression damage to the cranial nerves (Shuman, 1995; Stevenson, 2004). Non-communicating hydrocephalus results due to impaired CSF outflow from the fourth ventricle (Shuman, 1995; Stevenson, 2004; Vertinsky and Barnes, 2007).

Dandy-Walker malformations (DWM) are congenital brain malformations that include agenesis of the cerebellar vermis, dilation of the fourth ventricle and cyst formation filling the posterior cranial fossa, resulting in macrocephaly and hydrocephalus (Pascual-Castroviejo et al., 1991; Peter and Fieggen, 1999; Vintzileos et al., 1983). Approximately 2.4 to 4% of all hydrocephalus cases are caused by DWM (Pascual-Castroviejo et al., 1991). A combination of lateral and fourth ventricle shunts is often used to treat hydrocephalus with DWM; left untreated, hydrocephalus with DWM is generally fatal within 4 years (Vintzileos et al., 1983).

The aqueduct of Sylvius is the narrowest part of the ventricular system, and aqueductal stenosis is the most common cause of non-communicating hydrocephalus. Aqueductal stenosis can either be primary (congenital) or secondary (acquired) (Vertinsky and Barnes, 2007).

Hemorrhage, infection, tumors or ependymal cell loss may all cause aqueductal stenosis, leading to enlargement of the lateral and third ventricles (Vertinsky and Barnes, 2007; Wagner et al., 2003). Often, there is no clear precipitating factor for aqueductal stenosis (Vertinsky and Barnes, 2007).

Tumors and cysts. Cysts of the posterior cranial fossa resulting from Dandy-Walker malformations and arachnoid cysts are common causes of hydrocephalus. Arachnoid cysts are fluid collections in the arachnoidal membrane and subarachnoid space and can be either congenital or acquired (Pradilla and Jallo, 2007; Vertinsky and Barnes, 2007). Congenital arachnoid cysts result from developmental defects and consist of lesions composed of an arachnoid membrane that secretes CSF to expand the cyst (Pradilla and Jallo, 2007; Vertinsky and Barnes, 2007). These cysts likely result from alterations in CSF flow (Pradilla and Jallo, 2007). In contrast, acquired arachnoid cysts are caused by trauma, such as hemorrhage, and are associated with arachnoid scarring (Pradilla and Jallo, 2007; Vertinsky and Barnes, 2007). Although most cysts remain stable, the enlargement of cysts, often due to active CSF secretion from the cyst membrane, leading to elevated ICP, hypertension and hydrocephalus (di Rocco et al., 1981; Pradilla and Jallo, 2007).

Neoplasms occurring with in the first two years of life are rare and include astrocytomas, embryonic tumors and mesenchymal neoplasms (Vertinsky and Barnes, 2007). These tumors often occur along the midline of the ventricular pathways, resulting in elevated ICP and hydrocephalus (Vertinsky and Barnes, 2007). Choroid plexus tumors are the most common intraventricular tumors in children and arise from the epithelial cells of the choroid plexus. Because the choroid plexus is the primary producer of CSF, choroid plexus tumors often cause

hydrocephalus due to CSF overproduction (Coates et al., 1989; Vertinsky and Barnes, 2007). If the tumor becomes large enough, it can also cause obstructive hydrocephalus (Coates et al., 1989; Vertinsky and Barnes, 2007). Unfortunately, the high vascularity of these tumors often makes complete removal impossible, and shunts are often required (Kumar and Singh, 2005; Nagib and O'Fallon, 2000). Posterior fossa and third ventricular tumors also often lead to hydrocephalus. Posterior fossa tumors cause non-communicating hydrocephalus by obstructing CSF flow at or below the level of the aqueduct and fourth ventricle (Vertinsky and Barnes, 2007; Zimmerman et al., 1992). Similarly, third ventricle tumors cause non-communicating hydrocephalus by blocking CSF flow at the foramen of Monroe, body of the third ventricle or cerebral aqueduct (Ambrosino et al., 1988; Vertinsky and Barnes, 2007).

Ependymal cell denudation. Although ependymal cell loss is generally considered to result from enlargement of the ventricles and stretching of the ependymal lining (Bannister and Mundy, 1979; Bruni et al., 1985; Del Bigio, 1993; Sarnat, 1995), some studies suggest that ependymal cell denudation may be a causative factor in hydrocephalus (Jimenez et al., 2001; Wagner et al., 2003). In the hyh mouse model of hydrocephalus, the ependymal lining of the aqueduct of Sylvius denudes during embryonic and early postnatal life (Jimenez et al., 2001; Wagner et al., 2003). Subsequently, the aqueduct becomes stenosed (Wagner et al., 2003). It is possible that the negatively charged glycocalyx rich in sialic residues present on the surface of the ependyma creates a repellant effect, maintaining aqueductal patency. When the ependyma denude, these negatively charged residues are lost, resulting in aqueductal stenosis (Wagner et al., 2003). In support of this hypothesis, the aqueduct was never found to be obliterated in hyh mice where the ependyma remained intact (Wagner et al., 2003). However, evidence showing ependymal loss

prior to hydrocephalus in humans is limited (Dominguez-Pinos et al., 2005); thus, whether ependymal denudation is a causative factor in human hydrocephalus is unknown.

Loss of cilia function. Several studies suggest that impaired CSF flow caused by defective ependymal cilia results in hydrocephalus in both humans and animals (al-Shroof et al., 2001; Banizs et al., 2005; Bush, 2000; Davy and Robinson, 2003; Dawe et al., 2007; De Santi et al., 1990; Ibanez-Tallon et al., 2004; Picco et al., 1993). Many studies have shown that humans with immotile cilia or ciliary dyskinesia develop hydrocephalus (al-Shroof et al., 2001; Bush, 2000; De Santi et al., 1990; Picco et al., 1993). Multiple models of hydrocephalus have also been developed based on ciliary defects. Transgenic mice with ciliary defects either show defective CSF reabsorption (hy3 mice) (Davy and Robinson, 2003; Dawe et al., 2007), excessive CSF production ($Tg737^{orpk}$ mice) (Banizs et al., 2005) or non-communicating hydrocephalus caused by a loss of directional CSF flow leading to aqueductal stenosis (Mdnah5 mice) (Ibanez-Tallon et al., 2004). Thus, although there is a clear link between ciliary dysfunction and hydrocephalus, it remains unclear how ciliary defects cause hydrocephalus in humans.

Infection and dysregulation of cytokines. Hydrocephalus may also be caused by infection or dysregulation of cytokines. In infants, prenatal or postnatal infections are a common cause of hydrocephalus. Prenatal infections can be caused by bacterial or herpes infections traveling from the cervix to the amniotic fluid or by toxoplasmosis, rubella, cytomegalovirus (CMV) or herpes simplex infections traveling through the placenta (Vertinsky and Barnes, 2007). Of these infections, CMV is the most common cause of hydrocephalus. Hydrocephalus can also from meningeal or ependymal reactions leading to aqueductal stenosis (Becker, 1992; Boesch et al.,

1989; Vertinsky and Barnes, 2007). Meningitis is one of the most common infections that leads to hydrocephalus postnatally and can be caused by bacterial, viral, fungal or parasitic infections. Meningitis causes hydrocephalus due to inflammation of the arachnoid granulations and decreased absorption of CSF. Additionally, inflammatory and blood products can lead to arachnoiditis (Bell, 1992; Vertinsky and Barnes, 2007).

Dysregulation of cytokines has also been implicated in the pathogenesis of hydrocephalus. Altered concentrations of cytokines are found in the CSF in many animal models of hydrocephalus, including the H-Tx rat, and have been shown to affect normal cortical development (Owen-Lynch et al., 2003; Vetsika et al., 1999). Concentrations of transforming growth factor β1 and β2 (TGF-β1 and TGF-β2) have also been shown to be elevated in the CSF of adults and infants with ventricular dilation caused by intracerebroventricular hemorrhage (Flood et al., 2001; Whitelaw et al., 1999). In stronger support of a causative role of cytokines in the pathogenesis of hydrocephalus, injecting TGF-β into the subarachnoid space in mice and ventricular infusions of fibroblast growth factor 2 (FGF-2) in rats resulted in ventriculomegaly and communicating hydrocephalus (Johanson et al., 1999; Tada et al., 1994). Hydrocephalus in these animals was characterized by ventriculomegaly, elevated ICP, reduced CSF production and collagen deposits in the arachnoid villi (Hakvoort and Johanson, 2000; Johanson et al., 1999; Tada et al., 1994). Further, overexpression of TGF-β1 in GFAP-positive cells in mice resulted in communicating hydrocephalus with severe motor incoordination (Galbreath et al., 1995; Wyss-Coray et al., 1995). Whether TGF-β or FGF-2 plays a causative role in human hydrocephalus has yet to be determined.

Hemorrhage. Germinal matrix (GM) or intraventricular hemorrhage (IVH) occurs in 20% of premature infants and often results in hydrocephalus (Kazan et al., 2005; Vertinsky and Barnes, 2007). Hemorrhage in preterm infants results from the rich blood supply of the subependymal germinal matrix, which lacks astrocytic support, and fluctuations in intravascular pressures (Cherian et al., 2004). Fifteen percent of infants with IVH develop ventricular enlargement that requires shunt insertion; however, these infants have a high frequency of neurodevelopmental disabilities, including motor dysfunction and cognitive impairment (Cherian et al., 2004; Davis et al., 1987; Murphy et al., 2002). Hemorrhage results in hydrocephalus due to obstruction of the ventricular system or arachnoid villi by red blood cells and subsequent obliterative, fibrosing arachnoiditis, impairing CSF absorption (Cherian et al., 2004; Vertinsky and Barnes, 2007). Meningeal fibrosis and subependymal gliosis may also occur, obstructing CSF outflow from the foramina of the fourth ventricle and the aqueduct of Sylvius (Cherian et al., 2004; Hill et al., 1984; Larroche, 1972).

Hypertension. Venous hypertension can increase pressure within the dural sinuses, creating a decreased pressure gradient across the arachnoid villi, leading to decreased CSF absorption (Hayward, 2005; Vertinsky and Barnes, 2007). This most often results in hydrocephalus in patients younger than 18 months because the open sutures and soft, undermyelinated and immature white matter allow ventricular expansion without resistance (Hayward, 2005; Vertinsky and Barnes, 2007). In older patients in whom the skull is not capable of expanding, venous hypertension creates a pseudo-tumor-like state (Hayward, 2005; Karahalios et al., 1996). Venous hypertension may be caused by developmental conditions, such as malformations of the skull base restricting venous outflow, congenital heart disease, pulmonary disease with elevated

central venous pressure or thrombosis of central veins or sinuses caused by infection, vascular malformation or coagulopathy (Vertinsky and Barnes, 2007). Hydrocephalus caused by venous hypertension is often treated with shunt surgery to drain the excess CSF caused by reduced absorption (Hayward, 2005).

Aging. Changes in the CNS caused by aging have also been shown to contribute to hydrocephalus. In particular, normal pressure hydrocephalus is common in elderly patients and is often comorbid with Alzheimer's disease (Long, 1985; Silverberg et al., 2003). With normal aging, the choroid plexus epithelial layer becomes flattened and calcified, reducing CSF production (May et al., 1990; Preston, 2001; Silverberg et al., 2002). The production and secretion of CSF by the choroid plexus is also regulated by vasopressin, and elevations in vasopressin concentrations in aging lead to decreased CSF production (Faraci et al., 1990; Frolkis et al., 1999). Additionally, CSF absorption decreases due to thickening of the arachnoid villi and reduced drainage into the vascular system, resulting in the build-up of toxic products, such as amyloid beta, in the CSF (Albeck et al., 1998; Bech et al., 1997; Bellur et al., 1980). Increases in venous pressure may also reduce CSF absorption (Rubenstein, 1998). Reduced CSF turnover and increased CSF volume also occurs with age, likely due to tissue atrophy, further contributing to the build-up of toxic substances in the CSF and possibly leading to ventriculomegaly (Foundas et al., 1998; Matsumae et al., 1996; Wahlund et al., 1996). Age-related decline in the protective, antioxidant enzymes of the choroid plexus and other brain tissues also contributes to oxidative stress and DNA damage these tissues (Preston, 2001). Although all of these processes are common to normal aging, they may make certain individuals more susceptible to hydrocephalus.

Genetic mutations. Mutations in the L1 neural adhesion molecule, located on near the telomere of the long arm of the X chromosome in Xq28, are the only known genetic cause of hydrocephalus in humans (Fransen et al., 1995; Zhang et al., 2006). Deficiencies in this protein result in CRASH syndrome, characterized by corpus callosum hypoplasia, mental retardation, adducted thumbs, spastic paraplegia and hydrocephalus (Fransen et al., 1995; Yamasaki et al., 1997). The severity of the disease is strongly correlated to the type of mutation in the L1CAM gene, with mutations that produce truncations in the extracellular domain of the L1 protein being more likely to produce severe hydrocephalus with mental retardation and early death (Yamasaki et al., 1997). L1CAM normally plays a key role in axon outgrowth and pathfinding as well as synaptic plasticity; however, how mutations in L1CAM lead to hydrocephalus remain unclear (Panicker et al., 2003; Rolf et al., 2001; Sztriha et al., 2000). Some studies suggest that L1-related hydrocephalus develops ex vacuo due to increased degeneration of neural cell types due to disturbed interactions between cells and between cells and the extracellular matrix (Dahme et al., 1997; Rolf et al., 2001). It is also possible that severe brain malformations resulting from altered development produce aqueductal stenosis and hydrocephalus (Rolf et al., 2001).

c. Pathology

The ventriculomegaly and elevated intracranial pressure that accompany hydrocephalus result in a wide variety of pathological changes. Although hydrocephalus is a multifactorial disease, the pathological changes observed in human and animal models of hydrocephalus are fairly consistent and include ependymal and subependymal changes, changes to the choroid plexus and altered CSF flow, vascular changes, edema, white matter loss, cell death and disorganization and gliosis.

Ependymal and subependymal changes. As the ventricles enlarge, the ependymal layer stretches and is eventually destroyed, especially over white matter; the degree of ependymal damage is dependent on the severity and rate of ventricular expansion (Bannister and Mundy, 1979; Del Bigio, 1993; Sarnat, 1995). Slowly enlarging lateral ventricles are less likely to lose their ependymal lining; instead, ventricular enlargement causes the cuboidal and columnar ependymal cells to flatten and increase their surface area (Del Bigio, 1993; Page et al., 1979). Additionally, as ependymal cells stretch and are lost, the cilia and microvilli that line the ventricles are also lost, especially over the roof and dorsolateral angle of the lateral ventricles (Page, 1975; Raimondi et al., 1976). Macrophages then appear on the surface of the ventricular walls to remove the debris (Del Bigio, 1993; Go et al., 1976). Because ependymal cells do not proliferate (Spassky et al., 2005), reactive astrocytes form a barrier that separates the periventricular tissue from the CSF (Del Bigio, 1993; Takano and Becker, 1997). Additionally, the subventricular zone, which lies immediately beneath the ependymal cells around the lateral ventricles, becomes disorganized and shows a marked reduction of proliferative cells (Dominguez-Pinos et al., 2005; Jimenez et al., 2009). Neuroblasts become displaced to the ventricular surface and show reduced migration through the rostral migratory stream to the olfactory bulb (Dominguez-Pinos et al., 2005; Jimenez et al., 2009). These changes in the SVZ have been suggested to be caused by the aberrant expression of trophic factors (Del Bigio, 2004; Fukumitsu et al., 2000; Miyan et al., 2001).

Changes in CSF and the choroid plexus. Morphological and physiological changes to the choroid plexus include epithelial cell atrophy and cytological changes, which may reflect reduced secretory activity (Preston et al., 2003; Silverberg et al., 2002). Additional changes observed in

experimental models of hydrocephalus include distortion of CP microvilli, cell flattening and vacuolization and enlargement of intracellular spaces (Del Bigio, 2001; Dohrmann, 1971; Go et al., 1976; Lawson and Raimondi, 1973).

Reduced outflow of CSF is also common in hydrocephalus, causing CSF to accumulate in the ventricles and subarachnoid spaces (Del Bigio, 1993). Because normal CSF flow is important for distributing growth factors, signaling molecules and neurotransmitters throughout the brain and for clearing waste products from the brain, reduced CSF outflow impairs neuronal function (Bergsneider, 2001; Di Terlizzi and Platt, 2006; Johanson, 2003; Podell and Hadjiconstantinou, 1997; Vaughn et al., 1988). Because shunting does not restore normal CSF flow, neurological deficits caused by impaired CSF flow often persist even after shunting (Mashayekhi et al., 2002; McAllister and Chovan, 1998).

Vascular changes. Reductions in blood flow, especially in white matter, have been demonstrated in humans with hydrocephalus using Doppler blood flow, PET, SPECT, MRI and CT (Goh and Minns, 1995; Nakano et al., 1996; Shih and Tasdemiroglu, 1995). Reductions in blood flow are correlated with lateral ventricle size in infants (Hill and Volpe, 1982; Lui et al., 1990). A reduction in the quantity and caliber of capillaries has also been shown, resulting in ischemia and injury to oligodendrocytes and axons (Del Bigio, 1993; Klinge et al., 2003). This reduction in capillaries is thought to be due to a combination of increased ICP and distortion of the brain parenchyma (DE, 1950; Del Bigio and Bruni, 1988; Di Rocco et al., 1979). Interestingly, in the periventricular white matter of hydrocephalic animals, separations of endothelial tight junctions have been observed, suggesting an alternate pathway for CSF absorption in hydrocephalus (Nakada et al., 1992; Nakagawa et al., 1984; Nakagawa et al., 1985; Okuyama et al., 1987).

Tight junctions may therefore represent dynamic structures that allow the paracellular movement of substances across the blood-brain barrier and may contribute to molecular transfer under pathological conditions (Bundgaard, 1986; Madara, 1988).

Periventricular edema. Elevated ICP is accompanied by edema in the periventricular region (Drake et al., 1989; Hiratsuka et al., 1982; Murata et al., 1981). Comparisons of wet and dry tissue weights and specific gravity analyses have shown that tissue water content is increased above control values in the periventricular region in hydrocephalic animals, and histological analyses have shown increased extracellular spaces in the white matter surrounding the ventricles in humans (Di Rocco et al., 1977; Fishman and Greer, 1963; Higashi et al., 1986; Takei et al., 1987). This periventricular fluid likely represents stagnant extracellular fluid (Del Bigio, 1993). Edema and changes in the extracellular spaces may have severe consequences for neuronal function. Maintenance normal volume and tortuosity of the extracellular spaces is necessary for the movement of neurotransmitter and their metabolites and waste products from energy metabolism (Del Bigio, 1993; Moseley et al., 1990; Nicholson, 1988). Therefore, compression or impeded flow of extracellular fluid through the extracellular spaces can upset the homeostasis of the local microenvironment and disrupt normal neuronal function (Del Bigio, 1993).

White matter loss. Myelin loss and axonal damage are important neuropathological changes in hydrocephalus, and measurements of myelin basic protein (MBP) in the CSF of hydrocephalic humans have been used to determine the severity of brain damage (Del Bigio, 2004; Sutton et al., 1983). Atrophy of periventricular white matter, including the corpus callosum, and damage to periventricular axons are frequently found in humans and animal models of hydrocephalus (Del

Bigio and Zhang, 1998; Del Bigio, 2001; Gadsdon et al., 1979). Atrophy of the fimbria/fornix connections between the hippocampus and forebrain are common in hydrocephalus in animals and humans, resulting in cognitive changes and memory dysfunction in severe hydrocephalus (Del Bigio et al., 2003). Oligodendrocytes also appear to be directly damaged by hydrocephalus and can be seen in the white matter of hydrocephalic rats and cats, resulting in white matter hypomyelination (Del Bigio et al., 1994; Del Bigio and Zhang, 1998; Hanlo et al., 1997). Edema in the periventricular white matter has been suggested as a primary cause of myelin damage (Feigin, 1983; Weller et al., 1971).

Neuronal damage and cell death and disorganization. Severe hydrocephalus results in considerable loss of brain tissue, including thinning of the cortex, redundant cortical gyri and gross atrophy of the basal ganglia (Clark and Milhorat, 1970; DE, 1950; Del Bigio, 1993; Di Rocco et al., 1977). In the basal ganglia, hydrocephalus produces functional injuries of cholinergic, dopaminergic and GABAergic neurons due to mechanical distortion (Tashiro et al., 1997b). Similarly, in the cerebral cortex and hippocampus, the loss of nonpyramidal interneurons without overt changes in neuronal architecture suggests a functional impairment of these neuronal systems in the pathogenesis of hydrocephalus prior to gross morphological changes (Tashiro et al., 1997a). Shrunken, dark neurons and cytoplasmic vacuolization have also been found in hydrocephalic cats (Hale et al., 1992; Wright et al., 1990). Neuronal pyknosis, vacuolization and degeneration have all been demonstrated in hydrocephalic humans (Del Bigio, 1993; Glees and Voth, 1988). Pathological changes in neurons are likely secondary to myelin loss and axonal damage (Del Bigio, 2004). Reduction in the quantity of dendritic spines and branches and reduced synaptic contacts have also been demonstrated (Del Bigio and Zhang,

1998; Harris et al., 1997; McAllister et al., 1985). In the developing rat brain, cortical compression and reduced cell density have been detected in severe hydrocephalus, although there were no changes in total cell number (Jones et al., 1991).

Glial changes. Subependymal astrogliosis is commonly observed in humans and animals with chronic hydrocephalus; however, astrogliosis has only been demonstrated in cases of severe hydrocephalus (Bruni et al., 1985; Del Bigio, 1993; Yoshida et al., 1990). Additionally, following ependymal denudation, astrocytes have been shown to proliferate and form a superficial cell layer to replace the lost ependyma (Paez et al., 2007; Sarnat, 1995). Astrocyte metabolism has also been shown to be disturbed relatively early in the kaolin-model of hydrocephalus in rats, and these disturbances persist throughout the chronic phase of hydrocephalus and are not resolved upon shunting, contributing to the neurological deficits that persist after shunting (Kondziella et al., 2003; Kondziella et al., 2008). Alterations in aquaporin 4 channel expression on astrocytes and ependymal cells have also been shown to affect hydrocephalus. Upregulation of aquaporin 4 is associated with brain edema, and aquaporin 4 knock-out mice have reduced edema (Owler et al., 2010; Papadopoulos and Verkman, 2007; Verkman et al., 2006). However, aquaporin 4 knock-out mice have worse clinical outcomes in hydrocephalus, likely due to the role of astrocytes in glia limitans in removing the redundant water from the parenchyma to the subarachnoid space (Verkman et al., 2006).

Microglia also become reactive throughout the brain during the intermediate stages of hydrocephalus in H-Tx rats, and reactive microglia have been demonstrated in the periventricular region and basal ganglia of human fetal hydrocephalus (Mangano et al., 1998; Ulfig et al., 2004). With increasing severity of human fetal hydrocephalus, the microglial activation spreads from

the periventricular region throughout the rest of the brain (Ulfig et al., 2004). Additionally, activated phagocytic macrophages have been found on the ependymal ventricular lining in human hydrocephalus, and likely act to remove detached ependymal cells (Del Bigio, 1993; Ulfig et al., 2004). However, both reactive astrogliosis and microgliosis were shown to be reduced following shunting in an experimental model of hydrocephalus, suggesting that these changes are, at least in part, reversible (Miller and McAllister, 2007).

d. Diagnosis and treatment

Diagnosis. Macrocephaly and increased intracranial pressure (ICP) are common symptoms of hydrocephalus (Vertinsky and Barnes, 2007). Macrocephaly is defined as a head circumference more than two standard deviations above the mean and is often associated with developmental delays, seizures, a neurocutaneous syndrome and elevated venous pressure (Vertinsky and Barnes, 2007). Symptoms of elevated ICP depend on age and include macrocephaly, bulging fontanelles, split sutures, reduced eating, vomiting, irritability, vision impairment, headache, lethargy, stupor, encephalopathy, sixth nerve palsy and papilledema (Vertinsky and Barnes, 2007). When hydrocephalus develops later in life, macrocephaly does not occur due to the hardening of the skull; however, symptoms of elevated ICP are still present and can be used for diagnosis. Normal pressure hydrocephalus is characterized by gait and cognitive impairments and urinary incontinence (Shprecher et al., 2008; Siraj, 2011).

Diagnosis of hydrocephalus is confirmed using imaging through ultrasonography (US), computed tomography (CT) and/or magnetic resonance imaging (MRI). Ventricular enlargement in the absence of atrophy or underdevelopment detected by these tests is indicative of hydrocephalus (Vertinsky and Barnes, 2007). Enlargement of the anterior and posterior recesses

of the third ventricle, rounded configuration of the lateral ventricles, increased flow voids on the MRI and dilation of the temporal horns are also suggestive of hydrocephalus (Gammal et al., 1987; Vertinsky and Barnes, 2007). Periventricular edema, which is common in patients with hydrocephalus, can also be detected as blurred or ill-defined ventricular margins (Vertinsky and Barnes, 2007).

US or CT is initially used to diagnose hydrocephalus in the fetus and infant because they are more practical than MRI in these cases. Because it is a noninvasive and repeatable bedside procedure, doppler US is used to identify infants with enlarged ventricles and elevated ICP and to determine whether shunting is required (Hoon and Melhem, 2000; Vertinsky and Barnes, 2007). US provides a good assessment of brain structure and maturation and is therefore good at detecting abnormalities in the periventricular white matter (Hoon and Melhem, 2000). However, US lacks specificity and sensitivity and does not show subtle lesions in the brainstem or cerebellum (Hoon and Melhem, 2000; Kuban, 1998; Paneth, 1999). Similarly, CT scans are practical because they are less costly than MRIs and often do not require sedation (Hoon and Melhem, 2000). Additionally, CT scans can detect enlarged ventricles and are often used to determine whether surgery is required (Gammal et al., 1987; Hoon and Melhem, 2000; Vertinsky and Barnes, 2007). However, CT provides incomplete information in diagnosing small or isodense pathological changes in the aqueduct and foramen of Monroe (Gammal et al., 1987). As such, the use of MRI is often necessary to visualize small obstructions in midline structures (Gammal et al., 1987).

Because of its superior contrast resolution, multiplanar imaging capability, lack of bone artifacts, absence of ionizing radiation and the ability to assess CSF flow and tissue anisotrophy, MRI is the preferred imaging method for determining anatomical changes present and the type of

surgery required in patients with hydrocephalus (Hoon and Melhem, 2000; Vertinsky and Barnes, 2007). The information provided by MRI with respect to CSF flow is helpful in assessing complex, compartmentalized or encysted hydrocephalus (Gammal et al., 1987; Vertinsky and Barnes, 2007). MRI can also be used to visualize small obstructions in the ventricular system, which cannot be seen via CT, and to determine whether a cyst or tumor is present and blocking the ventricular system (Gammal et al., 1987; Vertinsky and Barnes, 2007). However, MRIs are more expensive and require sedation (Hoon and Melhem, 2000).

Shunts. Untreated hydrocephalus results in severe brain damage and has a high mortality rate of 50 – 96%; thus, treatment is required to prevent further brain damage and death (Laurence and Coats, 1962; Yashon, 1963). Treating hydrocephalus by redirecting CSF flow through the insertion of a shunt into the ventricular system was developed over fifty years ago by Nulsen and Spitz and remains the primary treatment for hydrocephalus today (Beni-Adani et al., 2006; Nulsen and Spitz, 1951). Although the original shunt diverted excess CSF into the jugular vein, today shunts drain excess CSF into the abdominal cavity, lungs or heart and use adjustable valves to tailor the drainage rate among patients (Del Bigio, 2004; Zemack and Romner, 2002). Shunt surgery is now primarily used for patients with communicating hydrocephalus or in non-communicating hydrocephalus in which absorptive problems are also present, whereas endoscopic third ventriculostomy (ETV, discussed in more detail below) is gaining acceptance as the preferred treatment for non-communicating hydrocephalus (Beni-Adani et al., 2006). However, as it is difficult to rule out an additional absorptive problem in patients with non-communicating hydrocephalus, ETV is less frequently used (Beni-Adani et al., 2006).

The placement of shunts greatly improves survival and outcomes of patients with hydrocephalus; however, early shunt surgery is necessary to prevent severe, irreversible effects, such as severe motor disabilities, epilepsy and intellectual impairment (Del Bigio et al., 1997; Takei and Sato, 1995; Tashiro and Drake, 1998). In children with shunted hydrocephalus, shunting restores myelination loss and changes in brain weight and size (Del Bigio, 2004; Gadsdon et al., 1979). Additionally, shunting has been shown to reduce the size of the ventricles, promote reexpansion of the cortical mantle and reduce edema of the periventricular tissues (Hale et al., 1992). Shunting of geriatric patients with normal pressure hydrocephalus has also been shown to improve memory, gait and urinary incontinence and reduce bradykinesia and Parkinson-like symptoms (Goodman and Meyer, 2001). Animal models have also suggested that cerebral blood flow and glucose utilization are restored, behavior and memory improve, myelin deposition improves, mild axonal damage is reversed and partial restoration of neurotransmitters occurs (Del Bigio et al., 1997; Del Bigio, 2004; Hale et al., 1992; Hawkins et al., 1997; Tashiro and Drake, 1998). However, not all pathological changes caused by hydrocephalus can be restored by shunting. Ventricles often remain enlarged, the ependymal lining is not restored, capillaries do not resume their normal configuration, severed axons cannot be restored and reactive astrogliosis causes persistent periventricular changes (Del Bigio, 1993; Del Bigio, 2001; Del Bigio, 2004; Takei and Sato, 1995)

Although shunts have greatly improved patient survival and outcomes, they have a high failure rate. Forty percent of shunts fail within the first year, and two-thirds of shunts fail within 10 years after surgery (Drake et al., 2000; Patwardhan and Nanda, 2005). Infection, obstruction of the shunt, overdrainage, slit ventricle syndrome, craniosynostosis and low cranial-brain compliance are all causes of shunt failure (Beni-Adani et al., 2006). The reported incidence of

shunt infections ranges from 2 to 39% and includes infections from *Staphylococcus epidermidis* and *S. aureus* (Turgut et al., 2005). In cases of infection, the infected shunt must be removed and replaced with a new shunt following a course of system antibiotics (Turgut et al., 2005). The high replacement rate of shunts, estimated to be between 1.6 and 3.6 revisions per patient, results in children receiving multiple neurosurgeries throughout their lives (Lazareff et al., 1998). Improvements made to shunt surgery have also not been without complications, such as cor pulmonale and shunt nephritis due to cardiac shunting, bowel erosion from spring-coiled catheters, obstruction of anti-siphon devices and tonsillar herniation due to lumboperitoneal shunts (Drake et al., 2000). As a result, further shunt improvements and new therapeutics are necessary to improve treatment of hydrocephalus.

Endoscopic third ventriculostomy. Endoscopic third ventriculostomy (ETV) is a relatively new endoscopic procedure used for patients with an obstruction at or distal to the posterior of the third ventricle who have patent subarachnoid spaces (Vertinsky and Barnes, 2007). To bypass this obstruction, a surgical opening is made in the floor of the third ventricle, restoring CSF flow (Vertinsky and Barnes, 2007). ETV is primarily used in patients older than two years with a well-defined anatomical obstruction, however, moderate success has been achieved in infants with posthemorrhagic or postinfectious HC as well as those with Chiari II malformations (Vertinsky and Barnes, 2007). ETV is successful and avoids the complications and need for repeat surgeries common with shunt placement. Additionally, there is no risk of overdrainage and a low risk of infection. However, the failure rate of ETV in infants ranges from 30 – 90% (Beni-Adani et al., 2006). This high failure rate is thought to be the result of the age of the patient, the underlying pathology (i.e., ETV did not eliminate the need for shunt placement) and

uncontrolled intraoperative bleeding (Beni-Adani et al., 2006). Additionally, in contrast to shunt placement, ventricular size decreases more slowly and to a lesser degree (Vertinsky and Barnes, 2007). Thus, better classification of hydrocephalus is necessary to determine whether a patient would benefit from ETV (Beni-Adani et al., 2006).

Pharmacological treatments. Although a variety of pharmacological agents have been administered to hydrocephalic patients for centuries, no current drug treatments exist (Del Bigio, 2004). Most treatments in the past half century have focused on reducing CSF production (Del Bigio, 2004). Although the carbonic anhydrase inhibitor acetazolamide reduced CSF production by 60%, it produced no clinical improvement in patients with hydrocephalus (ELVIDGE et al., 1957). Likewise, furosemide, a diuretic that inhibits sodium reabsorption in the renal tubules and is capable of affecting fluid balances in the brain showed no benefit in children with post-hemorrhagic hydrocephalus (Shinnar et al., 1985). The hyperosmolar agent isosorbide has been suggested as a treatment for hydrocephalus but lacked efficacy in clinical trials and has therefore not been tested in a randomized controlled trial (Lorber, 1975; Lorber et al., 1983). Further, the Na^+-K^+-ATPase pump ouabain has not been tested in clinical trials due to toxicity (Del Bigio, 2004). It is likely that drugs that attempt to reduce CSF production are ineffective because CSF plays an important role in flushing waste products into the blood, and reducing CSF production would not aid in cases of hydrocephalus where CSF flow or absorption is blocked because the pulse waves that cause ventricular enlargement would persist (Del Bigio, 2004).

Treatments that attempt to reopen obstructed CSF pathways have also been attempted. However, intrathecal injections of hyaluronidase in children with post-tuberculosis hydrocephalus had little effect (Schoeman et al., 1991). Additionally, urokinase and

streptokinase, which are fibrinolytic enzymes, were infused into the ventricular CSF following intraventricular hemorrhage to disperse blood clots and prevent scarring; however, these drugs also showed limited improvement (Hansen et al., 1997; Yapicioglu et al., 2003). Anti-inflammatory drugs have also been attempted in cases of hemorrhagic hydrocephalus with little improvement in preventing or treating hydrocephalus (Erler and Klaber, 2001; Wilkinson et al., 1974).

A number of treatments have also been attempted to prevent the brain damage that accompanies hydrocephalus; however, these treatments have only been attempted in animal models of hydrocephalus. Nonetheless, nimodipine, which blocks L-type calcium channels, and magnesium sulfate, which blocks NMDA receptors and voltage- and receptor-operated calcium channels, have shown behavioral and structural protection in the kaolin model of hydrocephalus (Del Bigio and Massicotte, 2001; Khan et al., 2003a; Khan et al., 2007). These protective effects are likely due to their effect on smooth muscle cell calcium channels and improved cerebral blood flow (Del Bigio and Massicotte, 2001; Khan et al., 2003a). In contrast, sodium channel blockers, such as mexiletine and riluzole, calcineurin inhibitors, such as tacrolimus and cyclosporine, and calpain inhibitor 1 showed no benefits in animal models of hydrocephalus (Del Bigio et al., 2002; Khan et al., 2003b). Further studies are necessary to confirm neuroprotective drug effects in humans to determine their benefit in the treatment of hydrocephalus.

e. Experimental models of hydrocephalus

Induced models. There are currently a number of animal models being used to gain insight into the pathophysiology of hydrocephalus. The first models of hydrocephalus were developed by inserting or injecting substances in the ventricular systems of various animals. The first model of

hydrocephalus involved inserting a cotton plug into the aqueduct dogs to mimic non-communicating hydrocephalus (Dandy, 1919). Since then, a number of other substances have been injected into the ventricular system to cause hydrocephalus. A commonly used inducible model of hydrocephalus involves injecting kaolin (aluminum silicate) into the cisterna magna of the rodent brain. This causes a strong inflammatory response in the meninges that results in obstruction of the outlets of the fourth ventricle and ventricular enlargement as a result of inflammatory scarring (da Silva Lopes et al., 2009). Injection of silicone oil into the cisterna magna also results in hydrocephalus due to mechanical obstruction of CSF flow out of the fourth ventricle, resulting in increased intracranial pressure and ventricular dilation (Del Bigio and Bruni, 1991). Injection of neuraminidase from *Clostridium perfingens* into the lateral ventricle of rats resulted in the death and detachment of ependymal cells from the lateral ventricles, third ventricle, cerebral aqueduct and the rostral half of the fourth ventricle, resulting in aqueductal stenosis (Grondona et al., 1996). Ventriculomegaly of the lateral and third ventricles also occurred (Grondona et al., 1996). These pathological changes were thought to be the result of cleavage of sialic acid residues from the ependymal surface glycoproteins and glycolipids (Grondona et al., 1996). Recently, a model of acute obstructive hydrocephalus was developed in rats using N-butyl cyanoacrylate (NBCA). Injection of NBCA into the fourth ventricle produced hydrocephalus in 73.3% of rats without diffuse inflammation (Park et al., 2011). However, the onset of hydrocephalus in these mice was rapid and there was a high mortality rate due to severe brain swelling and brain stem compression (Park et al., 2011). In all of these models, hydrocephalus is often accompanied by an inflammatory response or a physical tissue distortion that is not present in most cases of human hydrocephalus. As a result, it is difficult to determine

the specific cellular changes caused by hydrocephalus, and their relevance to human hydrocephalus is unclear.

Genetic models. The first congenital models of hydrocephalus were developed through spontaneous mutations in rats; namely, the hydrocephalic Texas strain (H-Tx) and the LEW/Jms strain. However, the penetrance in both of these models is low, at approximately 40% in the H-Tx rats and 28% in the LEW/Jms strain (Jones et al., 2000b). While the LEW/Jms strain presents with aqueductal stenosis and therefore represents a model of non-communicating hydrocephalus, it remains controversial whether the H-Tx model displays communicating or non-communicating hydrocephalus. Studies have demonstrated stenosis of the aqueduct of Sylvius in H-Tx rats (Boillat et al., 1999; Jones and Bucknall, 1988); however, hydrocephalus appears to develop prior to impaired CSF flow, suggesting that this is a model of communicating hydrocephalus (Kiefer et al., 1998). Additionally, in the H-Tx strain, the ependymal layer is maintained, which is in contrast to the loss of the ependymal layer (ependymal denudation) found in human cases of congenital non-communicating hydrocephalus (Jones et al., 2000a; Oi et al., 1996; Yamada et al., 1992; Zhang et al., 2006). Although these models have been useful in the study of hydrocephalus, the limited penetrance and severe pathology limits their usefulness in understanding the pathogenesis of hydrocephalus.

Many genetic animal models for studying hydrocephalus have been developed, including both models of communicating and non-communicating hydrocephalus. One genetic model of hydrocephalus is the hydrocephalus with hop gait (hyh) mice, which have a mutation in α-SNAP, leading to a neural progenitor defect that results in ependymal denudation, aqueductal stenosis, and enlargement of the lateral ventricles (Hong et al., 2004; Jimenez et al., 2001; Paez

et al., 2007; Wagner et al., 2003). In this model, mice have neural progenitor defects and are born with moderate, communicating hydrocephalus. In the first postnatal week, the aqueduct of Sylvius closes and severe hydrocephalus develops (Wagner et al., 2003). The development of hydrocephalus in this model appears to be dependent on ependymal denudation (Jimenez et al., 2001; Paez et al., 2007; Wagner et al., 2003). Deficiencies in the L1 neural adhesion molecule have been observed in both humans and mice, leading to CRASH syndrome (corpus callosum hypoplasia, mental retardation, adducted thumbs, spastic paraplegia and hydrocephalus) (Fransen et al., 1995). Hydrocephalus in L1 deficient mice appears to be communicating; the aqueduct only becomes stenosed in severe hydrocephalus due to brain compression (Rolf et al., 2001). Another genetic model of hydrocephalus are the E2f5 deficient mice, which lack the E2f5 transcription factor normally expressed in the choroid plexus (CP) (Lindeman et al., 1998). This mutation alters the secretory activity of the CP, resulting in a model of communicating hydrocephalus with excessive CSF production (Lindeman et al., 1998). Another model of hydrocephalus was developed by the insertional inactivation of the transcription factor RFX4 (Blackshear et al., 2003). Mice heterozygous for this mutation develop hydrocephalus due to the absence of the subcommissural organ (SCO). Without the Reissner's fibers produced by the SCO, which are necessary for the patency of the aqueduct in mice, the aqueduct becomes stenosed, resulting in non-communicating hydrocephalus (Blackshear et al., 2003; Zhang et al., 2007). Overexpression of the G-protein coupled receptor, PAC1, in the mouse nervous system was also found to cause hydrocephalus, including enlarged lateral and third ventricles; however, aqueductal enlargement was also observed, which is rarely observed in human hydrocephalus (Lang et al., 2006). Lastly, disruption in the RNA binding protein Msi1 results in aberrant

proliferation of the ependymal cells that surround the aqueduct of Sylvius, resulting in non-communicating hydrocephalus (Sakakibara et al., 2002).

Multiple models of hydrocephalus have also been developed based on ciliary defects, including the hy3 mouse (Davy and Robinson, 2003), the Tg737^{orpk} mouse (Banizs et al., 2005) and in mice with a disruption in Mdnah5, a gene that codes for the dynein heavy chain of cilia (Ibanez-Tallon et al., 2004). Hy3 mice show defective CSF reabsorption, resulting in communicating hydrocephalus with perinatal onset (Davy and Robinson, 2003; Dawe et al., 2007). In these mice, mild hydrocephalus develops by P14 with moderate ventricular dilation and a flattened but intact ependymal lining. As ventricular dilation becomes more severe, the ependyma and ependymal cilia of the hy3 mice disappear, especially at the roof of the lateral ventricle (Lawson and Raimondi, 1973). Tg737^{orpk} mice present with abnormal ion and water transport across the choroid plexus epithelium, resulting in excessive CSF production; stenosis of the aqueduct of Sylvius occurs late in the pathogenesis of hydrocephalus in this model (Banizs et al., 2005). Hydrocephalus is not the primary pathology in these mice, however; these mice also present with cystic kidney disease, sterility, biliary and bile duct hyperplasia in the liver, and retinal degeneration (Banizs et al., 2005). In contrast, mice with a mutation in Mdnah5 present with non-communicating hydrocephalus caused by a loss of directional CSF flow that leads to stenosis of the aqueduct of Sylvius (Ibanez-Tallon et al., 2004).

In all of these genetic mouse strains, the genetic mutations lead to developmental pathologies unrelated to hydrocephalus, making it difficult to identify cellular changes specific to the development of hydrocephalus. Additionally, the incomplete penetrance and inability to induce hydrocephalus in these models has made it impossible to specifically investigate the pathogenesis of hydrocephalus.

Chapter IV

The Ro1 model of hydrocephalus

Our understanding of the early changes in hydrocephalus requires the development of better animal models. In existing animal models, penetrance is often low and hydrocephalus appears to be one of a spectrum of diseases, making it difficult to sort out the cellular mechanisms that are contributing to hydrocephalus. Our lab has developed a novel model of hydrocephalus that gives us the unique ability to control the onset of the disease and thereby study early cellular changes that may lead to the development of hydrocephalus. This model was created using the tetracycline-inducible system to drive expression of a mutated Gi-coupled GPCR (Ro1 receptor) to cells expressing glial fibrillary acidic protein (GFAP). When mice are taken off doxycycline (a tetracycline derivative), allowing for Ro1 expression in GFAP+ cells, 100% of mice develop hydrocephalus. Unlike other models, hydrocephalus also appears to be the primary pathology.

The Ro1 RASSL (receptor activated solely by a synthetic ligand) was developed by Bruce Conklin's laboratory by replacing the second extracellular loop (EL2) of the human kappa opioid receptor (KOR) with the EL2 of the delta opioid receptor (DOR) (Coward et al., 1998b). As such, this receptor represents a transgenic Gi-coupled G protein-coupled receptor (GPCR). This receptor was also FLAG-tagged at the amino terminus (Figure 3). This transgenic receptor showed a 200-fold decrease in the K_i for dynorphin, an endogenous KOR agonist (Coward et al., 1998b). A high-throughput screening of 21 endogenous KOR agonists demonstrated that the Ro1 receptor has significantly reduced affinity for endogenous ligands (Coward et al., 1998b). However, binding of the small synthetic drug, spiradoline, was not significantly affected in the Ro1 receptor (Coward et al., 1998b). This receptor retained the ability to couple to adenylyl cylcase, causing a decrease in cAMP levels (Coward et al., 1998b). Additionally, the inverse agonist norbinaltorphamine (norBNI) was capable of inhibiting Ro1 signaling (Scearce-Levie et

al., 2005). A tetracycline-inducible system was subsequently used to drive Ro1 to a specific cell or tissue type using a cell- or tissue-specific promoter (Figure 4). This technique allowed for inducible expression of the receptor, thereby avoiding complications caused by expression during development, and cell- or tissue-specific activation of a Gi-coupled GPCR signaling cascades.

When the cardiac-specific α myosin heavy chain (αMHC) promoter was used to drive Ro1 expression to the heart, mice developed a lethal cardiomyopathy associated with a wide QRS complex arrhythmia (Redfern et al., 2000). These cardiac arrhythmias were blocked by a single injection of pertussis toxin (PTX), demonstrating that Ro1 signaling through Gi-coupled pathways in the heart caused this arrhythmia (Redfern et al., 2000). Interestingly, these changes were due to Ro1 expression alone, suggesting that expression of this receptor is sufficient to activate Gi-coupled signaling cascades (Redfern et al., 2000). Additionally, when the Ro1 receptor was expressed in osteoblasts using the mouse 2.3-α type 1 collagen promoter (Col I-2.3), mice developed trabecular osteopenia (Peng et al., 2008). More specifically, eight weeks of Ro1 expression resulted in a greater than 20% reduction in trabecular bone volume compared with sex-matched littermate controls (Peng et al., 2008). Again, Ro1 expression alone caused this phenotype, suggesting that the Ro1 receptor shows basal signaling in the absence of the agonist, spiradoline (Peng et al., 2008).

Our laboratory used the tetracycline-inducible system to drive Ro1 expression to GFAP-positive cells. Immunohistochemistry showed selective co-localization of the FLAG-tagged Ro1 receptor with GFAP-positive cells in the hippocampus (Figure 5) (Sweger et al., 2007). Additionally, Ro1 expression was shown to be regulated by dox. In wild-type control mice or in Ro1 mice maintained on dox, the FLAG-tagged Ro1 receptor could not be detected via western

blotting; however, when taken off dox, there was clear Ro1 expression in the whole brain, hippocampus and cerebellum (Figure 6) (Sweger et al., 2007). Additionally, 100% of double-transgenic Ro1 mice developed hydrocephalus when taken off dox (Sweger et al., 2007). When Ro1 were born to dams maintained off dox, mice developed severely enlarged heads, and by 11 weeks of age, 50% of Ro1 mice had died (Figure 7) (Sweger et al., 2007).

To demonstrate that signaling through the Gi-coupled Ro1 receptor was causing hydrocephalus in the Ro1 mice rather than the transgene interfering with cellular machinery, Ro1 mice and single-transgenic littermate control mice were taken off dox at P30 and injected with the KOR antagonist norBNI (7.6 mg/kg, i.p.) every three days for 30 days. The mice were then sacrificed, and the lateral ventricle to brain ratio (LV:brain ratio) was measured at the level of the striatum and anterior commisure. The LV:brain ratio was significantly higher in Ro1 mice off dox than in controls ($p = 0.02$); however, there were no significant differences in this ratio between control mice and Ro1 mice maintained on dox or Ro1 mice maintained off dox and given norBNI (Figure 8) (Sweger and McCarthy, 2009). The mitogen-activated protein kinase (MAPK) signaling cascade has been shown to be activated downstream of Gi-coupled GPCRs. Thus, because signaling through the Gi-coupled Ro1 receptor causes hydrocephalus, changes in phospho-ERK were investigated in hydrocephalic Ro1 mice. In P21 mice, phospho-ERK levels were shown to be elevated in hydrocephalic Ro1 mice, but not in littermate controls, around the lateral ventricles and in the entorhinal cortex (Figure 9) (Sweger et al., 2007). These findings implicate Gi-GPCR and MAPK signaling cascades in Ro1-mediated hydrocephalus. Given that we are selectively expressing the Ro1 receptor in a specific population of cells and activation of a specific signaling cascade is causing hydrocephalus in these mice, this model enables the investigation of signaling molecules that may be contributing to hydrocephalus. Additionally, the

complete penetrance and inducibility of this model allow us the unique ability to investigate the earliest changes in the pathogenesis of hydrocephalus. Together, these characteristics of the Ro1 model will increase our understanding of the early pathogenesis of hydrocephalus and may lead to the development of novel therapeutics to treat this disorder.

Chapter V

Characterization of the histological changes in the pathogenesis of hydrocephalus in Ro1 mice

Introduction

Hydrocephalus is a highly prevalent disorder that affects greater than 0.1% of the population, yet the primary treatment for hydrocephalus—the surgical placement of shunts to drain the excess cerebrospinal fluid—has not changed in over 50 years (Patwardhan and Nanda, 2005; Piatt and Carlson, 1993; Sainte-Rose et al., 1991). The lack of improved treatments for this disorder is due to the multifactorial causes of this disorder and our lack of understanding of the early cellular and morphological changes in the pathogenesis of this disorder. In existing animal models, penetrance is often low and hydrocephalus appears to be one of a spectrum of diseases, making it difficult to sort out the cellular mechanisms that are contributing to hydrocephalus. The Ro1 model of hydrocephalus developed by our laboratory has complete penetrance, is inducible and is free of complicating pathologies, giving us the unique ability to investigate the pathogenesis of hydrocephalus. In this study, we used histology, immunohistochemistry and electron microscopy to elucidate the cellular and morphological changes that lead to hydrocephalus in the Ro1 model.

Materials and Methods

Animals. All experiments were performed in accordance with the Institutional Animal Care and Use Committee at the University of North Carolina at Chapel Hill and federal guidelines. Animals were maintained in climate-controlled housing with a 12 h light/dark cycle and were given food and water *ad libitum*. Selected breeding pairs and weaned mice were given 50 μg/mL doxycycline (dox; Sigma) in their drinking water, which was changed twice a week. Dox was provided in black water bottles to protect the dox from light. Breeding pairs maintained off dox were never exposed to dox.

Transgenic mice. GFAP-tTA::tetO-Ro1 mice on a KOR knockout background were generated as described by Sweger et al., 2007. All mice were backcrossed onto the C57Bl/6J background (10 generations).

Real-time PCR. Two 1 mm-thick coronal brain sections at the level of the lateral ventricles per mouse were sliced on an acrylic matrix and placed in RNA later (Ambion) at -20ºC. RNA was isolated using the RNeasy Lipid Tissue Mini Kit (Qiagen), and the amount of RNA per sample was quantified using a NanoDrop spectrophotometer (Thermo Scientific). RNA from each mouse was sent for an RNA quality check at the Nucleic Acids Core Facility at the University of North Carolina. cDNA was then prepared using Superscript II Reverse Transcriptase with random primers and RNaseOUT to block RNase activity (Invitrogen). Real-time PCR was then conducted using hKOR2 and GAPDH primers and a SYBR green detection system (Applied Biosystems).

Hematoxylin and eosin staining. Mice were taken off dox at P30 and transcardially perfused with 4% paraformaldehyde at 9, 12, 18, 24, 30 and 48 days following dox removal. To study the effect of Ro1 expression throughout gestation and development, dams were maintained off dox, and weaned mice were perfused at P27. Following perfusion, the brains were removed and post-fixed overnight at room temperature in 10% formalin with gentle agitation. The brains were then rinsed in distilled water and stored in 70% ethanol. The brains were then taken to the University of North Carolina histology core facility for paraffin embedding. Serial coronal sections were sliced 5 μm-thick on a sliding microtome (Leica) and stained with hematoxylin and eosin.

Stained brain sections were imaged with a light microscope (Zeiss), and images were captured using a Dage Excel XL16 camera (Dage-MTI).

Measurements. Images from hematoxylin and eosin stained coronal brain sections (1.25x magnification) at 0.38 mm anterior to bregma were analyzed with MetaMorph image analysis software. The maximum width of the lateral ventricles was measured and divided by the maximum brain width to obtain the lateral ventricle to brain ratio (LV:brain ratio). For measurements of aqueduct disorganization, images of the aqueduct of Sylvius were captured from 18, 24, 30 and 48 days off dox mice at 20x magnification immediately posterior to the dorsal third ventricle (approximately 2.92 mm posterior to bregma). Aqueduct disorganization was scored by three observers blind to genotype based on the continuity of the ependyma and the degree of cilia coverage. A maximum score of 10 represented a continuous ependymal lining with a thick, continuous carpet of cilia, whereas a minimum score of 0 represented a complete loss of ependyma and cilia.

Immunohistochemistry. Mice were taken off dox at P30 and transcardially perfused with 4% paraformaldehyde at 9, 12 and 24 days after removal of dox. The brains were post-fixed for 4 h in 4% paraformaldehyde at 4ºC and subsequently transferred to a 30% sucrose solution in PBS (pH 7.4) at 4ºC for cryoprotection. The brains were then embedded and frozen in O.C.T. (Optimal Cutting Temperature; Tissue-Tek, Sakura, Japan) in an ethanol/dry ice bath and stored at -80ºC. Ten micrometer-thick coronal and sagittal slices were cut on a cryostat (Reichard-Jung) and melted onto Superfrost Plus slides (Fisher). The slices were washed three times with phosphate-buffered saline (PBS) and incubated in blocking solution (10% normal goat serum and

0.3% TritonX-100 in PBS). The slices were then incubated in primary antibody overnight in blocking solution at 4ºC. The primary antibodies used included doublecortin (DCX, 1:500; Cell Signaling) to stain for migrating neuroblasts, glial fibrillary acidic protein (GFAP, 1:500; Sigma) to stain for astrocytes and S100 (1:500; DAKO) to stain ependymal cells. The slices were then washed six times for 10 min in PBS and incubated in goat anti-rabbit 594 or goat anti-mouse 488 secondary antibodies (Alexa Fluor, 1:400; Invitrogen) in blocking solution for 2 h at room temperature. The slices were washed six times for 10 min in PBS and mounted in Vectashield with DAPI (Vector), coverslipped and sealed with nail polish. The sections were imaged with a fluorescent microscope (Zeiss).

Electron microscopy. Mice were taken off dox at P30 and transcardially perfused at 18 and 30 days off dox with Ringer's solution (1.36 M NaCl, 0.127 M Na_2HPO_4, 0.503 M KCl, 0.098 M $MgCl_2$, 0.595 M $NaHCO_3$, 0.204 M $CaCl_2$ and 2.2 mM dextrose, with 0.004% xylocaine to anesthetize smooth muscle and 5 U/mL heparin to prevent blood clotting) followed by 2% paraformaldehyde and 2.5% glutaraldehyde in 0.1 M phosphate buffer for 10 min at a rate of 3 mL/min. Brains were post-fixed in the same fixative for 1 h on ice and sliced 50 μm-thick on a Vibratome (Leica) in ice-cold fixative. The tissue slices were then post-fixed overnight in the same fixative at 4ºC. The sections were post-fixed in 0.5% osmium tetraoxide in 0.1 M phosphate buffer for 45 min and then stained with 1% uranyl acetate in maleate buffer for 45 min. After dehydrating in an ascending ethanol series, sections were embedded in Epon/Spurr resin (Electron Microscopy Services) and mounted between sheets of Aclar within glass slides. After embedding, sections were cut 60 nm-thick on an Ultracut (Leica), mounted onto T200

copper grids (Electron Microscopy Services) and post-stained with 2% uranyl acetate and Sato's lead.

Statistics. An F-test was used to calculate a p-value for linear regression analyses. P-values < 0.05 were considered to be statistically significant. StatView statistical software (version 5.0) was used for all statistical tests (SAS).

Results

Ro1 expression is detectable by 9 days off dox. When taken off dox at P30, Ro1 receptor expression was detectable by real-time PCR in 1 mm-thick coronal brain slices at the level of the lateral ventricle at 9 days off dox. However, the degree of Ro1 expression varied considerably among double-transgenic mice (Figure 10; n = 6). This variability was surprising given that all of the mice were derived from the same transgenic lines and all mice were on the C57/bl6 background. It is possible that this variability is due to variability in the consumption or metabolism of dox among the mice. For example, the rate at which dox leaves the fat deposits and bone may vary from mouse to mouse, thereby affecting the timing and degree of Ro1 expression.

Ventriculomegaly and disorganization of the aqueduct of Sylvius are the first signs of pathology in the Ro1 model. To determine the early histological changes in the Ro1 model of hydrocephalus, Ro1 and littermate control mice were taken off dox at P30 and perfused 9 (n = 4), 12 (n = 7), 18 (n = 6), 24 (n = 6), 30 (n = 5) and 48 (control, n = 21; Ro1, n = 17) days after removal of dox. Serial coronal sections were taken from the beginning of the lateral ventricle

through the fourth ventricle and stained with hematoxylin and eosin (H&E). Although we saw clear Ro1 receptor expression by 9 days off dox, there were no detectable morphological changes at 9, 12 or 18 days off dox. Ventriculomegaly was first observed at 24 days off dox (Figure 11). However, likely due to the variability observed in Ro1 receptor expression among double-transgenic mice, there was considerable variability in ventricle size among Ro1 mice (average LV:brain ratio = 0.22; range = 0.14 – 0.39). Ventriculomegaly was more pronounced at 30 and 48 days off dox (Figure 11), with an average LV:brain ratio of 0.25 at 30 days (range = 0.15 – 0.43) and 0.38 at 48 days (range = 0.18 – 0.64). Concomitant with the increase in ventricle size, we observed disorganization of the ependymal cells and their cilia lining the aqueduct of Sylvius. The degree of aqueductal disorganization was highly correlated with the severity of ventriculomegaly, as measured by the lateral ventricle to brain ratio ($r^2 = 0.67$; $p < 0.0001$; Figures 12 and 13). Interestingly, there was considerable variability in the size of the aqueduct of Sylvius. However, closure of the aqueduct of Sylvius was never observed, despite analysis of serial coronal sections from the third to fourth ventricles. These data suggest that the Ro1 model is a model of communicating hydrocephalus.

Ependymal denudation of the lateral ventricles is secondary to ventriculomegaly. Ependymal denudation of the lateral ventricles often accompanies enlargement of the lateral ventricles in humans and other animal models. When taken off dox at P30, brains from Ro1 mice rarely showed denudation; denudation was only present with severe ventriculomegaly. However, the ependymal lining became thinner with increasing lateral ventricle size (Figure 14). The thinning of the ependymal lining observed at the lateral ventricles differed from the considerable ependymal cell loss and disorganization observed at the aqueduct of Sylvius. Thus, in the Ro1

model of hydrocephalus, ependymal thinning and denudation of the ventricles appears to be a consequence of the enlargement of the lateral ventricles, rather than a causative event in the pathogenesis of hydrocephalus.

Despite ventriculomegaly, there is no change in subventricular zone organization in early hydrocephalus. Because we are driving Ro1 expression to GFAP-positive cells and GFAP is expressed in both subventricular zone (SVZ) astrocytes and at low levels in ependymal cells, we hypothesized that Ro1 expression might be affecting SVZ organization. Furthermore, SVZ astrocytes extend processes that both integrate into the ependymal layer and contact blood vessels (Danilov et al., 2009), positioning them to play a potential role in ventriculomegaly and ependymal denudation in the pathogenesis of hydrocephalus. These SVZ astrocytes are also the progenitor cells of the SVZ, giving rise to neuroblasts that migrate to the olfactory bulb where they form olfactory interneurons (Doetsch et al., 1999b; Lois and Alvarez-Buylla, 1994; Luskin, 1993). Moreover, astrocytes direct the migration of the SVZ-born neuroblasts (Anton et al., 2004; Conover et al., 2000; Lois et al., 1996). To determine whether Ro1 expression in these cells causes changes in SVZ organization and neuroblast migration early in the pathogenesis of hydrocephalus, 10 μm-thick coronal and sagittal slices were stained with glial fibrillary acidic protein (GFAP), an astrocytic marker, S100, an ependymal cell marker, and doublecortin (DCX), a marker of migrating neuroblasts. Although there appeared to be thinning of the ependymal layer in mice with ventriculomegaly at 24 days off dox, there were no changes observed in the number or intensity of staining of astrocytes or ependymal cells at 9 (n = 4), 12 (n = 3) or 24 days (n = 5) off dox (Figure 15 A-F). Additionally, sagittal slices stained with DCX showed no

changes in the number or migration of SVZ-born neuroblasts at 12 (data not shown; n = 3) or 24 days (n = 5) off dox (Figure 15 G-H).

Ventriculomegaly causes thinning of the ependymal layer, resulting in edema and patches of the ventricular wall barren of microvilli. Because no gross morphological changes were observed with either H&E staining or immunohistochemistry, transmission electron microscopy was performed to investigate the ultrastructure of the ependymal and subependymal layers of the lateral ventricles of Ro1 mice early in the development of hydrocephalus. No changes were observed in Ro1 mice off dox for 18 days, which corroborates the findings from the light microscopy experiments (data not shown; n = 8). However, at 30 days off dox (n = 3), considerable thinning of the ependymal layer was observed (Figure 16). Additionally, there were patches of the lateral ventricle walls that were barren of microvilli (Figure 16). Edema was also present in the periventricular area (Figure 16).

Mice maintained off dox show similar disease progression to mice taken off dox at P30. To investigate whether Ro1 expression throughout gestation and development alters disease progression in double-transgenic mice, dams were never given dox, and pups were maintained off dox until perfusion at P27 (n = 4). Double-transgenic Ro1 mice showed severely enlarged heads at P27 (data not shown). Histological analysis using H&E staining showed severe but variable ventriculomegaly of Ro1 mice (Figure 17). Interestingly, ependymal denudation was not present in any Ro1 mice (Figure 17). Ependymal denudation was only present with severely enlarged lateral ventricles, further demonstrating that ependymal denudation is a result of ventricular enlargement rather than a causative factor in the development of hydrocephalus in the

Ro1 model. Additionally, despite analysis of serial coronal sections from the third ventricle through the fourth ventricle, stenosis of the aqueduct of Sylvius was never observed even in the most severely hydrocephalic brains studied, although disorganization of the aqueduct was present in all Ro1 mice with ventriculomegaly (Figure 17). These data further suggest that the Ro1 model is a model of communicating hydrocephalus, as blockage within the ventricular system does not appear to be a causative factor for hydrocephalus in this model.

Discussion

Selectively expressing the transgenic Ro1 receptor in astrocytes using a tetracycline-inducible system results in a novel and inducible model of hydrocephalus that can be used to study the early pathogenesis of this disorder. The careful histological analysis of the Ro1 model presented in this study demonstrates that ventriculomegaly and disorganization of the aqueduct of Sylvius are the earliest morphological changes observed in the pathogenesis of hydrocephalus in the Ro1 model. Ependymal denudation and cilia loss, a common feature of hydrocephalus in humans and animal models, appear to result from enlargement of the lateral ventricles. This finding suggests that ependymal loss and cilia dysfunction are not a cause of hydrocephalus but rather due to the resulting pathology. Interestingly, thinning of the ependymal layer due to ventriculomegaly appears to lead to edema and a loss of microvilli lining the walls of the lateral ventricles. Other studies have suggested that edema is a result of transependymal flow of CSF due to the loss of tight junctions between the ependymal cells caused by ventriculomegaly (Jensen, 1979; Rahme and Bojanowski, 2010; Del Bigio, 1993). Furthermore, stenosis of the aqueduct of Sylvius, the narrowest part of the ventricular system, was never observed, suggesting that the Ro1 model represents a model of communicating hydrocephalus. It is interesting that

although the aqueduct never closed, disorganization of the ependyma of the aqueduct was observed. The mechanism leading to the disorganization of the aqueduct, as well as the role of this disorganization in the pathogenesis of hydrocephalus, remain unclear. The progression of hydrocephalus in the Ro1 model appears to be the same, although perhaps more rapid, when mice are maintained off dox throughout gestation and development as compared to mice taken off dox at P30.

The Ro1 model of hydrocephalus appears to mirror human hydrocephalus in many respects. Multiple studies have suggested that ependymal denudation is subsequent to ventriculomegaly and the degree of denudation appears to be dependent on the size of the lateral ventricles and the rate at which hydrocephalus progresses; more rapid disease progression leads to increased ependymal loss (Bannister and Mundy, 1979; Bruni et al., 1985; Del Bigio, 1993; Sarnat, 1995). The progressive loss of microvilli and cilia as well as periventricular edema have also been shown to occur in humans with increasing ventricular size and thinning and denudation of the ependymal lining (Bannister and Mundy, 1979; Bruni et al., 1985; DaSilva, 2004; Del Bigio et al., 1985; Di Rocco et al., 1977). Previous studies have proposed that stretching and disruption of the tight junctions of the ependyma secondary to ventricular dilation may result in transependymal CSF flow and edema (Levine, 2008; Raimondi, 1994). Interestingly, a previous study on human fetuses with moderate communicating hydrocephalus showed consistent ependymal denudation. However, all of the fetuses studied presented with ventricular dilation, and the ventricular surface area devoid of ependyma increased with increasing severity of hydrocephalus and age of the fetus (Dominguez-Pinos et al., 2005). We also observed increased ependymal denudation and cilia loss with increasing ventricular size and a correlation between the rate of hydrocephalus development and both denudation and cilia density. Whereas extensive

denudation and loss of cilia was found in P27 mice maintained off dox throughout gestation and development, denudation was rarely observed in Ro1 mice taken off dox at P30, even with severe ventriculomegaly. These data suggest that in the Ro1 model the progression of hydrocephalus occurs more slowly when hydrocephalus is induced by the removal of dox in young adults; this may provide the ependyma with greater time to compensate for the enlargement of the ventricles, thereby reducing the degree of denudation observed.

Subependymal gliosis is commonly observed in humans and animals with chronic hydrocephalus; however, gliosis has been shown to be subsequent to ependymal loss (Bruni et al., 1985; Del Bigio, 1993). Thus, although we did not observe gliosis early in the pathogenesis of hydrocephalus in Ro1 mice, a previous study demonstrated gliosis in the hippocampus and cortex of severely hydrocephalic Ro1 mice (Sweger et al., 2007), suggesting that gliosis occurs in Ro1 mice with severe hydrocephalus. Although changes in the subventricular zone of human fetuses with moderate communicating hydrocephalus have also been observed, these changes were shown to be subsequent to ventricular dilation and ependymal loss (Dominguez-Pinos et al., 2005). Therefore, it is possible that SVZ disorganization is also present in Ro1 mice, but only in mice with severe hydrocephalus and ependymal denudation.

Many studies in animal models corroborate our findings. Most animal studies of both communicating and non-communicating hydrocephalus have shown that ventriculomegaly and early tissue damage is accompanied by a flattening, stretching and subsequent disruption of the ependyma. For example, in the H-Tx rat and the hy3 mouse models, both of which are models of communicating hydrocephalus, ventricular enlargement initially causes stretching of the ependyma. However, with more severe ventriculomegaly, ependymal loss occurs, especially at the roof of the lateral ventricles (Bannister and Mundy, 1979; Kiefer et al., 1998). Previous TEM

studies have also shown stretching of the ependymal layer, intact but widely separated clusters of cilia and edematous tissue with enlarged extracellular spaces, which mirrors the results obtained in our study (Del Bigio, 1993; Raimondi et al., 1976). Our data from mice maintained off dox throughout gestation and development showed that ependymal denudation was most common on the roof of the lateral ventricle with severely enlarged ventricles. The Ro1 model of hydrocephalus may also be similar to the H-Tx rat in that obstruction of the aqueduct of Sylvius may occur only in severely hydrocephalic animals. A previous study on hydrocephalic Ro1 mice demonstrated aqueductal stenosis in severely hydrocephalic mice maintained off dox throughout gestation and development (Sweger et al., 2007). Although aqueductal stenosis was never observed in this study, even in mice with severe ventriculomegaly and a similar dox dosing schedule as the previous study, it remains possible that stenosis of the aqueduct of Sylvius may require hydrocephalus even more severe than presented herein. It is possible that the loss of cilia and ependyma of the aqueduct of Sylvius demonstrated in this study may lead to subsequent aqueduct stenosis; ependymal loss of the aqueduct of Sylvius has been proposed to lead to aqueduct stenosis and hydrocephalus in the hyh mouse model of hydrocephalus (Jimenez et al., 2001; Paez et al., 2007; Wagner et al., 2003).

In sum, the Ro1 model of hydrocephalus represents a novel model of communicating hydrocephalus. This model has many similarities to both human hydrocephalus and experimental models of hydrocephalus. However, the complete penetrance, inducibility and lack of complicating pathologies in this model provide the unique opportunity to investigate the pathogenesis of hydrocephalus, which may provide insight into the development and progression of this disorder. Moreover, because the Ro1 receptor is a G protein-coupled receptor and is restricted to GFAP-positive cells, this model provides the unique ability to investigate specific

signaling cascades that may cause hydrocephalus. The data presented herein provide insight into the earliest cellular and histological changes in the development and progression of hydrocephalus, which may help to improve the early diagnosis and treatment of this disorder.

Chapter VI

Astrocyte-specific Ro1 expression causes hydrocephalus but does not affect mouse behavior

Introduction

A variety of behavioral changes have been observed in various animal models of hydrocephalus. However, most of these changes appear in mice with severe hydrocephalus and the rate of disease progression appears to affect behavioral changes. Nonetheless, reduced swim speeds, abnormal gait, hypoactivity and reduced performance on the wire hang and inclined slope tests have been demonstrated in various models of hydrocephalus (Del Bigio et al., 1997; Del Bigio et al., 2003; Fransen et al., 1998; Khan et al., 2007; Lopes Lda et al., 2009; Tsubokawa et al., 1988; Wada, 1988). Additionally, animal models of hydrocephalus have shown reduced learning in the Y maze, 8-arm radial maze and Morris water maze tests (Del Bigio et al., 1997; Jones et al., 1996; Khan et al., 2007; Miyazawa and Sato, 1991; Miyazawa et al., 1997; Morrisey et al., 1996). However, findings from these tests differed considerably depending on the model studied. In humans with hydrocephalus, gait abnormalities, motor disorders and memory and cognitive defects are the most common behavioral changes (Bakar and Bakar, 2010; Estanol, 1981; Fletcher et al., 1996; Tarazi et al., 2008; Yeates et al., 2003), which parallels the changes found in animal models of hydrocephalus in some respects. However, whether early behavioral changes exist prior to apparent pathology, such as ventriculomegaly, remains unknown. A better understanding of these early behavioral changes may aid in the early diagnosis of hydrocephalus.

Materials and Methods

Animals. All experiments were performed in accordance with the Institutional Animal Care and Use Committee at the University of North Carolina at Chapel Hill and federal guidelines. Animals were maintained in climate-controlled housing with a 12 h light/dark cycle and were given food and water *ad libitum*. Selected breeding pairs and weaned mice were given 50 μg/mL

doxycycline (dox; Sigma) in their drinking water, which was changed twice a week. Dox was provided in black water bottles to protect the dox from light. Breeding pairs maintained off dox were never exposed to dox.

Transgenic mice. GFAP-tTA::tetO-Ro1 mice on a KOR knockout background were generated as described by Sweger et al., 2007. All mice were backcrossed onto the C57Bl/6J background (10 generations).

Behavior. To investigate progressive changes in weight and general motor ability, mice (controls, n = 11; Ro1, n = 10) were taken off dox at P30, and weight, grip strength (wire hang), motor coordination (rotarod), exploratory behavior (open field), startle responses and sensorimotor gating (acoustic startle) were measured immediately following removal of dox and every week thereafter for a total of seven weeks. For the wire hang test, the mice were placed, one at a time, on a wire grid and inverted approximately 20 cm above a soft sponge. The latency to fall off of the grid was recorded; the maximum cut-off time was 60 s. For the rotarod test, the mice were placed on an accelerating cylinder (rotarod), and the latency to fall off the rotarod was recorded; the maximum cut-off time was 300 s. The mice were first given a series of three trials to evaluate motor learning; on each subsequent testing day, the mice were given two trials on the accelerating rotarod to measure motor coordination. For the open field test, mice were placed in a large Plexiglas enclosure with a photobeam array (Accuscan Instruments) and allowed to freely explore for 1 h. Total distance traveled (cm), horizontal activity, stereotypy counts and rearing activity were measured. For the acoustic startle test, the SR-LAB startle response system was used (San Diego Instruments). Briefly, mice were placed in a plexiglas cylinder with white noise

at a level of 70 dB. Mice were given a loud startle (120 dB) or a prepulse (74, 78, 82, 86 or 90 dB) followed by the loud startle (120 dB), and the force displaced by a whole-body startle response was measured by an accelerometer. Responses to the startle alone or prepulse followed by the startle were randomized; the response to each stimulus was tested six times with 15 s between stimuli.

A second cohort of mice (control, n = 10; Ro1, n = 11) was used to test learning and memory in the Morris water maze. The Morris water maze consists of a circular pool (diameter = 122 cm) partially filled with water (45 cm deep, 24 – 26°C) containing non-toxic white paint. The pool was visually divided into four quadrants. Visual cues were placed in the room surrounding the pool. Visual learning was tested at 10 – 12 days after removal of dox by placing the mice in the pool and measuring their latency to swim to a visible platform. Learning acquisition of the location of a hidden platform (diameter = 12 cm) was then tested until the average latency of the mice was less than 15 s. This test was conducted from 15 – 19 days off dox by placing the escape platform below the surface of the water and measuring their latency to learn the location of the hidden platform based on the visual cues in the surrounding room. A probe trial was then conducted at 19 days off dox by measuring the time spent in each of the quadrants; increased time spent swimming in the quadrant where the platform had been previously located (quadrant 1) was considered indicative of learning. The platform was then moved to the opposite quadrant (quadrant 3) and the time required to learn the new location of the platform was measured. Mice were trained in the reversal learning paradigm until the latency to find the hidden platform was, on average, less than 15 s. Reversal learning occurred from 22 – 32 days off dox, and the probe trial for reversal was conducted at 32 days off dox. Mice were

then tested for the ability to remember the location of the hidden platform (quadrant 3) by recording their latency to find the platform at 46 – 47 days off dox (retention).

A third group of mice (control, n = 17; Ro1, n = 13) was used to test the development of anxiety and depression in early hydrocephalus. At 24 days off dox, mice were tested on the elevated plus maze, which has two open arms and two closed arms (20 cm in height). The maze is elevated 50 cm from the floor and the arms are 30 cm long. Animals were placed in the center section (8 cm x 8 cm) and allowed to freely explore the maze for 5 min. The time spent in the open and closed arms and the number of entries into each arm was recorded. Mice were subsequently tested in the forced swim test at 25 days off dox. In this test, mice were placed in a cylinder (28 cm high; 20.2 cm in diameter) filled with water (14.5 deep; 23°C), and their time spent immobile in a 6 min-period was recorded. The time spent in the center of the open field apparatus (AccuScan Instruments) in 1 h was used as a measure of anxiety in mice 31 days off dox. Lastly, passive avoidance was tested in mice 32 – 33 days off dox. The passive avoidance test consisted of two trials. On the first day of testing, mice were placed in the apparatus, which consists of a light chamber and a dark chamber, separated by a door. After a 30 s acclimation period, the door is opened, and when the mice enter the dark chamber, they received a mild footshock (0.5 mA, 2 s). On the second day of testing, the latency to enter the dark chamber was measured; a 300 s cut-off was used.

Statistics. For comparisons between control and Ro1 mice at a single time point, Student's t-test was used. To analyze changes in the behavioral tests over time as well as changes in the acoustic startle test, a repeated-measures ANOVA was used. An F-test was used to calculate a p-value for

linear regression analyses. P-values < 0.05 were considered to be statistically significant. StatView statistical software (version 5.0) was used for all statistical tests (SAS).

Results

There are no changes in weight, motor or sensory ability of Ro1 mice with hydrocephalus. Over seven weeks of testing, no statistically significant changes in weight were observed between Ro1 and control mice (Figure 18). Additionally, there were no significant changes in any of the measures of the open field test, including total distance traveled (Figure 19), rearing, stereotypy or center time. Ro1 mice also did not show reduced motor coordination on the rotarod test or reduced startle responses or sensorimotor gating in the acoustic startle test as compared to control mice at any week tested (Figures 20 and 21). There were also no changes in grip strength, as measured by the wire hang test, between Ro1 and control mice (Figure 22). Of the two Ro1 mice that died prior to completion of the study, weight, activity, ability on the rotarod and wire hang tests and startle responses appeared to drop off immediately prior to death; however, there was no correlation between the lateral ventricle to brain ratio and the performance on any of these tests. No sex differences were observed in any test. These data are summarized in Table 1 below.

Table 1
Changes in weight and general motor ability of Ro1 mice and littermate controls over seven weeks of testing[a]

	Week 1			Week 4			Week 7			p-value
	Control	Ro1	p-value	Control	Ro1	p-value	Control	Ro1	p-value	(7 weeks)[b]
Weight (g)	12.5 ± 0.5	12.7 ± 0.5	0.77	18.1 ± 0.67	17.7 ± 0.79	0.71	20.3 ± 0.8	19.7 ± 0.8	0.67	0.90
Wire hang (latency, s)	58 ± 2	56 ± 4	0.75	60 ± 0	55 ± 5	0.31	60 ± 0	51 ± 7	0.15	NA[c]
Rotarod (latency, s)	219 ± 27	229 ± 23	0.79	287 ± 7	232 ± 31	0.08	259 ± 18	250 ± 24	0.77	0.22
Total distance (cm)	5790 ± 563	5816 ± 411	0.97	7817 ± 1144	6045 ± 901	0.25	8573 ± 1051	11817 ± 2189	0.16	0.62
Startle response (to 120 dB)	615.8 ± 58.4	520.9 ± 20.7	0.18	970.5 ± 113.3	899.2 ± 94.3	0.65	862.1 ± 98.6	814.3 ± 102.0	0.75	0.23

Ro1, n = 10; Control, n = 11

[a]Weeks 1, 4 and 7 are shown for simplicity. There were also no significant changes at weeks 2, 3, 5 or 6.

[b]Student's t-test was used to measure differences between Ro1 and control mice at each week; a repeated measures ANOVA was used to measure changes across all seven weeks of testing.

[c]A repeated measures ANOVA across all seven weeks of testing could not be calculated for the wire hang test due to lack of variance.

There are no changes in learning and memory in Ro1 mice with hydrocephalus. The Morris water maze was used to assess learning and memory. Ro1 mice were not different from controls in their ability to find a visual platform at 10 – 12 days off dox (data not shown). Additionally, Ro1 mice learned the location of the hidden platform at the same speed as control mice from 15 – 19 days off dox (Figure 23) and remembered the location of the hidden platform during the probe trial at 19 days off dox (Figure 24). Although ventriculomegaly was likely present in most Ro1 mice during reversal learning and the reversal probe trial, the Ro1 mice were not significantly different from controls in either of these tests (Figures 25 and 26). However, when tested for their ability to remember the location of the hidden platform two weeks later (retention), the Ro1 mice showed an increased latency to find the hidden platform, suggesting impaired learning as compared to controls, although this difference in latency was not statistically significant (Figure 27). However, when lateral ventricle to brain ratio was plotted against performance in the retention test, there was a moderate, but significant correlation (r^2 = 0.59; p = 0.026; Figure 28). No sex differences were found in any test. These results are summarized in Table 2 below.

Table 2
Performance of Ro1 mice and littermate controls in the Morris water maze

	Days off dox	Control	Ro1	p-value
Hidden platform acquisition (latency, trial 4, s)	19	14 ± 2	11 ± 1	0.6
Hidden probe trial (duration quadrant 1, s)	21	25 ± 3	23 ± 2	0.86
Reversal platform acquisition (latency, trial 9, s)	32	12 ± 2	16 ± 4	0.93
Reversal probe trial (duration quadrant 3, s)	34	14 ± 1	19 ± 3	0.17
Retention (latency, trial 1, s)	47	18 ± 4	26 ± 6	0.26

Ro1, n = 10; Control, n = 11

Hydrocephalic Ro1 mice show no changes in anxiety, fear or depression. The elevated plus maze and the forced swim tests are commonly used measures of anxiety and depression, respectively. No changes were found between control and Ro1 mice at 24 and 25 days off dox, respectively, in either of these tests (Figures 29 and 30); histological studies suggest that approximately 20% of Ro1 mice have clear ventriculomegaly by this time (Table 3). Additionally, no changes in center time were found in the open field test, another measure of anxiety, at 31 days off dox (Figure 31). By this point, approximately 40% of mice display ventriculomegaly (Table 3). Fear conditioning and amygdala-dependent learning and memory were tested in the passive avoidance test at 32 – 33 days off dox. No significant changes in latency to enter the room where the mice had previously received a mild foot shock were recorded (Figure 32). There were no sex differences in any of these tests, and no correlations to lateral ventricle to brain ratio were found. The results from these tests are summarized in Table 4 below.

Table 3
Degree of lateral ventricle enlargement in Ro1 mice at various time points following removal of dox at P30

Days off dox	Average LV:brain ratio	Range (LV:brain ratio)	Percentage of mice with a LV:brain ratio > 0.3
18	0.14	0.10 – 0.18	0%
24	0.22	0.14 – 0.39	20% (1 of 5)
30	0.25	0.11 – 0.43	40% (2 of 5)
48	0.31	0.20 – 0.59	50% (5 of 10)

Table 4
Assessment of anxiety and depression in Ro1 mice and littermate controls

	Days off dox	Control	Ro1	p-value
Elevated plus maze (open arm time, s)	24	59.5 ± 4.8	61.5 ± 4.9	0.78
Forced swim test (time immobile, s)	25	81.6 ± 12.5	74.5 ± 8.7	0.66
Open field (center time, s)	31	19.6 ± 4.1	25.2 ± 3.8	0.33
Passive avoidance (latency, s)	33	68.3 ± 19.1	42.4 ± 9.8	0.45

Ro1, n = 13; Control, n = 17

Discussion

Although we were surprised to discover a lack of significant behavioral changes in Ro1 mice even in the presence of ventriculomegaly, our data are perhaps unsurprising considering the slow development of hydrocephalus when Ro1 mice are taken off dox at P30. Del Bigio et al. (2003) have suggested that a slower rate of disease progression results in less severe morphological and behavioral changes. Additionally, studies in H-Tx rats and rats with kaolin-induced hydrocephalus showed a rapid reduction of motor activity and body weight immediately prior to death (Del Bigio et al., 1997; Wada, 1988). In our study we also found hypoactivity, reduced rotarod performance and increased latency in the retention test of the Morris water maze in mice immediately prior to death. Moreover, studies investigating behavioral changes in animal models of hydrocephalus have shown conflicting results. For example, there was no change in rotarod performance in juvenile or adult mice injected with kaolin at 7 or 14 days post-injection (Lopes Lda et al., 2009) or in kaolin-induced neonatal rats at P20, 19 days after kaolin injection (Khan et al., 2006). In contrast, when rats were injected with kaolin to induce hydrocephalus at three weeks, there was a significant decrease in rotarod performance at eight months post-injection (Del Bigio et al., 2003), suggesting that severe hydrocephalus is necessary in the kaolin-injected model before behavioral changes on the rotarod are apparent. Del Bigio et al. (2003) suggested that there is a threshold of ventricle size beyond which functional changes appear, which is dependent on various factors, such as age of onset and rate of ventricular enlargement. It is therefore likely that in the Ro1 model, taking the mice off dox to induce astrocyte-specific Ro1 expression and hydrocephalus at P30 results in a slow rate of ventricular enlargement that reduces the likelihood of observing behavioral changes. It is possible that compensation is occurring in the brains of these mice, allowing them to adapt to the gross

morphological changes resulting from ventriculomegaly. Considering that we see more rapid disease progression in Ro1 mice maintained off dox throughout gestation and development, it is possible that Ro1 mice taken off dox at a younger age would show a more rapid rate of ventricular enlargement and behavioral changes. It should be noted, however, that the Ro1 receptor is expressed in astrocytes throughout the brain; therefore, any changes in behavior observed in this model may be due to Ro1 affecting astrocyte signaling in a specific brain region and may not necessarily be due to hydrocephalus. Taken together, these results suggest that treatments that slow the rate of the progression of this disorder may have therapeutic potential by allowing the brain to compensate and increasing the therapeutic window for shunt placement or alternative treatments.

Chapter VII

Lack of demonstrable changes in protein expression in early hydrocephalus

Introduction

Little is known about the early cellular changes that cause hydrocephalus; as a result, there are currently no drug-based therapeutic approaches for treating this disease. A handful of genomic and proteomic studies have been conducted to address this problem. In 2001, Balasubramaniam and Del Bigio published the results from a microarray study in which hydrocephalus was induced using the kaolin method (Balasubramaniam and Del Bigio, 2002). Kaolin injection into the cisterna magna causes an inflammatory response that results in non-communicating hydrocephalus. The goal of this study was not to identify early changes in hydrocephalus, however. Instead, the authors sought to compare differences in gene expression profiles between adult and young hydrocephalic brains. Additionally, the results of their study are complicated by the fact that hydrocephalus is secondary to the inflammatory response in the kaolin model. Thus, it is not clear whether the changes in gene expression they discovered are a result of the induction of hydrocephalus or the inflammation itself. To circumvent this problem, Morgan et al. (2005) chose to use a congenital model of hydrocephalus, the H-Tx rat, to conduct a microarray study in which they analyzed changes in stress response genes between E18 H-Tx rats and age matched Sprague-Dawley (SD) rats (Morgan et al., 2005). Closure of the aqueduct and resulting hydrocephalus is thought to occur between E18 and P5 in this model, making E18 a good time point to analyze early changes in the pathology of hydrocephalus. They discovered distinct heat shock protein gene expression patterns relative to SD rats. However, since the authors did not verify hydrocephalus in their rats, and H-Tx rats have a low penetrance of approximately 40% (Morgan et al., 2005), this calls into question the validity of their results. Additionally, the authors used whole brain for RNA isolation; isolating RNA from tissues most likely to be involved in the development of hydrocephalus would have likely yielded differences

in gene expression that were much greater in magnitude. A similar report using H-Tx rats to understand early gene expression changes in hydrocephalus was published by Miller et al. (2006) (Miller et al., 2006). In this study, the authors isolated tissue from the area of the cerebral aqueduct of P5 hydrocephalic H-Tx rats and healthy littermate controls. Interestingly, they found only a small number of genes that were differentially expressed: 47 transcripts were changed, 23 of which have known functions. However, with this study there is the concern that they are investigating effects secondary to the development of hydrocephalus, since at P5 the authors noted that the rats already had enlarged lateral ventricles. Therefore, an earlier time point would be necessary to identify early changes central to the development of hydrocephalus. With the H-Tx model, however, this is not possible since penetrance is low and the only way to ensure that the rats studied will develop hydrocephalus is to wait until the disease is already present.

Currently, there is only one proteomic study that has been conducted to investigate early changes in the development of hydrocephalus. Li et al. used 2D-gel electrophoresis and mass spectrometry to investigate changes in protein expression among P1 hydrocephalic H-Tx rats, age-matched littermate controls, and P1 Sprague-Dawley rats (Li et al., 2005). The authors identified 7 proteins altered in H-Tx rats at this stage, which included HMG-1, CDCrel-1A, mitochondrial ATP synthase, ERp29, NADP+-ICDH, CCT β and γ. These changes suggest that at P1, H-Tx rats have abnormal energy metabolism and protein folding, which implies that congenital hydrocephalus may be related to mitochondrial and ER dysfunction. However, as with the study by Miller et al., these rats already had an enlarged cranium; therefore an earlier time point is necessary to investigate early changes that lead to hydrocephalus. Additionally, 2D gel-electrophoresis and mass spectrometry can only identify a handful of altered proteins. As a result, in this study, we investigated early protein and phospho-protein expression changes in

early hydrocephalus using antibody microarrays, western blotting and immunohistochemistry. A large-scale antibody microarray was used to investigate changes in 800 proteins, including 300-phospho-specific antibodies (Pelech and Zhang, 2007). Because our mice have 100% penetrance and no complicating pathologies, we have the unique ability to investigate early changes in the development of hydrocephalus. Changes in protein and phospho-protein expression were analyzed via antibody microarrays and western blotting at 9 days following the removal of doxycycline; at this time point, there is expression of the Ro1 receptor detectable by real-time PCR (Figure 10), but no histological changes in brain or cellular morphology are observed. The strength of the antibody microarray approach lies in its ability to analyze changes across a large number of proteins in an unbiased manner. Considering that there is no definite pathological hypothesis as to how hydrocephalus develops, there is no hypothesis to prove or disprove; rather, the goal of this study was to create a breakthrough in our understanding of the mechanisms that cause hydrocephalus. However, as a result of the high false negative rates of this approach, immunohistochemical analysis of various proteins and phospho-proteins likely to play a role in the Ro1 model of hydrocephalus was also conducted. Further, primary astrocyte cell culture with western blotting was used to investigate signaling cascades activated downstream of the Ro1 receptor. Together, the goal of these approaches was to identify early changes in protein and phospho-protein expression in the development of hydrocephalus that may be contributing to the pathophysiology of this disorder.

Materials and Methods

Ependymal and subependymal cell dissection and lysis. Mice were taken off dox at P30 and sacrificed for analysis of protein expression and phosphorylation levels at 9 days off dox.

Following anesthesia with isoflurane, double-transgenic Ro1 and single-transgenic control mice were decapitated, and their brains were cut into 1 mm-thick coronal sections using an acrylic matrix. The slices containing the lateral ventricles were immediately transferred to ice-cold dissection buffer, containing 20 mM MOPS, pH 7.0, 2 mM EGTA, 5 mM EDTA, 30 mM sodium fluoride, 60 mM β-glycerophosphate, 20 mM sodium pyrosphosphate, 1 mM sodium orthovanadate, 1 mM phenylmethylsulfonylfluoride, 3 mM benzamidine, 10 μM leupeptin and 2 mg/mL pepstatin A. The ependymal and subependymal layers were dissected from the lateral ventricles using 30 gauge needles and transferred to a 0.5 mL centrifuge tube containing 100 μL of dissection buffer. Tissue was pooled from four mice per genotype to generate enough protein. Following the dissections, the samples were spun at 1000 x*g* for 10 min at 4ºC to pellet the tissue. The dissection buffer was then removed, and 60 μL of lysis buffer was added. The lysis buffer consisted of dissection buffer plus 1% Triton X-100 and 1 mM dithiothreitol (DTT). Samples were then sonicated four times for 10 s and spun at 90,000 x*g* for 30 min at 4ºC. The supernatant fraction was transferred to a new tube and subjected to the Thermo 660 nm protein assay (Thermo Scientific). The lysates were then stored at -80°C.

Kinexus antibody microarray. For the Kinexus antibody microarray, tissue was prepared as described in "Ependymal and subependymal dissection and lysis." The tissue lysates were shipped to Kinexus overnight on dry ice and run on their 800 antibody microarrays. These arrays contain 300 phospho-site specific antibodies and 500 antibodies for total protein. Additionally, for each sample analyzed, each antibody is spotted twice as a quality control measure. "Hits" were identified based on fold change from control and quality control parameters.

Primary astrocyte cell culture. P0 – 2 pups were sterilized with 70% ethanol and decapitated. The brain was then removed, and the cortex was peeled away and placed in Hank's Balanced Salt Solution containing calcium and magnesium (HBSS+; Invitrogen). The meninges were then removed with fine forceps, and each hemisphere of the cortex was cut into 2 – 3 pieces and placed into fresh HBSS+. The cortical pieces from each pup were placed into a separate 35 mm dish with HBSS+, and tail cuttings were taken for genotyping. The pieces of cortex were then transferred to a 14-mL Falcon tube (BD Biosciences) with 1 mL of 1x Trypsin-EDTA (CellGro), and incubated for 30 min at 37ºC at 100 rpm. Following incubation, 1 mL of Dulbecco's Modified Eagle Medium – high glucose (DMEM-H; CellGro), containing 10% fetal bovine serum (CellGro), penicillin/streptomycin and glutamine, was added. The tissue pieces were then titrurated using a 5 mL transfer pipet, and tissue pieces from each mouse were placed in a separate well in a 6-well plate containing DMEM-H. The 6-well plates were then placed in an incubator at 37°C and 95%O_2/5%CO_2. Half of the media was changed the subsequent day, and all of the media was changed two days after the initial culture. The media was then changed every two days.

Real-time PCR. For real-time PCR experiments, cultured astrocytes from four pups per genotype were combined into a 25 cm^2 flask, 10 days after the initial culture. Twenty-five days later, RNA was isolated using the RNeasy Lipid Tissue Mini Kit (Qiagen), and the amount of RNA per sample was quantified using a NanoDrop spectrophotometer (Thermo Scientific). RNA from each mouse was sent for an RNA quality check at the Nucleic Acids Core Facility at the University of North Carolina. cDNA was then prepared using Superscript II Reverse Transcriptase with random primers and RNaseOUT to block RNase activity (Invitrogen). Real-

time PCR was then conducted using hKOR2 and GAPDH primers and a SYBR green detection system (Applied Biosystems).

Immunocytochemistry. For FLAG staining of cultured astrocytes, cultured astrocytes were split 12 days after initial culture onto poly-D-lysine coated coverslips (BD Biosciences); two pups per genotype were combined for staining. Three days later, the cells were rinsed in HBSS and fixed for 15 min in 4% paraformaldehyde (PFA) in 1x phosphate-buffered saline (PBS). Cells were then washed three times for 5 min in 1x PBS and permeabilized for 10 min in ice-cold methanol. Following washes in 1x PBS, the cells were blocked in 5% normal goat serum (NGS) and 0.3% Triton-X100 in 1x PBS for 1 h at room temperature. The cells were then incubated overnight in primary antibodies in antibody dilution buffer, containing 1% bovine serum albumin and 0.3% Triton-X100 in 1x PBS at 4ºC. The primary antibodies used were mouse anti-GFAP (1:500; Sigma) to stain for astrocytes and rabbit anti-FLAG (1:500; Sigma) to stain for the FLAG-tagged Ro1 receptor. Following washes in 1x PBS, the cells were incubated in antibody dilution buffer for 2 h at room temperature in the following secondary antibodies: goat anti-mouse Alexa Fluor 488 (1:400; Invitrogen) and goat anti-rabbit Alexa Fluor 594 (1:400; Invitrogen). After washing in 1x PBS, the cells were mounted onto glass slides in Vectashield plus DAPI mounting media (Vector Laboratories) and imaged with a fluorescent microscope (Zeiss).

Western blotting. For western blotting on tissue lysates derived from Ro1 and control mice at 9 days off dox, the tissue was prepared as described in "Ependymal and subependymal cell dissection and lysis." Twenty micrograms of tissue lysates (except phospho-RSK, 40 μg) were added to 5x loading buffer and heated at 95°C for 5 min. The lysates were then loaded onto a

10% Tris-glycine gel and subjected to SDS-PAGE at 120 V. Four samples per genotype were run on each gel. The proteins were then transferred to nitrocellulose at 100 V for 1 h at room temperature. The membranes were blocked for room temperature for 1 h in 5% milk for all antibodies except ERK and phospho-ERK, which were blocked in 3% gelatin. The blots were then incubated overnight at 4ºC in primary antibody (all 1:1000), washed in TBST and incubated in HRP-conjugated secondary antibody (goat anti-rabbit or goat anti-mouse, 1:5000; Jackson ImmunoResearch) for 2 h at room temperature. Following washes in TBST, ECL reagent (SuperSignal West Pico, Thermo Scientific) was applied for 5 min and blots were exposed to film and developed. To ensure even loading, blots were stripped with Restore^{TM} stripping buffer (Thermo Scientific) for 15 min at room temperature before reprobing with actin (Sigma). For p38γ, phospho-c-Jun, Bcl-2, MKK4, MKK3β, RSK and phospho-RSK, the primary antibody (1:1000) was incubated in 5% bovine serum albumin (BSA) in TBST, and the secondary antibody was incubated in 1% non-fat dry milk in TBST. For ERK and phospho-ERK (1:1000), the primary and secondary antibodies were incubated in 1% gelatin. For actin, the primary and secondary antibodies were incubated in 1% mik. All primary antibodies were purchased from Cell Signaling except the actin antibody, which was purchased from Sigma.

For western blotting on cultured astrocytes, cells were cultured in 6-well plates, as described in "Primary astrocyte cell culture," until confluent (9 days after initial culture). The cells were then gently washed with 1x PBS and lysed on ice with ice-cold lysis buffer, containing 20 mM Tris, pH 7.4, 150 mM NaCl, 1 mM EDTA, 1 mM EGTA, 1% Triton X-100, 1 mM PMSF, 2 mM sodium vanadate, 20 mM sodium fluoride, 0.05 mM DTT, 1 mg/mL leupeptin and 17 mg/mL aprotinin. Cells were then transferred to a microcentrifuge tube on ice, vortexed and incubated on ice for 10 min with occasional vortexing. The lysates were then spun at 13,000

rpm for 10 min at 4ºC, and the supernatant was transferred to a fresh microcentrifuge tube. The Thermo 660 nm (Thermo Scientific) protein assay was used to determine the concentration of protein per lysate. Lysates were stored at -80ºC until use. Western blotting for ERK and phospho-ERK was conducted as previously described, loading seven samples per genotype on a single gel.

Immunohistochemistry. Mice were taken off dox at P30 and transcardially perfused at 12, 18 and 24 days off dox with 4% paraformaldehyde (PFA). The brains were then removed and post-fixed in 4% PFA for 4 h and cryoprotected in 30% sucrose at 4ºC. The brains were then frozen in O.C.T. (Optimal Cutting Temperature, Sakura, Japan) on dry ice and stored at -80ºC. The brains were sliced 10 μm thick on a cryostat and mounted onto glass slides. Following washes in 1x PBS, the tissue was blocked for 1 h in 4% normal goat serum (NGS) and 1% BSA in 1x PBS. The tissue was then incubated overnight at 4ºC in aquaporin 4 (1:100; Santa Cruz Biotechnology) and GFAP (1:500; Sigma) primary antibodies in 0.25% Triton X-100 and 1% DMSO in 1x PBS. Following washes in 1x PBS, the tissue was incubated in goat anti-rabbit Alexa Fluor 594 and goat anti-mouse Alexa Fluor 488 (1:400; Invitrogen) for 1.5 h at room temperature in 0.25% Triton X-100 and 1% DMSO in 1x PBS. The tissue slices were then washed, mounted with Vectashield plus DAPI (Vector Laboratories) and coverslipped. Staining was imaged using a fluorescent microscope (Zeiss).

Results

There are no proteins or phospho-proteins with significantly altered levels of expression in vivo *in early hydrocephalus*. Using a $\log_2$(fold change) cutoff of greater than 0.5 or less than –0.5,

which corresponds to a 40% change from control, and filtering the dataset for various quality control measures, 55 proteins or phospho-proteins were found to be altered consistently across all three paired samples. The $\log_2$(fold change) was used because this value linearizes the data; as a result, this is a better measure of the degree of change because the fold change and the percent change from control (%CFC) underestimate the magnitude of the decreases. This list was further reduced based on consistency across samples and quality parameters, including the signal to noise ratio and the variability between the two spots for each antibody on the array. Table 5 shows the final list of proteins and phospho-proteins with a $\log_2$(fold change) greater than 0.5 or less than -0.5 across three paired samples, each of which were prepared on the same day.

Table 5
Changes in protein and phospho-protein expression levels across three paired samples analyzed on the Kinexus antibody microarrays

Protein abbreviation (phospho-site) and full name	**Sample 1: Log2 (%CFC)**	**Sample 2: Log2 (%CFC)**	**Sample 3: Log2 (%CFC)**
Bcl2 (Pan) B-cell lymphoma protein 2	-0.73 (-40)	-1.3 (-59)	-1.55 (-66)
EGFR (Pan) Epidermal growth factor receptor-tyrosine kinase	1.22 (134)	0.82 (76)	0.88 (84)
Erk1 (Pan) Extracellular regulated protein-serine kianse 1 (p44 MAPK)	2.68 (542)	1.80 (248)	2.25 (377)
Erk1 (T202+Y204; T185/Y187) Extracellular regulated protein-serine kianse 1 (p44 MAPK)	1.35 (155)	0.96 (94)	0.67 (59)
FAK (Y397) Focal adhesion protein-tyrosine kinase	-0.93 (-48)	-0.74 (-40)	-1.03 (-51)
FAK (Y576) Focal adhesion protein-tyrosine kinase	-0.72 (-39)	-0.93 (-48)	-0.76 (-41)
FGFR1 (Pan) Fibroblast growth factor receptor-tyrosine kinase 1	-1.03 (-51)	-2.13 (-77)	-1.11 (-54)
FKHRL1 (T32) Forkhead-like transcription factor 1 (FOXO3A)	-0.67 (-37)	-1.22 (-57)	-1.51 (-65)
GFAP (S8) Glial fibrillary acidic protein	-0.96 (-48)	-0.94 (-48)	-1.20 (-56)
GRK3 (Pan) G protein-coupled receptor-serine kinase 3	-0.76 (-41)	-0.98 (-49)	-1.40 (-62)
GSK3b (Pan) Glycogen synthase-serine kinase 3 beta	-1.25 (-58)	-1.20 (-56)	-1.53 (-63)
Histone H1 (phospho CDK1 sites)	0.96 (95)	1.26 (140)	0.63 (55)
Histone H2A.X (S139)	0.78 (71)	0.87 (83)	1.21 (131)
IKKα (Pan) Inhibitor of NFκB protein-serine kinase alpha	-1.08 (-53)	-1.20 (-57)	-1.38 (-62)
Jun (S73) Jun proto-oncogene-encoded AP1 transcription factor	0.72 (65)	0.64 (56)	0.53 (44)
MEK3b (MAP2K3) (Pan) MAPK/ERK protein-serine kinase 3 beta isoform	-0.98 (-49)	-0.5 (-30)	-1.16 (-55)
MEK4 (MAP2K4) (Pan) MAPK/ERK protein-serine kinase 4 (MKK4)	-1.79 (-71)	-1.42 (-63)	-0.82 (-55)
MEKK1 (MAP3K1) (Pan) MAPK/ERK kinase kinase 1	-0.63 (-35)	-0.79 (-42)	-0.99 (-51)
MEKK2 (MAP3K2) (Pan) MAPK/ERK kinase kinase 2	-0.68 (-38)	-0.86 (-45)	-0.74 (-40)

p38g MAPK (Erk6) (Pan) Mitogen activated protein-serine kinase p38 gamma	-0.61 (-34)	-0.60 (-34)	-0.64 (-36)
PKA R1a (Pan) cAMP-dependent protein-serine kinase type I-alpha regulatory subunit	-1.53 (-65)	-1.08 (-53)	-0.81 (-43)
RSK1 (Pan) Ribosomal S6 protein-serine kinase 1	-1.31 (-60)	-0.92 (-47)	-1.33 (-60)
RSK1/2/3 (T573/T477) Ribosomal S6 protein-serine kinase 1/2/3	-0.56 (-32)	-1.12 (-54)	-1.23 (-57)

A signaling pathway diagram for these changes in protein and phospho-protein expression was then created to illustrate how potential signaling pathways may be altered early in the Ro1 model of hydrocephalus (Figure 33). Interestingly, there was a consistent increase in phospho-ERK levels in the Ro1 mice; ERK has been shown to be activated downstream of the KOR and is therefore likely to be activated by the Ro1 receptor (Bruchas et al., 2008; Bruchas and Chavkin, 2010). Additionally, past studies in our laboratory have demonstrated that phospho-ERK staining is increased in Ro1 mice as compared to controls (Sweger et al., 2007).

Western blotting was then used to confirm the changes observed in the antibody microarray analysis. However, no changes were found via western blotting for p38γ, phospho-c-jun, Bcl-2, phospho-ERK, ERK, MKK4, MKK3, RSK or phospho-RSK at 9 days off dox (data not shown).

Despite Ro1 expression, primary astrocyte cultures do not show changes in phospho-ERK expression, a protein known to be activated downstream of the Ro1 receptor. Although the primary astrocyte cultures were shown to expression the Ro1 receptor via real-time PCR and FLAG staining (Figures 34 and 35), there were no changes in phospho-ERK expression after 9 days in culture (data not shown).

Considerable variability in aquaporin 4 expression is present early in hydrocephalus. Immunohistochemistry was used to analyze changes in aquaporin 4 expression at 12, 18 and 24 days off dox. Although there was a trend suggesting a decrease in aquaporin 4 expression at 18 days off dox (Figure 36), due to the high degree of variability of staining among mice, no statistically significant changes were observed between Ro1 and control mice at any time point analyzed.

Discussion

Nine days off dox may be too early to observe changes in protein or phospho-protein expression in the Ro1 model of hydrocephalus. Most of the changes in protein or phospho-protein expression found using the antibody microarray analysis were small and none were confirmed via western blotting, suggesting that there may be no changes in protein expression at 9 days off dox. Preliminary studies in our laboratory suggested that ependymal denudation was present at 9 days off dox, resulting in the selection of this time point for the antibody microarray analysis. However, further and more careful histological analysis of the progression of hydrocephalus in the Ro1 model (see Chapter IV) revealed that ependymal denudation does not occur until severe ventriculomegaly is present and was not observed prior to 48 days off dox. Additionally, in this careful histological analysis, no morphological or cellular changes were found until 24 days off dox, at which point ventriculomegaly and disorganization of the aqueduct of Sylvius was observed in approximate 33% of mice (Chapter IV). Therefore, it is likely that 9 days off dox was too early a time point to observe changes in protein or phospho-protein expression in the pathogenesis of hydrocephalus in the Ro1 model. Future studies using western blotting or immunohistochemistry to investigate changes in protein and phospho-protein expression at a

later time point may reveal early changes that contribute to the development of hydrocephalus in this model.

Additionally, it is possible that the wrong cell type was isolated for analysis. As previously mentioned, prior studies in our laboratory suggested that ependymal denudation was the earliest change observed in the pathogenesis of hydrocephalus in the Ro1 model; therefore, the ependymal and subepenymal cells were isolated for analysis for antibody microarrays and western blotting. However, the careful histological analysis described in Chapter IV demonstrated that ependymal denudation at the lateral ventricles is a result of severe enlargement of the ventricular walls and not a causative factor in the development of hydrocephalus in this model. Therefore, it is possible that the wrong population of cells was isolated for these studies. The use of fluorescent-activated cell sorting (FACS) to selective isolate and analyze GFAP-positive astrocytes (Cahoy et al., 2008), which should be expressing the Ro1 receptor, may provide better insight into the early signaling events that lead to the development of hydrocephalus in this model.

Considerable variability in rate of disease progression in Ro1 mice makes analysis of changes in protein or phospho-protein expression difficult. As shown in Figure 10 in Chapter IV, there is considerable variability in the degree of Ro1 expression among Ro1 mice. It is likely that this variability is contributing to the variability we observe in the rate of the development of hydrocephalus in Ro1 mice (Chapter IV). Due to this variability in the rate of disease progression among Ro1 mice, it is perhaps unsurprising that there was considerable variability observed in aquaporin 4 expression among Ro1 mice. As a result, although there was a trend suggesting a reduction in aquaporin staining at 18 days off dox, this reduction was not significant. If Ro1

expression levels correlate with rate of disease progression, then it is possible that correlating levels of Ro1 expression using real-time PCR with immunohistochemistry on fresh frozen brain tissue from the same mouse may reveal changes in protein or phospho-protein expression at a specific level of Ro1 expression.

Difficulties in mimicking Ro1 signaling in vitro. Although increases in phospho-ERK expression have been previously shown around the lateral ventricles and in the entorhinal cortex of Ro1 mice, there were no changes in phospho-ERK expression in primary astrocytes cultures (n = 7). This lack of changes in phospho-ERK expression was demonstrated despite expression of the Ro1 receptor, as detected by real-time PCR and FLAG staining. It is possible that 9 days in culture without dox was not the correct time point to observe changes in phospho-ERK expression; receptor expression may have been too low at this time point or, more likely, receptor downregulation may have occurred, thereby reducing Ro1 signaling. Because dox leaves bone and adipose tissue slowly, it takes longer for dox to be completely removed *in vivo*, resulting in a relatively slow onset of Ro1 expression. In contrast, *in vitro*, the dox is eliminated as soon as the cells are cultured. As a result, Ro1 expression should be present shortly after culturing. However, it is unclear what dose of dox primary astrocyte cultures should be given to suppress Ro1 expression and at which point following removal of dox from cultured astrocytes Ro1 signaling mimics that which we observe *in vivo*. Therefore, the feasibility of using primary astrocyte cultures for examining Ro1 signaling *in vitro* is questionable.

Gi-coupled GPCR signaling and possible role in hydrocephalus. The Ro1 receptor was created by removing the second extracellular loop of the kappa opioid receptor and replacing it with the second extracellular loop of the delta opioid receptor (Coward et al., 1998a; Redfern et al., 1999; Scearce-Levie et al., 2005; Sweger et al., 2007). Because both of these receptors are Gi-coupled GPCRs, it is likely that the Ro1 receptor also signals via Gi-coupled GPCR pathways. The major signaling pathways shown to be activated downstream of the KOR and other Gi-coupled GPCRs include inhibition of adenylyl cyclase, modulation of calcium and potassium channels and activation of the mitogen-activated protein kinase (MAPK) family, including ERK1/2, p38 and JNK (Bruchas and Chavkin, 2010).

The Gβγ subunit of Gi-coupled GPCRs has been shown to directly activate the inwardly rectifying potassium channel, Kir3, and reduce conductance through voltage-gated calcium channels (Krapivinsky et al., 1995; Sadja et al., 2003; Wickman and Clapham, 1995). Interestingly, KOR activation has been suggested to mobilize intracellular calcium via the inositol tris-phosphate (IP3) pathway (Spencer et al., 1997), and kappa opioids have been shown to increase intracellular calcium in astrocytes (Gurwell et al., 1996; Stiene-Martin et al., 1993). However, it is possible that this calcium mobilization is due to the KOR promiscuously coupling to Gq-coupled G proteins (Bruchas and Chavkin, 2010).

GRK3- and arrestin-mediated desensitization and internalization of the KOR have been shown to recruit MAPKs, the best characterized of which is ERK1/2 (Bruchas and Chavkin, 2010). Interestingly, ERK1/2 activation in astrocytes was shown to stimulate the proliferation of astrocytes (McLennan et al., 2008), and previous studies in our laboratory have demonstrated that basal levels of Ro1 signaling activate phospho-ERK (Sweger et al., 2007). ERK1/2 has also been shown to be activated downstream of KOR in an arrestin-independent manner (McLennan

et al., 2008). Activation of ERK1/2 is known to activate cAMP response element binding protein (CREB), a transcription factor that controls the expression of several proteins. p38 has also been shown to be activated downstream of the KOR in astrocytes and is thought to be arrestin-dependent (Bruchas et al., 2006; Bruchas et al., 2007a). p38 activation leads to the production of inflammatory cytokines in astrocytes as well as the induction of nitric oxide synthase (Ashwell, 2006). Other studies have shown p38-induced Src activation following stimulation of the KOR (Clayton et al., 2009). Although there have been fewer studies on opioid receptor-mediated activation of JNK, arrestin-dependent activation of JNK has been shown downstream of Gi-coupled GPCR activation (Kam et al., 2004; McDonald et al., 2000; Song et al., 2009). Additionally, KOR activation has been shown to cause protein kinase B (PKB)-dependent JNK phosphorylation (Bruchas et al., 2007b; Kam et al., 2004).

Additionally, GPCR promiscuity has been demonstrated in other systems, especially upon overexpression of the receptor (Hermans, 2003); as such, with high levels of expression and high basal activity of the Ro1 receptor, it is possible that receptor promiscuity is also occurring in our mice. As a result, it is unclear which signaling pathways are being activated by Ro1 expression to cause hydrocephalus. Future studies involving FACS sorting with antibody microarrays and western blotting at various time points to investigate changes in signaling pathways in the development of hydrocephalus in the Ro1 model may provide insight into the pathogenesis of this disorder. Additionally, correlating levels of Ro1 expression to changes in protein and phospho-protein expression via real-time PCR and immunohistochemistry, respectively, may aid in the determination of Ro1-mediated changes in protein and phospho-protein expression that lead to hydrocephalus in this model.

Chapter VIII

Discussion

a. Current problems in hydrocephalus research and treatment

There have been few improvements in the treatment and diagnosis of hydrocephalus since shunt placement surgery was developed over 50 years ago, in large part due to limited clinical and basic research focused on understanding hydrocephalus. This is astounding considering that the prevalence of hydrocephalus is high, affecting 0.1% of the population (Patwardhan and Nanda, 2005). Unfortunately, with the development of shunt surgery for the treatment hydrocephalus, research into other treatments of hydrocephalus slowed considerably. This is especially unfortunate because shunt infection and failure are extremely common, with two-thirds of shunts failing within a ten-year period, and most individuals suffering from hydrocephalus require multiple shunt revision surgeries throughout their lives (Patwardhan and Nanda, 2005). Further research into the pathogenesis, pathology and recovery mechanisms of hydrocephalus are necessary to improve the diagnosis and treatment of this disorder.

The vast majority of hydrocephalus cases are idiopathic in nature. It is likely that many of these cases result from aberrant signaling within the CNS; however, to date, few proteins and signaling pathways have been implicated in the development of hydrocephalus. The only signaling pathways identified to play a possible role in the development of hydrocephalus were demonstrated through the creation of transgenic mice. Suppressor of cytokine signaling 7 (SOCS7) knock-out mice and mice with overexpression of the pituitary adenylate cyclase-activating polypeptide receptor type 1 (PAC1) developed hydrocephalus (Krebs et al., 2004; Lang et al., 2006). Thus, it is possible that phosphatidylinositol-3 kinase (PI3K), phospholipase Cγ (PLCγ) and the Jak/STAT pathway, which are downstream of SOCS7, as well as protein kinases A and C (PKA and PKC), which are activated downstream of the PAC1 receptor, may play a role in the development of hydrocephalus (Lang et al., 2006; Martens et al., 2005;

Matuoka et al., 1997). Genomic and proteomic studies have shown altered expression of proteins involved in energy metabolism and the stress response in hydrocephalic rats (Li et al., 2005; Morgan et al., 2005); however, further investigation is necessary to determine if these changes are specific to hydrocephalus and are involved in the development of this disorder. The Ro1 receptor also implicates Gi-coupled GPCR signaling in the pathogenesis of hydrocephalus; however, the specific signaling pathways leading to hydrocephalus in this model remain unclear.

Most of our current knowledge of hydrocephalus is related to the secondary neuropathological changes resulting from hydrocephalus, some of which can be improved or reversed by shunting. These pathological changes are discussed in more detail in Chapter III and include ependymal loss, reactive gliosis, periventricular edema, white matter loss, destruction of periventricular axons and atrophy of dendritic processes, decreased levels of neurotransmitters and reduced metabolism. These changes lead to severe defects in motor coordination, cognition and quality of life in hydrocephalic individuals. However, our understanding of how these changes develop and how treatment is capable of reversing these changes is extremely limited. The development of new drugs to treat these neuropathological changes, especially those changes unaffected by shunting, may improve patient outcome after shunt surgery.

Although pharmacological therapy to treat or prevent hydrocephalus is the ultimate goal, new medical devices and/or procedures for the treatment of hydrocephalus are required in the interim. For example, the development of shunts with reduced risk of infection or blockage would greatly reduce the need for shunt revision in patients with hydrocephalus. Drake and colleagues suggest that neurosurgeons should be able to achieve a one-year failure rate of 5%, including an infection rate of 1%, in the near future (Drake et al., 2000). They suggest that improvements in mathematical models to better understand the interactions between the patient

and the shunt, animal models of shunt failure to improve our understanding of the mechanisms of catheter occlusion, ongoing clinical trials and new shunts designs and materials will enable neurosurgeons to reach this goal (Drake et al., 2000). Additionally, the development and use of devices that record the ICP and monitor shunt flow would likely improve short- and long-term treatment options (Williams et al., 2007). Further, finding ways in which to reopen blocked pathways of CSF, similar to endoscopic third ventriculostomy, rather than inserting foreign objects into the body may reduce the need for recurrent neurosurgery. Optimizing treatment for a specific individual depending on the type of hydrocephalus present would also greatly improve outcomes following shunt surgery or ETV.

Improved early diagnosis is also necessary because the earlier hydrocephalus is treated, the better the outcome. Diagnosis of hydrocephalus is currently conducted using patient history, physical examination, imaging (US, CT and/or MRI) of the brain and measurements of ICP (Williams et al., 2007). Once ventriculomegaly is apparent and ICP is greatly elevated, the diagnosis of hydrocephalus is obvious; however, early hydrocephalus with mild to moderate ventriculomegaly and elevated ICP may be missed. Additionally, the classification of hydrocephalus, the decision of whether or not to treat the patient and the treatment best suited for the patient are often not straightforward. For example, compensated or arrested hydrocephalus in asymptomatic children and cerebral atrophy (hydrocephalus ex vacuo) in the elderly rarely require treatment; however, differentiating them from progressive hydrocephalus is often difficult (Williams et al., 2007). Detecting CSF flow and absorption abnormalities using MRI and infusion methods, respectively (Williams et al., 2007), may aid in the appropriate diagnosis and treatment. Further, identification of biomarkers, especially elevations of compounds in the CSF that can be identified by lumbar puncture, and improved behavioral and neuropsychological

testing may improve early diagnosis. Therefore, research into proteins elevated in the CSF of hydrocephalic individuals and the early behavioral and psychological changes found in patients with hydrocephalus will likely improve early diagnosis of this disorder and improve patient outcomes.

b. The Ro1 model of hydrocephalus

Advantages of the Ro1 model. Expression of the transgenic Gi-coupled Ro1 receptor selectively in GFAP-positive cells in mice results in communicating hydrocephalus with complete penetrance. Additionally, we are able to control the onset of hydrocephalus through the use of the tetracycline inducible system; removal of doxycycline from the drinking water of double-transgenic mice results in Ro1 receptor expression and hydrocephalus. This model of hydrocephalus has a number of advantages. First, because all double-transgenic mice will develop hydrocephalus when taken off dox, we have the unique ability to study the earliest stages of hydrocephalus, which has provided insight into the pathogenesis of this disorder. Additionally, because hydrocephalus appears to be the primary pathology in this model, it is likely that any changes observed in this model are due to hydrocephalus and not the result of a secondary condition. No other animal model exists that allows for the investigation of early cellular changes in hydrocephalus without interference from secondary pathologies. Further, the selective expression of a Gi-coupled G protein-coupled receptor (GPCR) in GFAP-positive cells enables the investigation of specific signaling cascades in specific cell populations, providing a tractable model for determining the signaling cascades involved in the pathogenesis of hydrocephalus.

The Ro1 model of hydrocephalus also closely mirrors human hydrocephalus in many respects. In the Ro1 model, for example, we first see ventriculomegaly followed by the stretching and eventual loss of the ependyma layer. Further, the degree of ependymal loss appeared to be dependent on the rate of disease progression; when mice were maintained off dox throughout gestation, hydrocephalus appeared to develop more rapidly and ependymal loss appeared to be greater as compared to ventricles of equivalent sizes from mice taken off dox at P30. Multiple studies on humans have suggested that ependymal denudation is subsequent to ventriculomegaly, and the degree of denudation appears to be dependent on the size of the lateral ventricles and the rate at which hydrocephalus progresses; more rapid disease progression has been shown to increase ependymal loss (Bannister and Mundy, 1979; Bruni et al., 1985; Del Bigio, 1993; Sarnat, 1995). In the Ro1 model, we also showed through electron microscopy that reduced microvilli and cilia coverage of the ventricular walls as well as periventricular edema accompanied enlarged lateral ventricles and thinned ependymal linings. These changes have also been observed in humans with hydrocephalus (Bannister and Mundy, 1979; Bruni et al., 1985; DaSilva, 2004; Del Bigio et al., 1985; Di Rocco et al., 1977). Subependymal gliosis is also commonly observed in humans and animals with chronic hydrocephalus; however, gliosis has been shown to be subsequent to ependymal loss (Bruni et al., 1985; Del Bigio, 1993). Thus, although we did not observe gliosis early in the pathogenesis of hydrocephalus in Ro1 mice, a previous study using the Ro1 model demonstrated gliosis in the hippocampus and cortex of severely hydrocephalic Ro1 mice (Sweger et al., 2007), suggesting that gliosis occurs in Ro1 mice with severe hydrocephalus. Although changes in the subventricular zone of human fetuses with moderate communicating hydrocephalus have also been observed, these changes were shown to be subsequent to ventricular dilation and ependymal loss (Dominguez-Pinos et al.,

2005). Therefore, it is possible that SVZ disorganization is also present in Ro1 mice, but only in mice with severe hydrocephalus and ependymal denudation, which was not investigated in this study.

Disadvantages of the Ro1 model. Although all double-transgenic mice taken off dox will express the Ro1 receptor and develop hydrocephalus, there was considerable variability in the level of Ro1 expression and the rate of disease progression in double-transgenic mice. This is the greatest disadvantage of the Ro1 model because it impairs the investigation of the cellular and morphological changes present at a specific time point following the removal of dox. For example, at 30 d following the removal off dox from P30 mice, only two out of five double-transgenic mice showed moderate to severe hydrocephalus (Table 4); the lateral ventricle to brain ratio of the remaining three double-transgenic mice was indistinguishable from single-transgenic control mice. Thus, any tissue processed for histology or electron microscopy at a specific time point must take this variability into consideration. Additionally, it becomes nearly impossible to compare signaling changes between double-transgenic Ro1 mice and single-transgenic controls via western blotting without correlating the changes in protein expression or phosphorylation to the severity of hydrocephalus in the same mouse. Therefore, by pooling ependymal and subependymal tissues from four different mice for the Kinexus antibody array and subsequent western blotting (as described in Chapter VII of this dissertation), any changes that might have been present at this time point would likely have been cancelled out due to the variability in disease progression among mice. (Here, it must be noted that the wrong cell population at the wrong time point was also likely isolated for these experiments. Please see Chapter VII for further explanation.) As a result, studies using the Ro1 model of hydrocephalus

must take this variability into consideration and correlate cellular and histological changes to a marker of disease severity, such as the lateral ventricle to brain ratio.

c. Possible signaling mechanisms

The Ro1 receptor was created by removing the second extracellular loop of the kappa opioid receptor and replacing it with the second extracellular loop of the delta opioid receptor (Coward et al., 1998a; Redfern et al., 1999; Scearce-Levie et al., 2005; Sweger et al., 2007). Because both of these receptors are Gi-coupled GPCRs, it is likely that the Ro1 receptor also signals via Gi-coupled GPCR pathways. The major signaling pathways shown to be activated downstream of the KOR and other Gi-coupled GPCRs include inhibition of adenylyl cyclase, modulation of calcium and potassium channels and activation of the mitogen-activated protein kinase (MAPK) family, including ERK1/2, p38 and JNK (see Chapter VII for more detail on signaling pathways activated downstream of Gi-coupled GPCRs) (Bruchas and Chavkin, 2010). The Ro1 receptor has been shown to couple to adenylyl cylcase, causing a decrease in cAMP levels, providing further evidence that it couples to Gi-coupled signaling cascades (Coward et al., 1998b). Additionally, cardiac arrhythmias caused by Ro1 expression in the heart were blocked by a single injection of pertussis toxin (PTX), demonstrating that Ro1 signaling through Gi-coupled pathways in the heart caused this arrhythmia (Redfern et al., 2000). Further, previous studies in our laboratory have demonstrated upregulation of phospho-ERK around the lateral ventricle and entorhinal cortex of Ro1 mice (Sweger et al., 2007). Nonetheless, GPCR promiscuity has been demonstrated in other systems, especially upon overexpression of the receptor (Hermans, 2003); as such, with the high levels of expression and high basal activity of the Ro1 receptor, it is possible that receptor promiscuity is also occurring in our mice.

Administration of PTX to Ro1 mice to determine whether Gi-coupled signaling cascades are necessary for the development of hydrocephalus in this model would therefore narrow our investigation of specific proteins involved in the pathogenesis of hydrocephalus to proteins involved in Gi-coupled GPCR signaling and thereby improve the likelihood of identifying therapeutic targets to treat this disorder.

d. Future directions

The Ro1 model of hydrocephalus represents a unique tool for the study of hydrocephalus, and further studies using this model should focus elucidating signaling pathways involved in the pathogenesis of hydrocephalus and improving our understanding of the neuropathological changes that accompany this disorder. Determining how altered GPCR signaling cascades downstream of the Ro1 receptor lead to hydrocephalus should be a priority of future research. Due to the variability in Ro1 expression and the rate of progression of hydrocephalus in these mice, signaling changes will need to be correlated with Ro1 expression to determine when these signaling changes occur in the progression of this disorder. One method for doing this may be to coexpress green fluorescent protein (GFP) with Ro1 in GFAP-positive cells and use fluorescence-activated cell sorting to isolate GFAP-positive cells. This population can then be used to measure both Ro1 expression (either by real-time PCR or western blotting) and changes in signaling proteins via western blotting. Alternatively, fresh tissue can be isolated from one hemisphere of the Ro1 mouse brain for real-time PCR to determine levels of Ro1 expression, and the other half can be fresh frozen, fixed and processed for immunohistochemistry. Preliminary studies have suggested that this approach is feasible. Once signaling changes have been identified, administration of inhibitors to specific proteins believed to be involved in the

pathogenesis of hydrocephalus will help to elucidate whether these proteins are necessary for the development of hydrocephalus. Intracerebroventricular infusions likely represent the best approach to selectively target these drugs to the brain and avoid non-specific and potentially deleterious systemic effects. Transgenic mice with cell- or brain-specific removal or overexpression for specific proteins could also be developed, although this approach is less feasible because the Ro1 mice are double-transgenic animals on a KOR knock-out background, and the breeding of mice with an additional transgenic construct could become complicated.

Further analysis of the pathological changes that occur in the brains of Ro1 mice would also be beneficial. For example, although we did not see any changes in the subventricular zone in early hydrocephalus in Ro1 mice, it is likely that changes in this region occur as hydrocephalus progresses. Also, investigating changes in adhesion molecules and cilia function could provide insight into early cellular changes that may contribute to the development of hydrocephalus. Further, it would be interesting and worthwhile to investigate changes in proteins, growth factors, neurotransmitters and other chemicals in the CSF of Ro1 mice through lumbar puncture and western blotting to better understand the early signaling changes in hydrocephalus and identify potential biomarkers for various stages of hydrocephalus. All of these changes should be correlated to Ro1 receptor expression to determine the timing and sequence of pathological changes in the Ro1 model of hydrocephalus. A better understanding of the neuropathological changes in the Ro1 model of hydrocephalus would improve our understanding of this disorder and possibly lead to the development of therapeutics to both prevent hydrocephalus and treat the adverse neuropathological changes that accompany this disorder

e. Summary and conclusions

Hydrocephalus is a highly prevalent and devastating disorder for which the only treatment is recurrent neurosurgery to insert and revise shunts that drain the CSF. Better treatments are required for hydrocephalus, and the study of animal models of hydrocephalus will likely improve our understanding of the development and pathology of this disorder, leading to better diagnosis and treatments. The Ro1 model represents a unique model of hydrocephalus in that hydrocephalus can be induced at any age with complete penetrance and without interfering pathologies, enabling the investigation of the earliest pathological changes that lead to hydrocephalus. Also, the specific activation of a G-protein coupled receptor (the transgenic Ro1 receptor) in a specific subset of cells (GFAP-positive cells) makes investigating signaling pathways involved in hydrocephalus extremely tractable. The experiments presented herein provide insight into the previously unknown cellular and morphological changes that occur in the pathogenesis of the Ro1 model of hydrocephalus, which may lead to the development of pharmacological treatments for hydrocephalus. Additionally, the behavioral data suggest that treatments that slow the rate of progression of this disorder may have therapeutic potential by allowing the brain to compensate and increasing the therapeutic window for shunt placement or alternative treatments.

Appendix I

Figures

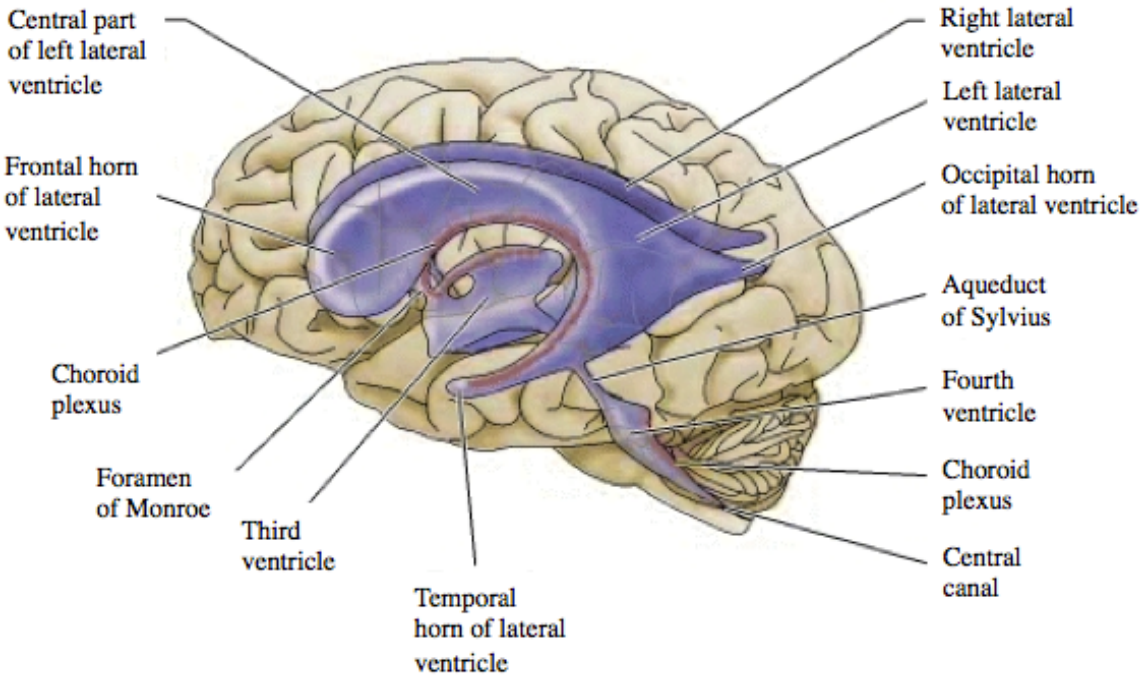

Figure 1. The ventricular system. The ventricular system is composed of four ventricles—two lateral ventricles, a third ventricle and a fourth ventricle—through which the cerebrospinal fluid (CSF) flows. CSF, which is produced primarily by the choroid plexus found in each of the four ventricles, flows from the lateral ventricles through the foramen of Monroe to the third ventricle and travels from the third ventricle through the aqueduct of Sylvius to the fourth ventricle. The CSF flows out of the fourth ventricle through the midline foramen of Magendie and two lateral foramina of Lushka into the cisterna magna and the basal cisterns of the subarachnoid space, respectively. The cavity of the fourth ventricle also extends into the central canal of the spinal cord. After exiting into the cisterna magna, the CSF then traverses the subarachnoid space over the surface of the cortex and drains back into the blood via the arachnoid granulations, spinal nerve roots and the olfactory tracts. Figure modified from Purves et al., 2001.

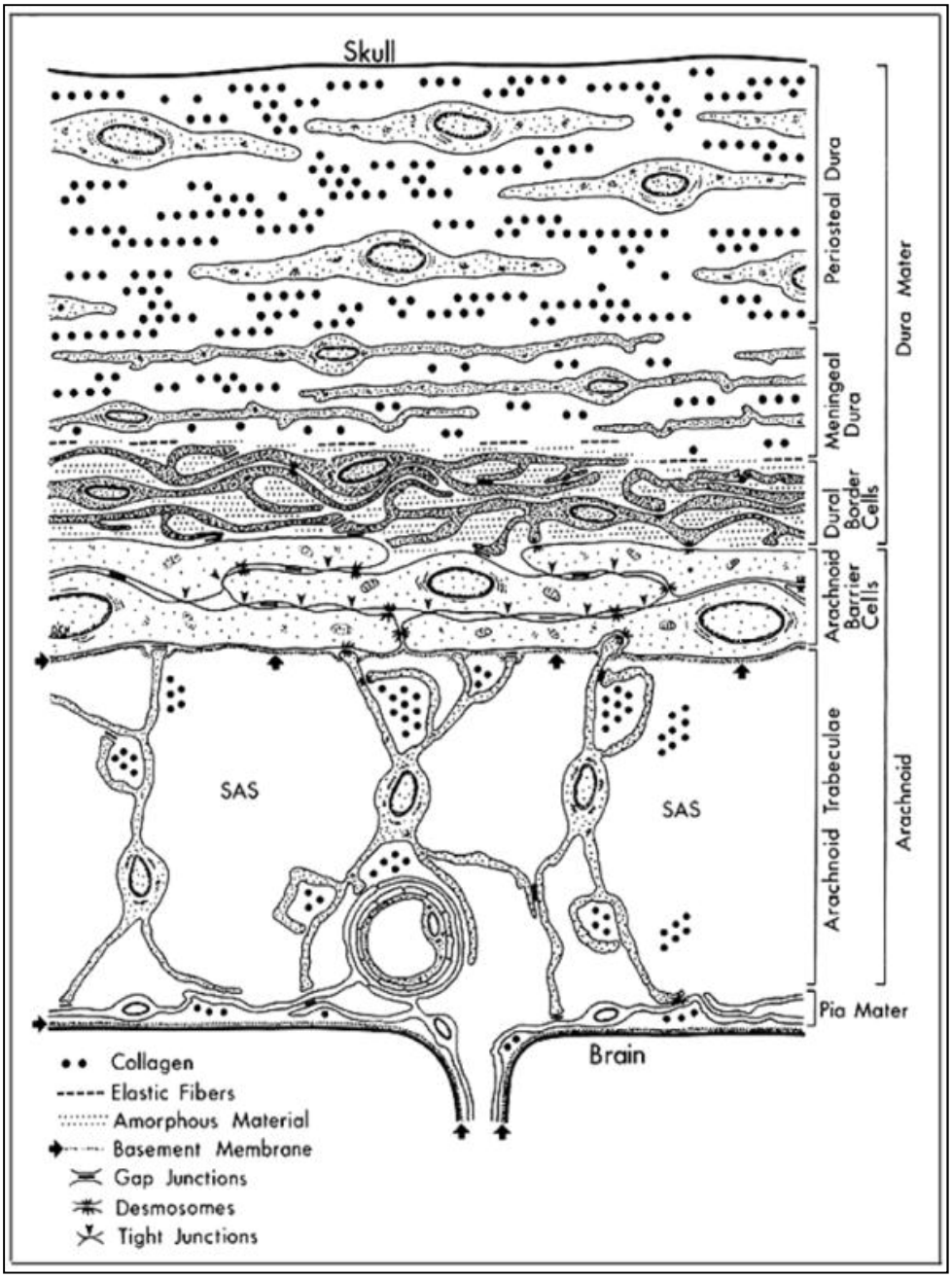

Figure 2. The meninges. In this schematic, the inner surface of the skull is located at the top, and the external surface of the brain is located at the bottom. The meninges are composed of dura, arachnoid and pia mater, and a fluid-containing compartment called the subarachnoid space is present between the pia and arachnoid layers. Image reprinted from Haines et al., 1993.

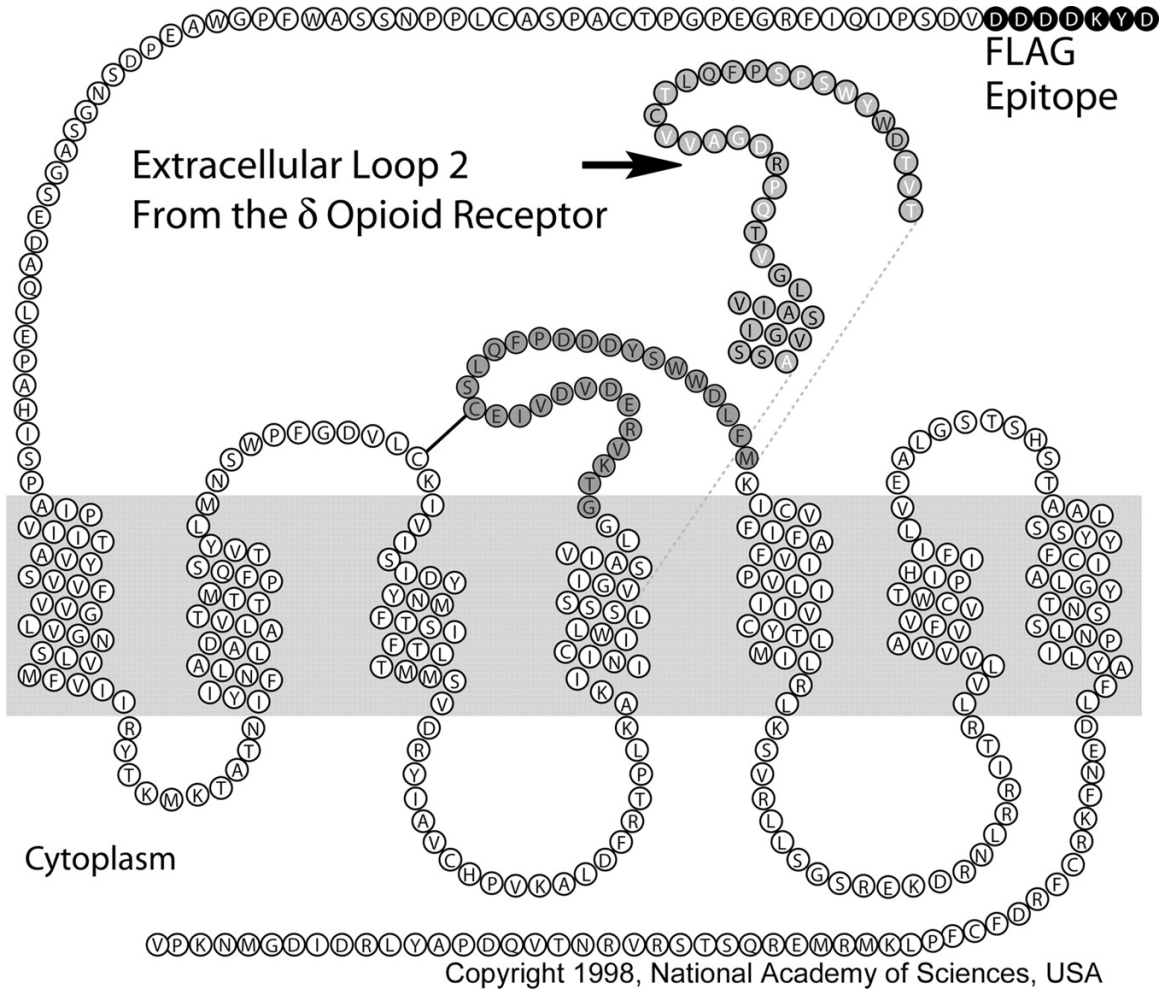

Figure 3. The Ro1 receptor. The Ro1 receptor was developed by replacing the second extracellular loop of the κ-opioid receptor with the second extracellular loop of the δ-opioid receptor. A FLAG tag was added to the N terminus for detection. The affinity of the Ro1 receptor for endogenous ligands is greatly reduced; however, it still responds to the small molecule drug spiradoline and the antagonist norbinaltorphamine (norBNI). Figure modified from Coward et al., 1998.

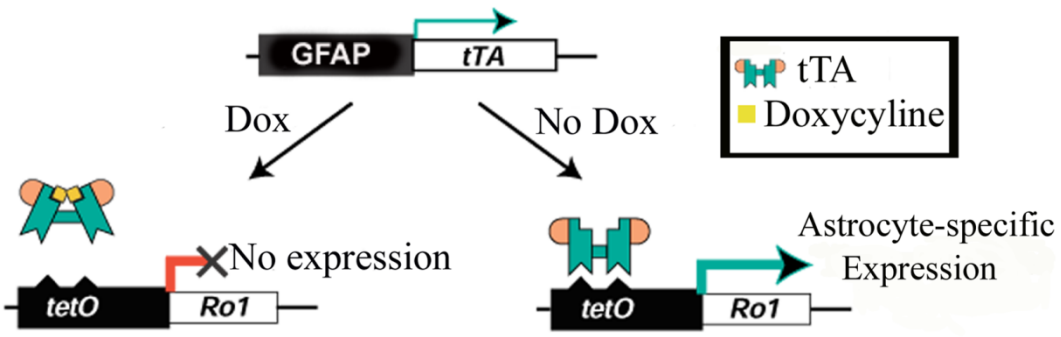

Figure 4. The tet-off system. Ro1 mice were created by crossing two lines of mice: in one line the GFAP promoter drives tTA expression. In the other line the tetO minimal promoter drives Ro1 expression. In the absence of doxycycline, tTA binds to the tetO promoter, driving Ro1 expression to GFAP+ cells. When mice are given dox, the dox binds to tTA, preventing tTA binding to the tetO promoter and thereby blocking Ro1 expression. Figure modified from Scearce-Levie et al., 2001.

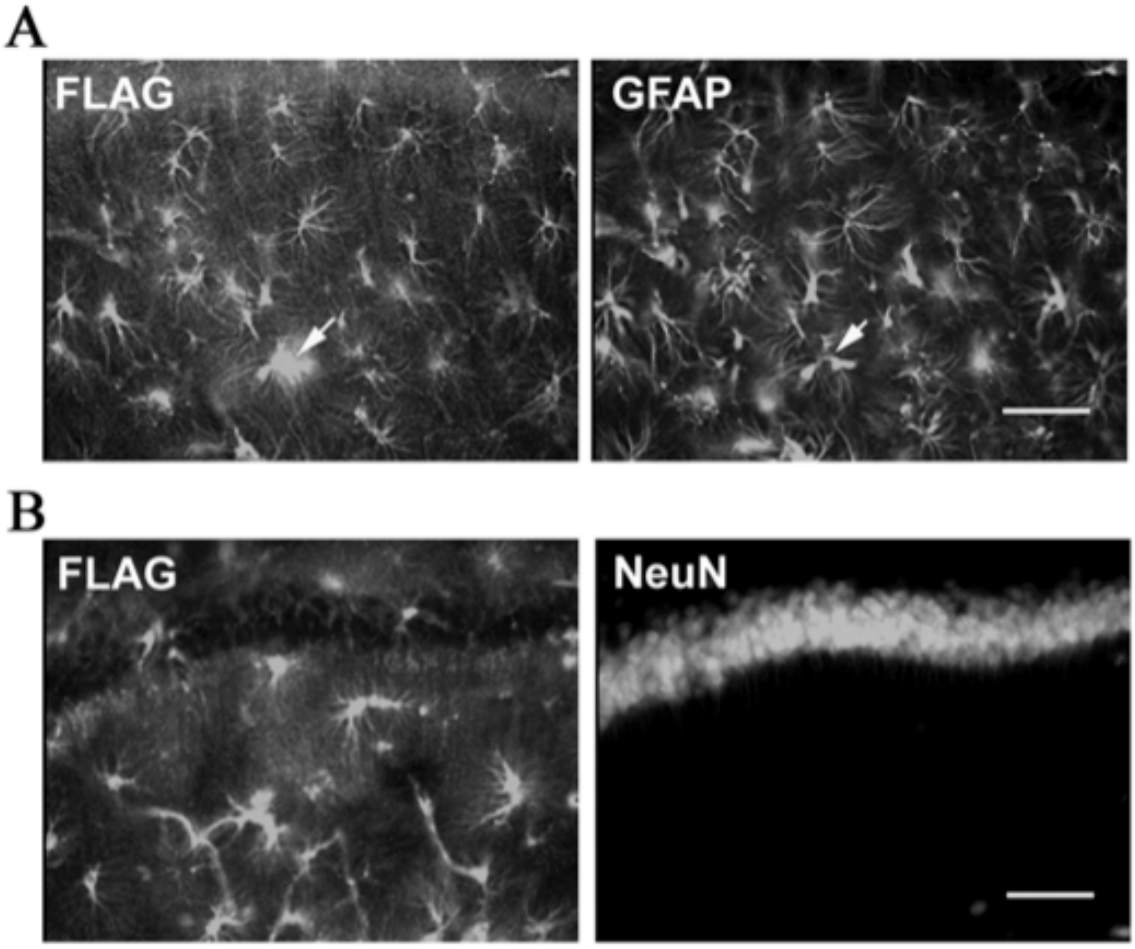

Figure 5. The Ro1 receptor is selectively expressed in astrocytes. Hippocampal brain sections were double-stained for FLAG and GFAP (astrocyte marker) or FLAG and NeuN (neuronal marker). A) FLAG staining (left, arrow) was colocalized with GFAP (right, arrow) but not with NeuN (B). The arrows point to the same cell. Scale bars, 100 μm. Figure reprinted from Sweger et al., 2007.

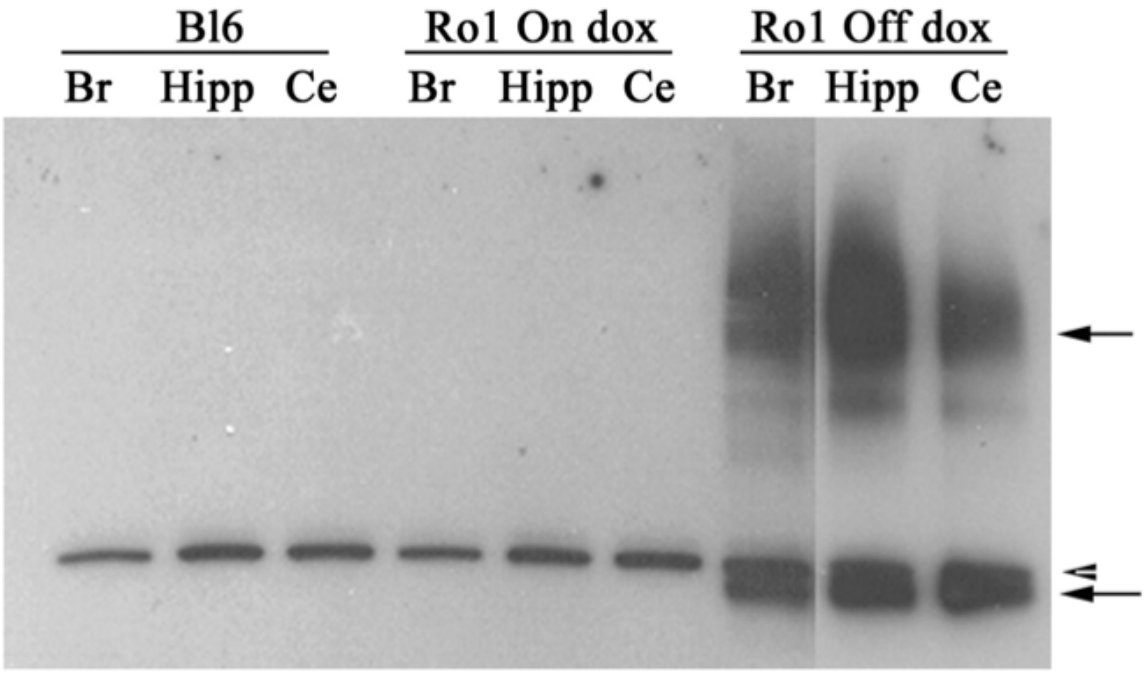

Figure 6. Ro1 expression can be regulated by doxycycline. Brain lysates from a C57BL/6 control mouse, an Ro1 mouse maintained on dox (25 μg/ml) and Ro1 mouse maintained off dox were immunoprecipitated with a FLAG monoclonal antibody and subjected to western blotting using a FLAG polyclonal antibody. Only the Ro1 mouse maintained off dox showed FLAG-tagged Ro1 expression. A nonspecific band was found in all samples (arrowhead). Br, Brain; Hipp, hippocampus; Ce, cerebellum. Figure reprinted from Sweger et al., 2007.

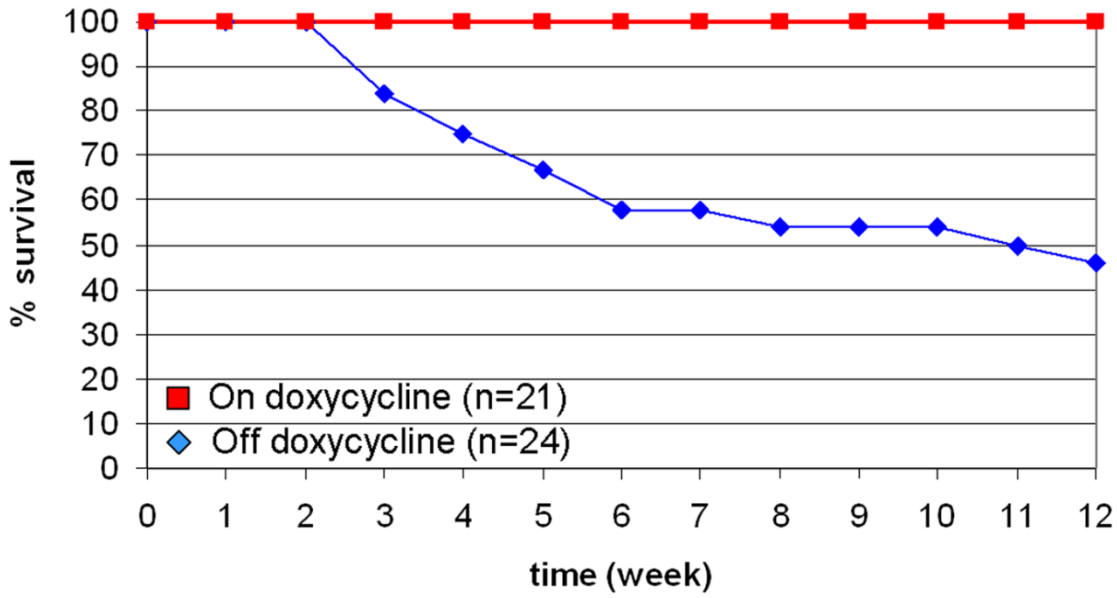

Figure 7. Survival curve of Ro1 mice maintained off doxycycline. All Ro1 mice maintained off dox develop hydrocephalus, and >50% die by 12 weeks of age. Figure reprinted from Sweger et al., 2007.

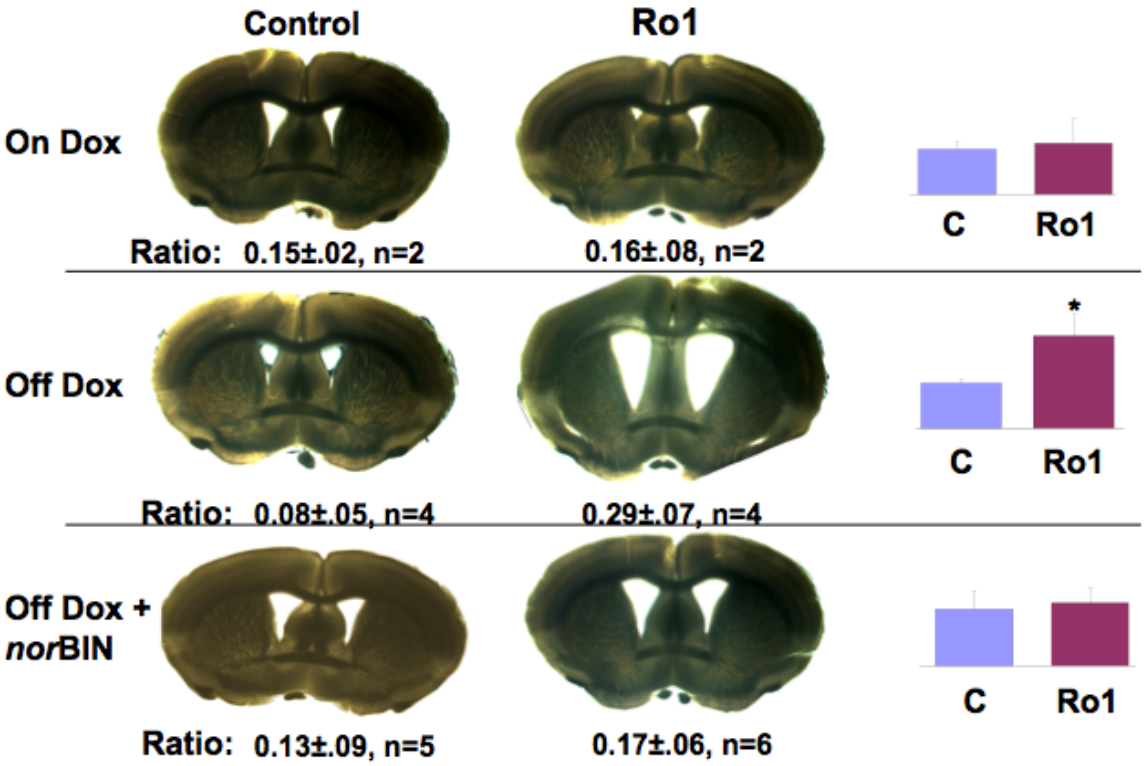

Figure 8. Signaling through the Ro1 receptor causes hydrocephalus. Mice were maintained on dox, taken off dox at P30 or taken off dox at P30 and given injections of norBNI (7.6 mg/kg i.p.) every three days for 30 days. At P60, the mice were sacrificed and the lateral ventricle to brain ratio was measured. Ro1 mice off dox for 30 days showed significantly greater lateral ventricle to brain ratios than control mice; there were no significant differences between controls or Ro1 mice maintained on dox or taken off dox for 30 days and given norBNI. Figure courtesy Sweger and McCarthy, 2009.

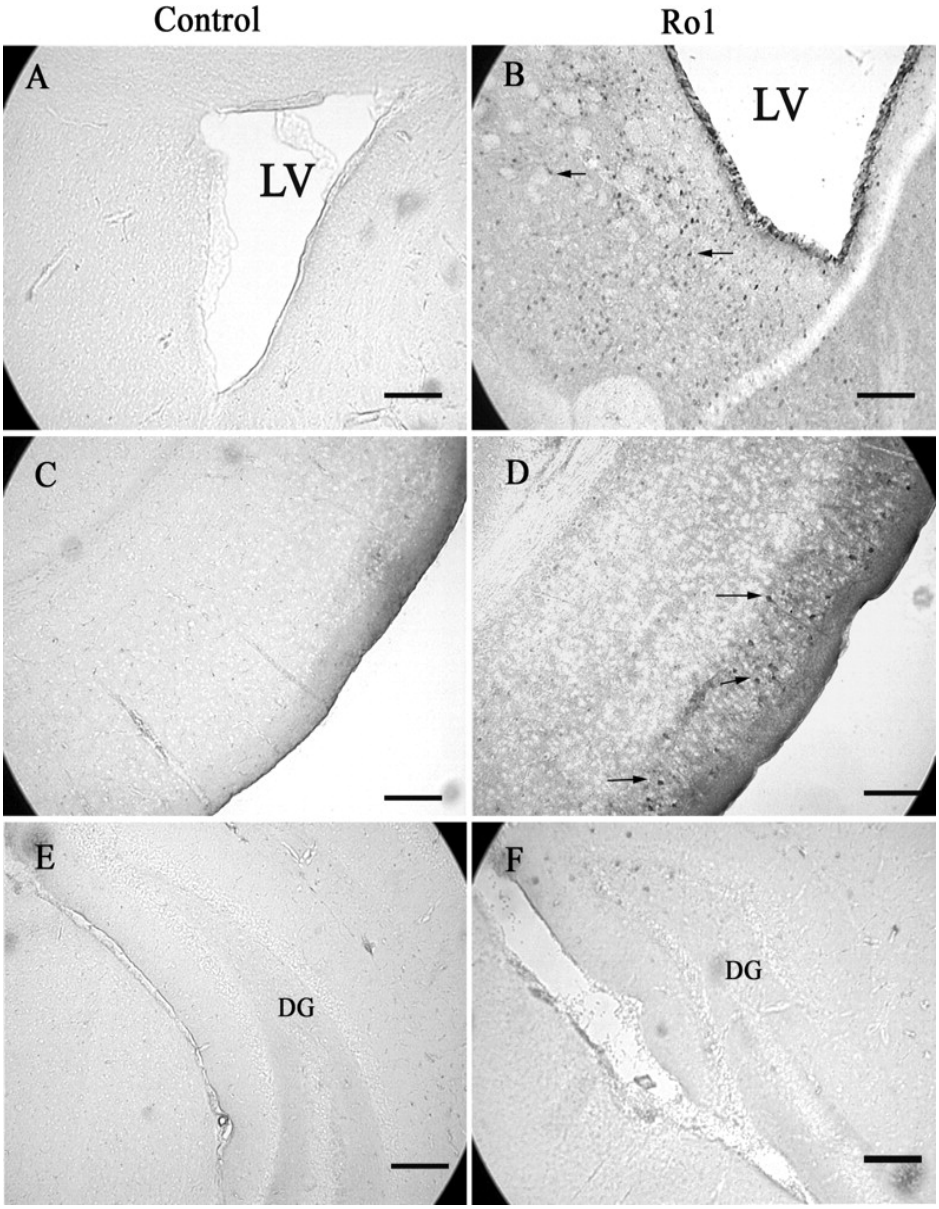

Figure 9. Phospho-ERK is upregulated in mice with hydrocephalus. Increased phospho-Erk staining was observed around the lateral ventricles (B) and in the entorhinal cortex (D) of hydrocephalic Ro1 mice but not in littermate controls (P21, always off dox) (A, C). No increases in phospho-Erk were observed in the hippocampus (F). Sections shown in A and B are at the level of the anterior commissure and striatum; C–F are at the level of the subcommissural organ. Scale bars, 150 μm. LV, Lateral ventricle; DG, dentate gyrus. Reprinted from Sweger et al., 2007.

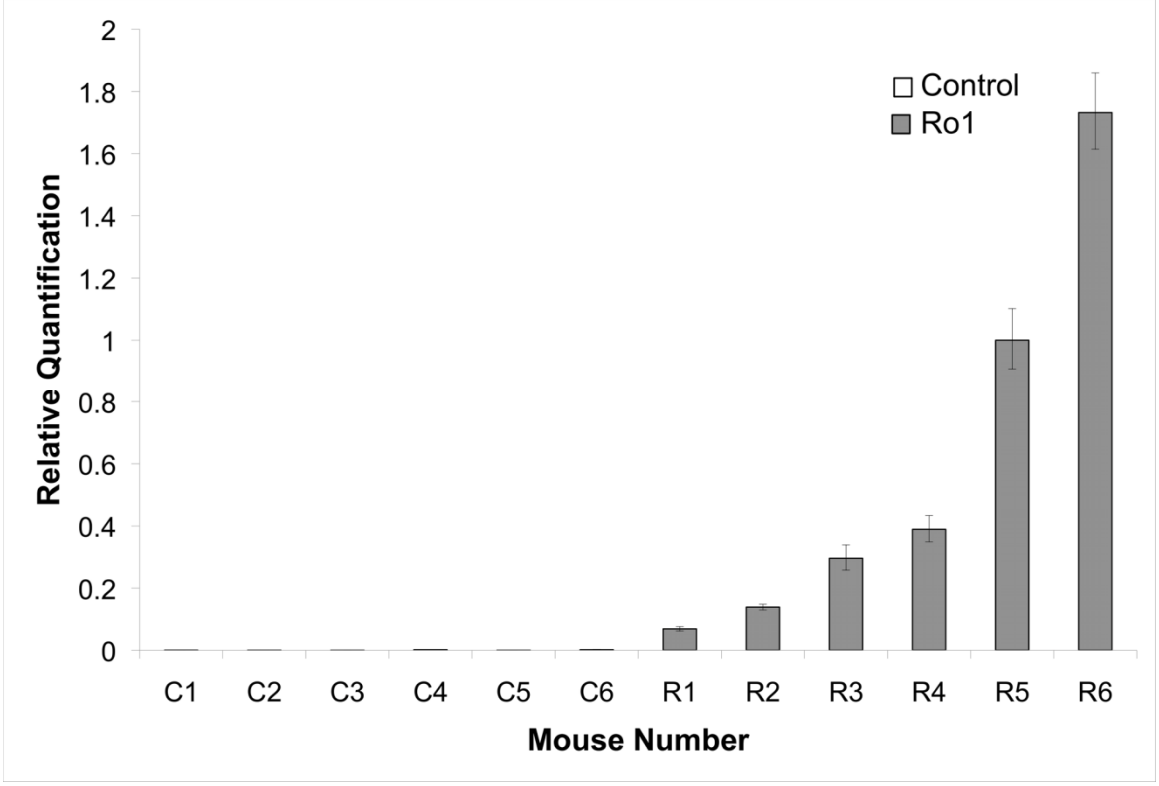

Figure 10. Variable expression of Ro1 receptor mRNA in Ro1 mice at 9 days off dox. Real-time PCR was used to measure Ro1 receptor mRNA expression levels using human KOR primers in lysates isolated from mouse brain tissue. This graph shows the relative quantification of Ro1 receptor expression in Ro1 mice and littermate controls (n = 6). Although Ro1 receptor mRNA was clearly expressed by Ro1 mice by 9 days after the removal of dox at P30, there was considerable variability in the levels of Ro1 mRNA expression among Ro1 mice.

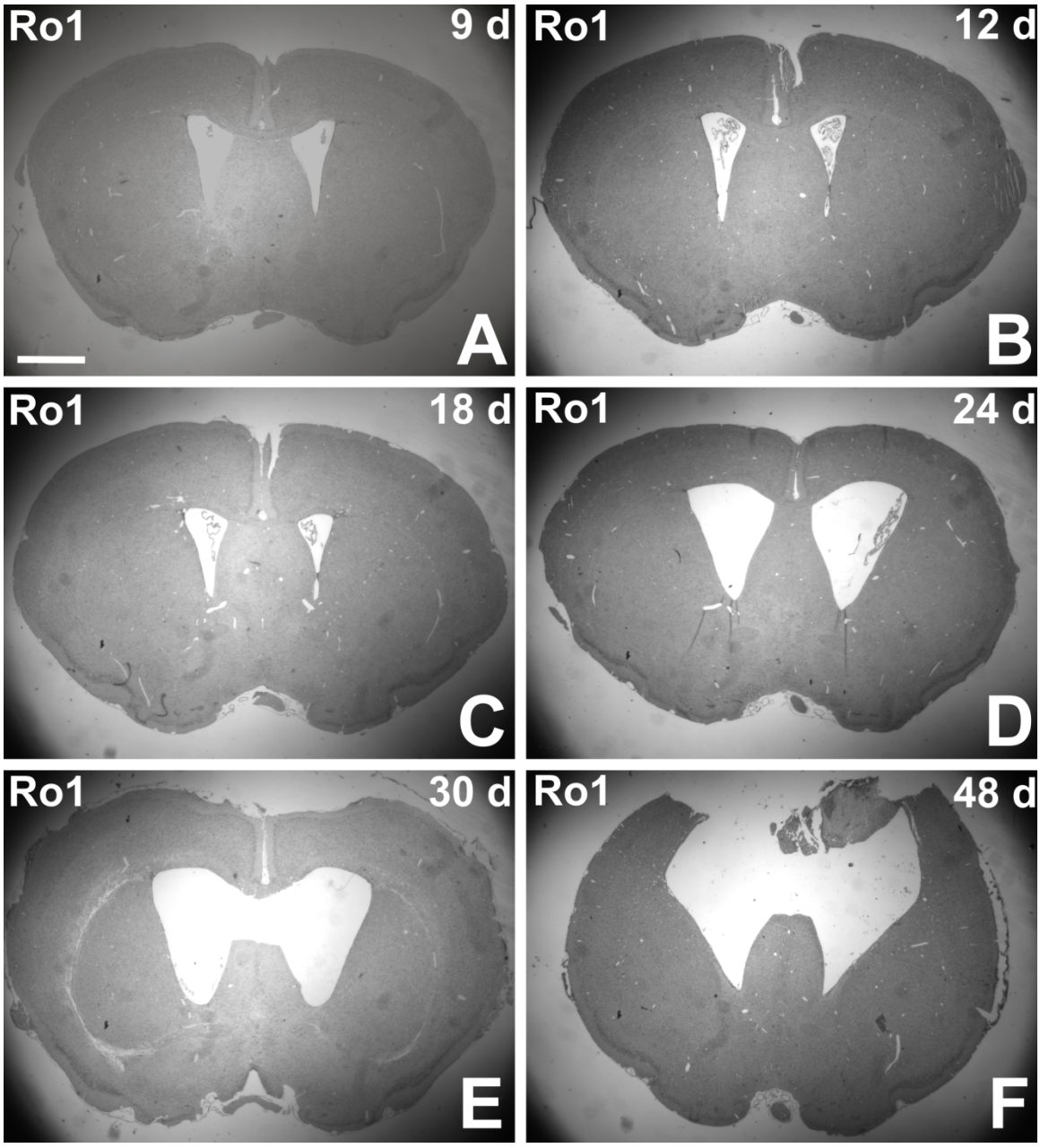

Figure 11. Lateral ventricle size increases as hydrocephalus progresses in the Ro1 model. At 9 (A), 12 (B) and 18 (C) days off dox, there were no changes in lateral ventricle (LV) size between Ro1 mice and littermate controls. (At 18 d off dox, the average LV:brain ratio = 0.20 and 0.14 for control and Ro1 mice, respectively; range (Ro1) = 0.10 – 0.18.) Increases in ventricle size were first observed at 24 days off dox (D; The average LV:brain ratio = 0.14 and 0.22 for control and Ro1 mice, respectively; range (Ro1) = 0.14 – 0.39). Ventriculomegaly

became increasingly more severe as hydrocephalus progressed; (E) 30 days off dox (The average LV:brain ratio = 0.14 and 0.25 for control and Ro1 mice, respectively; range (Ro1) = 0.15 – 0.43), (F) 48 days off dox (The average LV:brain ratio = 0.18 and 0.32 for control and Ro1 mice, respectively; range (Ro1) = 0.18 – 0.64). Scale bar = 1.0 mm.

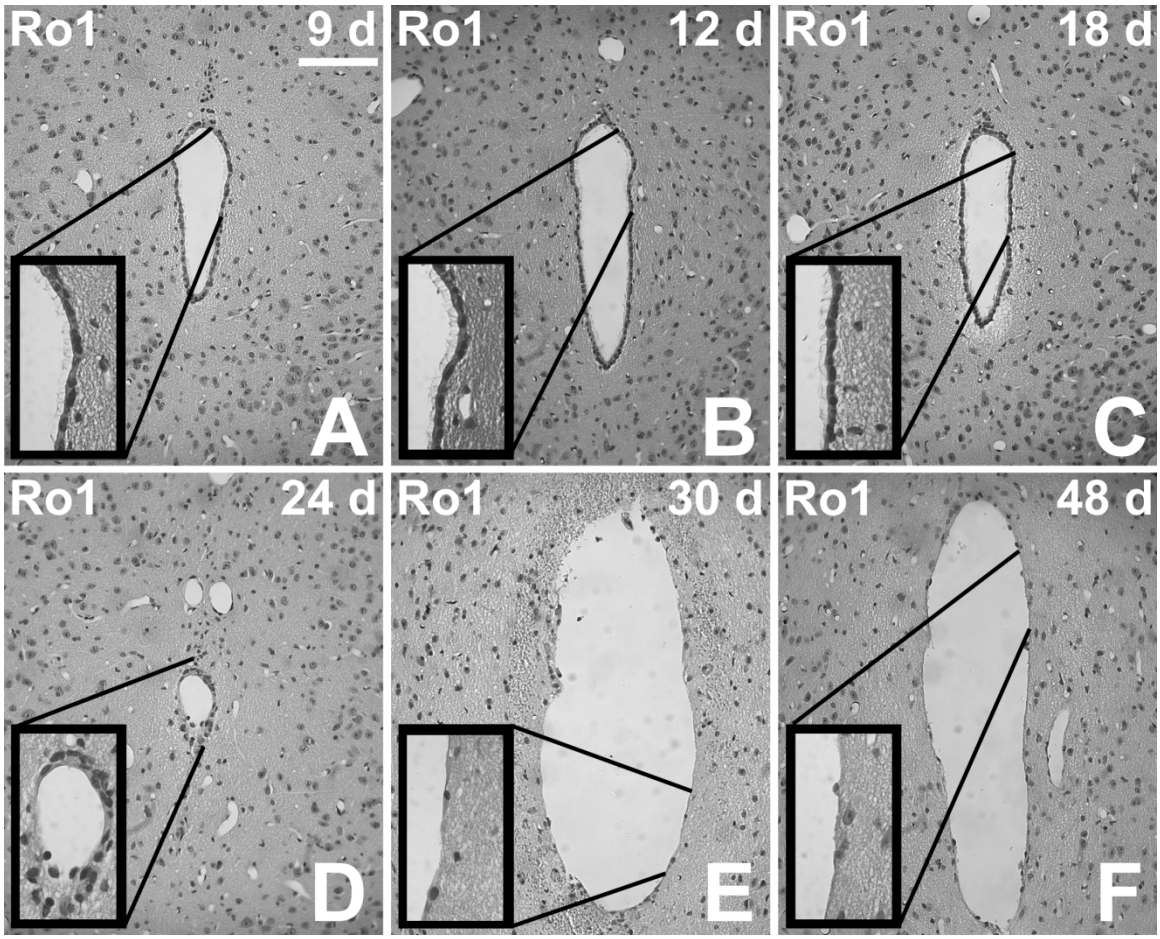

Figure 12. Progressive disorganization of the aqueduct of Sylvius occurs in the Ro1 model. At 9 (A), 12 (B) and 18 (C) days off dox, there were no changes in the ependymal lining of the aqueduct between Ro1 mice and littermate controls. Disorganization of the ependymal lining of the aqueduct was first observed at 24 days off dox (D). This disorganization became increasingly more severe as hydrocephalus progressed and lateral ventricle size increased; (E) 30 days off dox, (F) 48 days off dox. These images were taken from the brains of the same Ro1 mice shown in Figures 2 and 5. Scale bar = 100 μm.

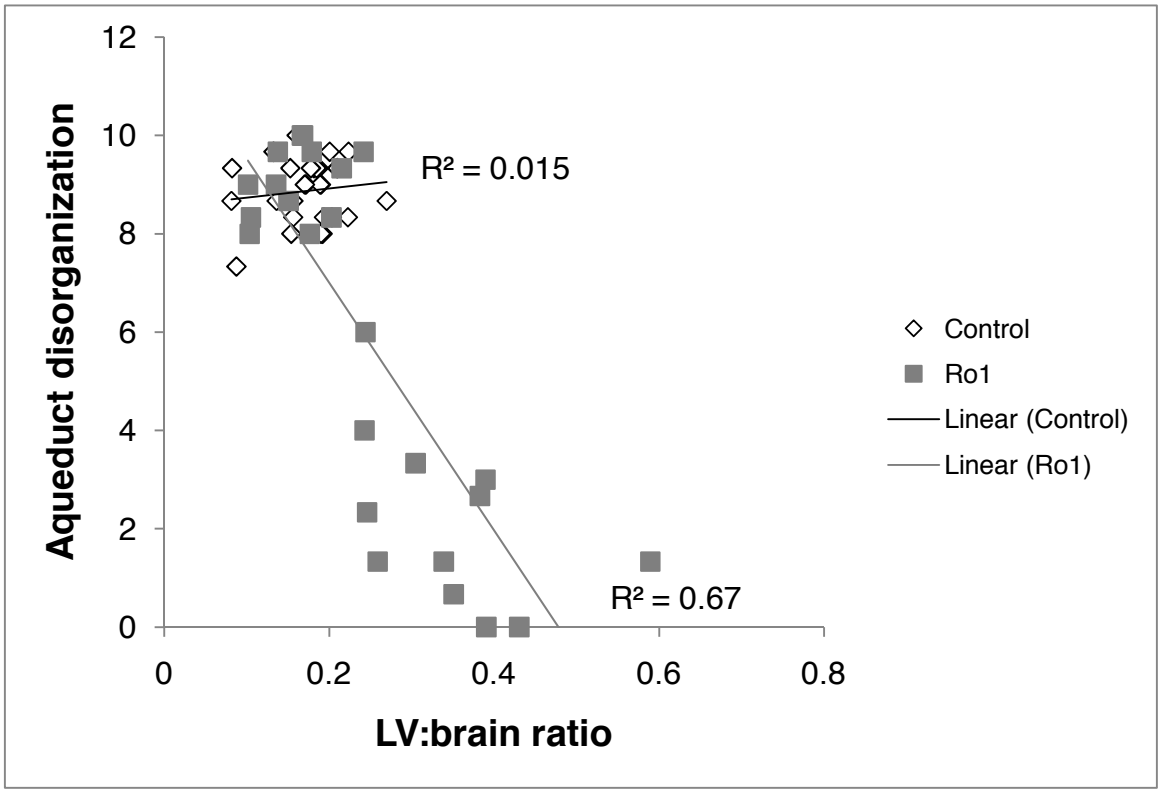

Figure 13. Lateral ventricle size is correlated with the degree of aqueduct disorganization. In Ro1 mice, lateral ventricle size is significantly correlated to disorganization of the aqueduct of Sylvius (r^2 = 0.67; $p < 0.0001$). As lateral ventricle size increased, the aqueduct became increasingly disorganized.

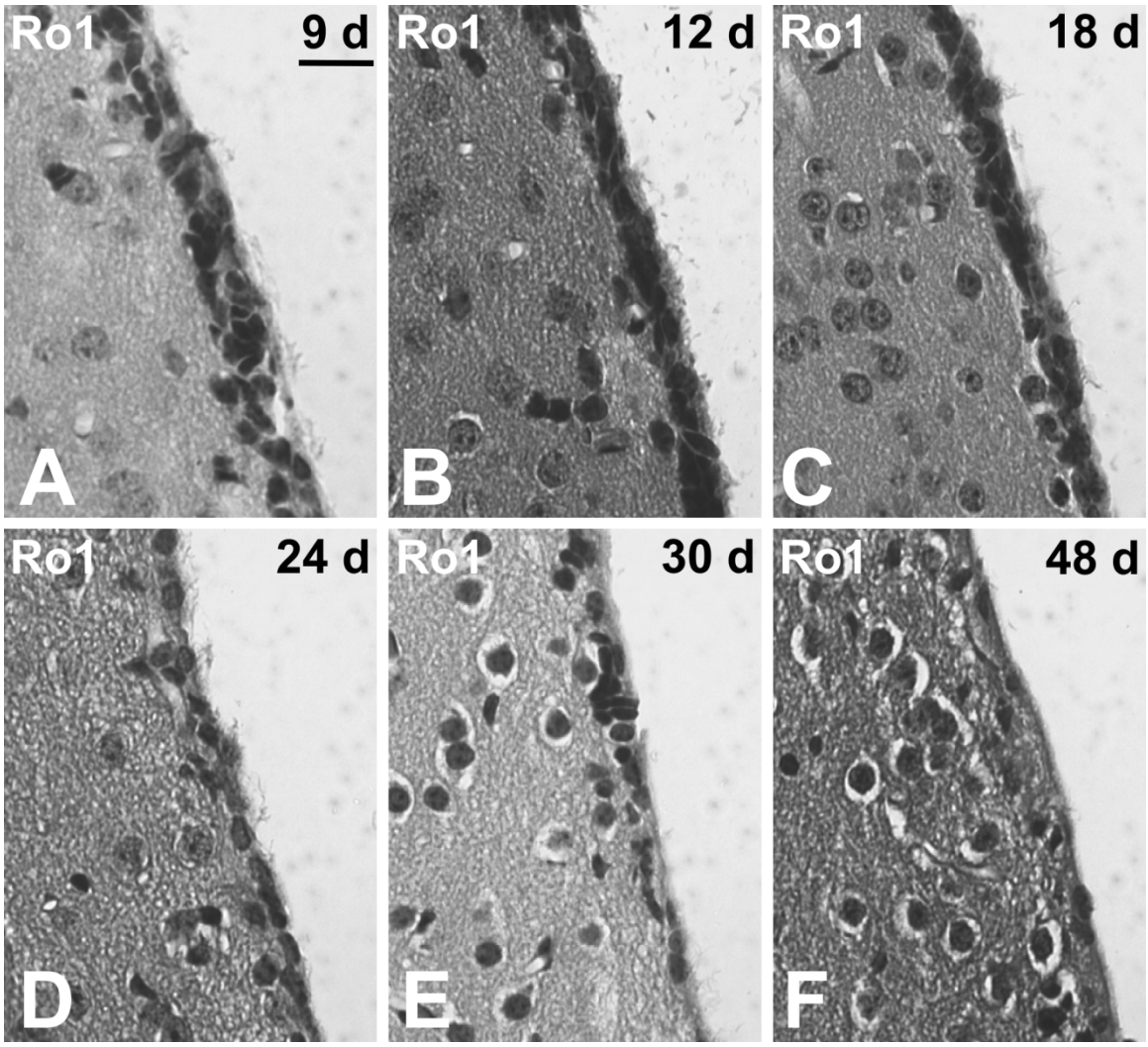

Figure 14. Changes in the ependymal lining of the ventricles are subsequent to ventriculomegaly. There were no changes in the ependymal lining of the lateral ventricles at 9 (A), 12 (B) or 18 (C) days off dox. As the lateral ventricle size increased, the ependymal layer became thinner; (D) 24 days off dox, (E) 30 days off dox and (F) 48 days off dox. These images were taken from the lateral wall of the left lateral ventricle. These images were taken from the brains of the same Ro1 mice shown in Figures 2 and 3. Scale bar = 20 μm.

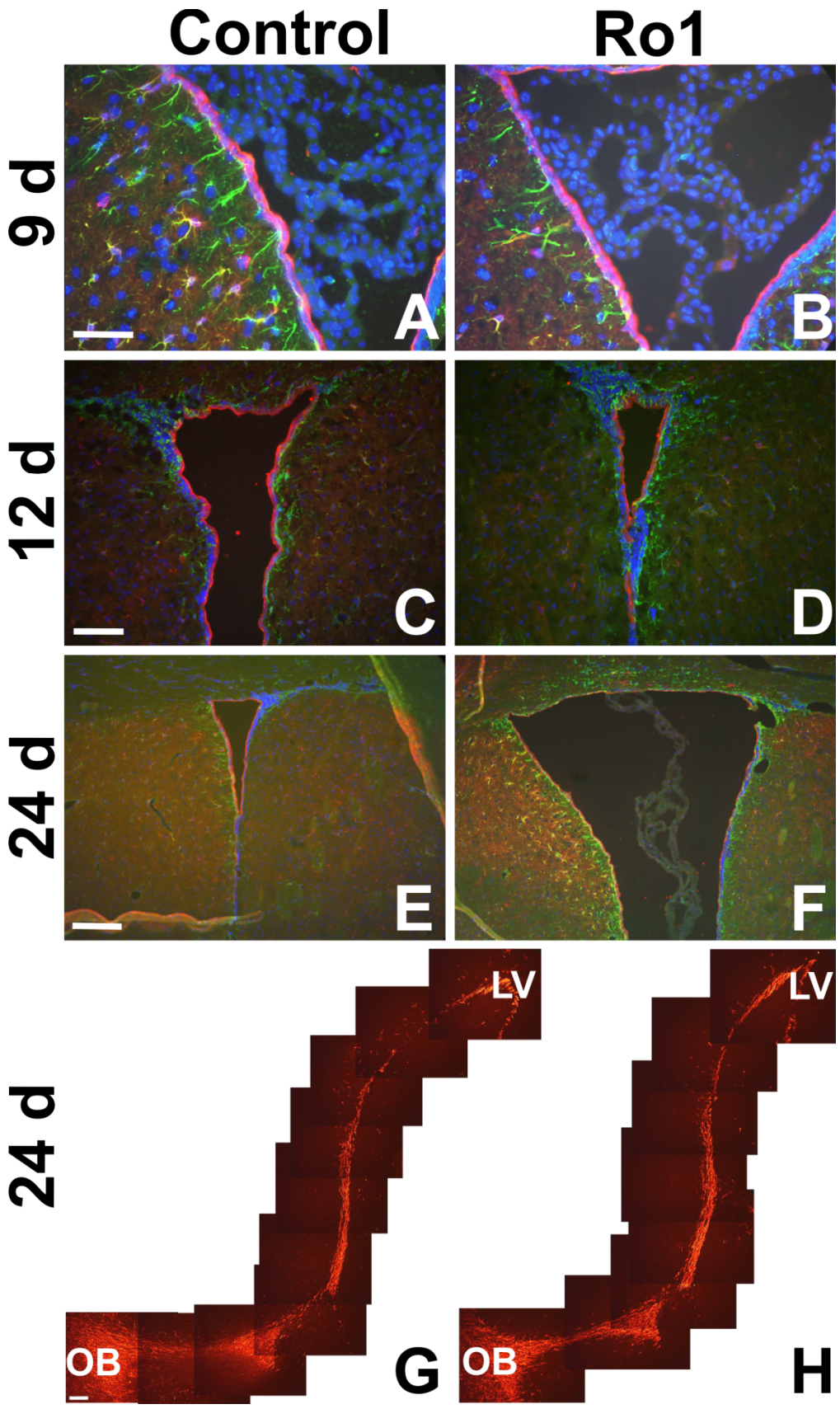
Control
Ro1
9 d
12 d
24 d
A
B
C
D
E
F
24 d
LV
LV
OB
OB
G
H

Figure 15. Lack of cellular changes in subventricular zone organization in early hydrocephalus in Ro1 mice. (A) and (B) show GFAP (green) and S100 (red) expression at 9 days off dox in control and Ro1 mice, respectively (n = 4; scale bar = 50 μm). (C) and (D) show GFAP (green) and S100 (red) expression at 12 days off dox in control and Ro1 mice, respectively (n = 3; scale bar = 100 μm). (E) and (F) show GFAP (green) and S100 (red) expression at 24 days off dox of control and Ro1 mice, respectively (n = 5; scale bar = 200 μm). These images were taken from the right lateral ventricle in coronal slices. There were no detectable changes in GFAP or S100 expression at any time point analyzed. (G) and (H) show DCX (red) expression from the lateral ventricle to the olfactory bulb in sagittal sections from control and Ro1 mice, respectively, at 24 days off dox. There were no detectable changes in DCX expression or migration at 24 days off dox (n = 5; scale bar = 100 μm).

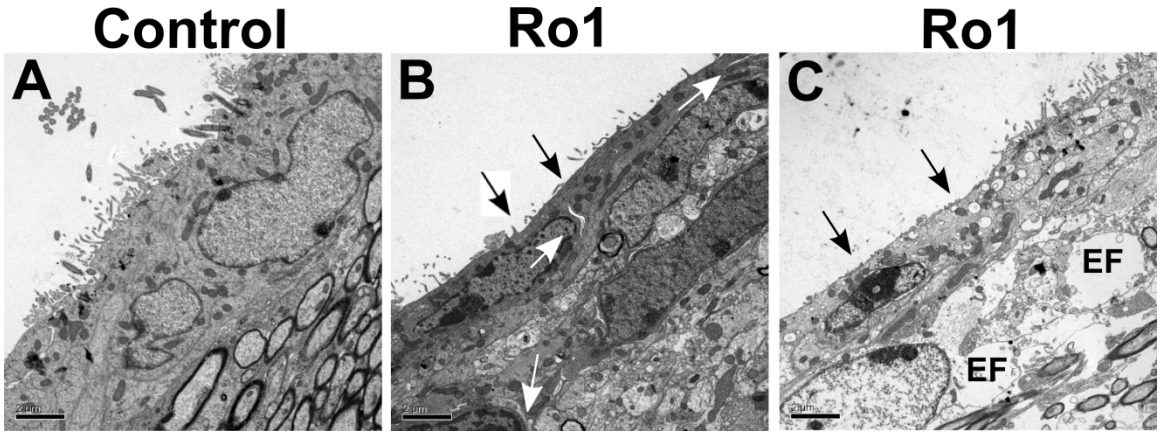

Figure 16. Ultrastructural changes in the periventricular region in Ro1 mice. Ventriculomegaly leads to thinning of the ependymal layer, which was associated with edema and patches of the ventricular wall barren of microvilli. A control (A) and two Ro1 (B and C) mice at 30 days off dox are shown (n = 3). Ro1 mice showed considerable thinning of the ependymal layer and a reduction in the number of microvilli lining the ventricles (black arrows). In the Ro1 mouse with an enlarged head and moderate ventriculomegaly (B), spaces appear to be developing between cells (white arrows). In the Ro1 mouse with an enlarged head and severe ventriculomegaly (C), vacuoles were present in the ependymal cell cytoplasm, and edema was present in the subependymal area (EF = edematous fluid). These images were taken from the lateral wall of the lateral ventricle. Scale bar = 2 μm.

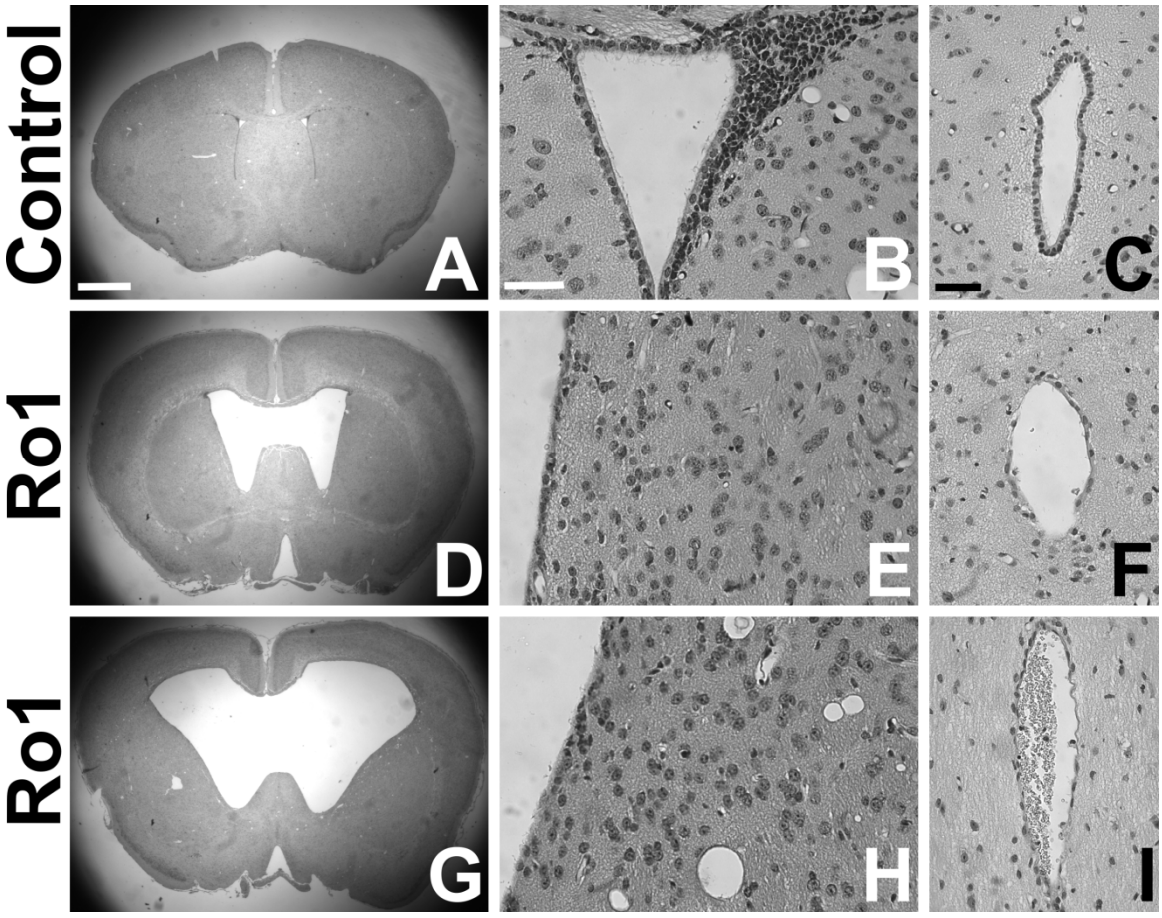

Figure 17. Morphological changes in the progression of hydrocephalus in mice maintained off dox. The progression of hydrocephalus in mice maintained off dox throughout gestation and development mirrors that found in mice taken off dox at P30. Images of coronal brain slices (A, D and G; scale bar = 1.0 mm), the lateral wall of the right lateral ventricle (B, E and H; scale bar = 50 μm) and the aqueduct of Sylvius (C, F and I; scale bar = 50 μm) are shown from a control mouse (A – C) and two Ro1 mice (D – F and G – I) at P27. Ro1 mice showed variable enlargement of the lateral ventricles (D and G), thinning (E) or loss (H) of the ependymal layer and disorganization of the ependymal lining of the aqueduct (F and I). The average LV:brain ratio was 0.34, and the range = 0.18 – 0.64. (n = 4)

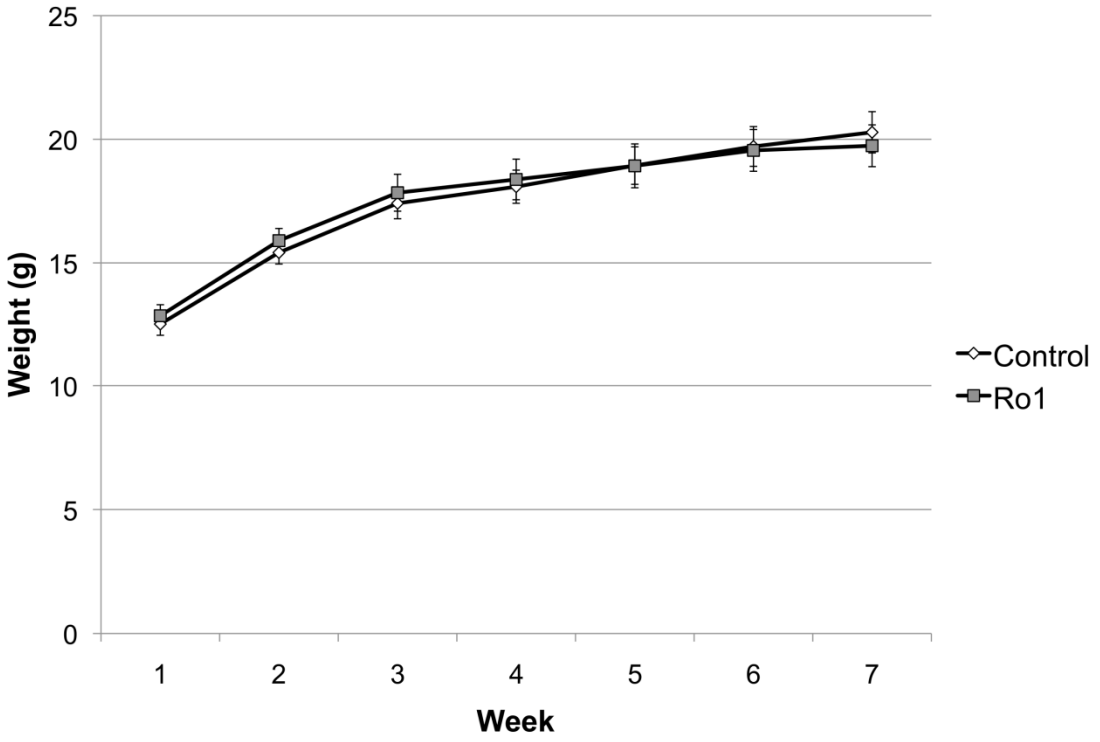

Figure 18. There are no differences in weight between Ro1 mice and littermate controls up to seven weeks following the removal of dox. Weight was measured weekly following the removal of dox from Ro1 and control mice at P30. $p = 0.90$. Control, $n = 11$; Ro1, $n = 10$.

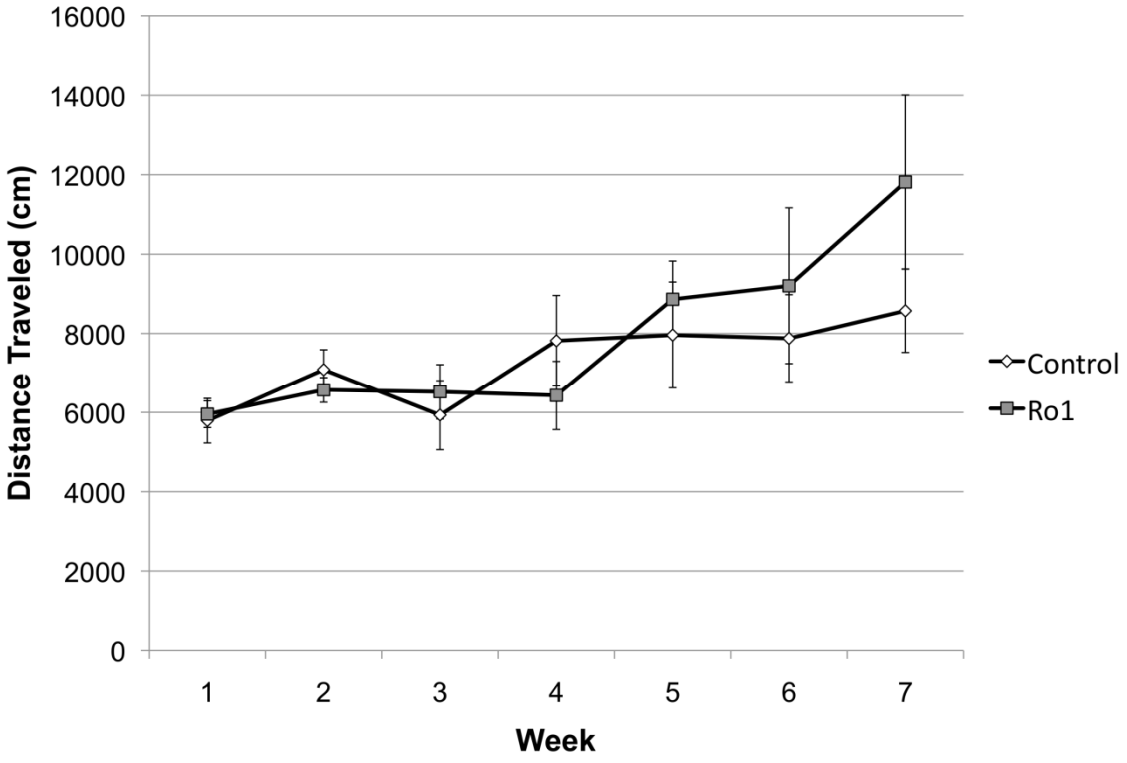

Figure 19. There are no differences in the total distance traveled between Ro1 mice and littermate controls up to seven weeks following the removal of dox. Total distance traveled was measured weekly in an open field activity box following the removal of dox from Ro1 and control mice at P30. $p = 0.62$. Control, $n = 11$; Ro1, $n = 10$.

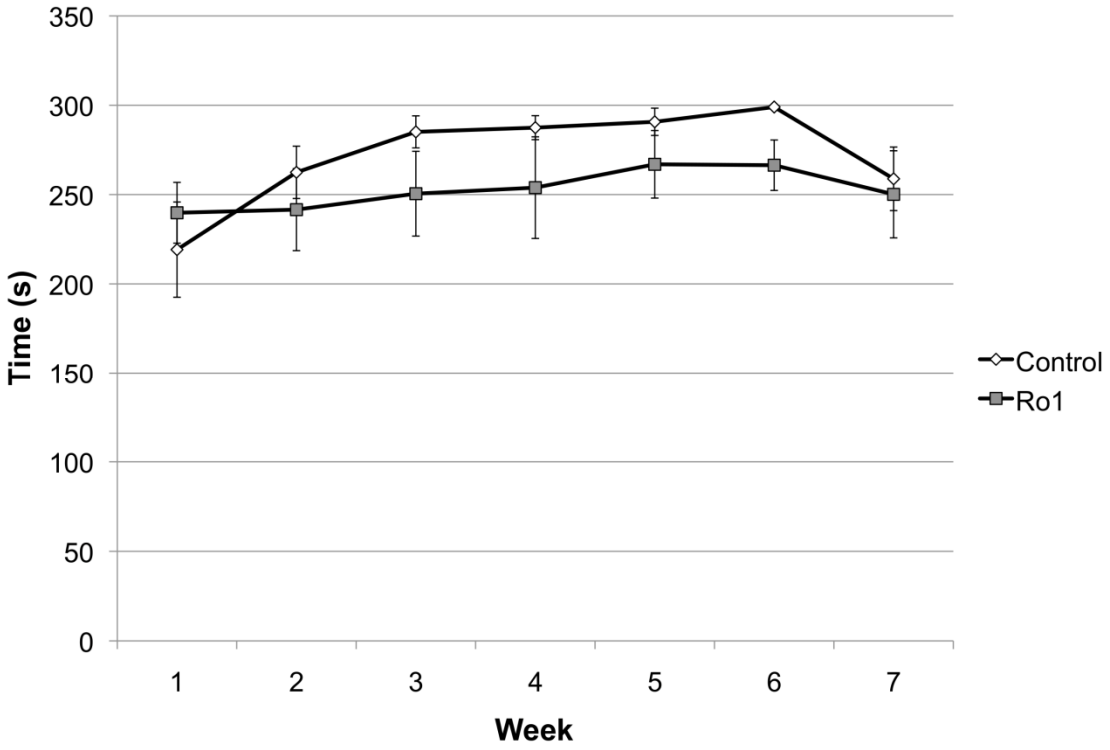

Figure 20. There are no differences in rotarod performance between Ro1 mice and littermate controls up to seven weeks following the removal of dox. Performance for a maximum of five minutes on an accelerating rotarod was measured twice weekly. Data from each trial were averaged for each week. $p = 0.22$. Control, $n = 11$; Ro1, $n = 10$

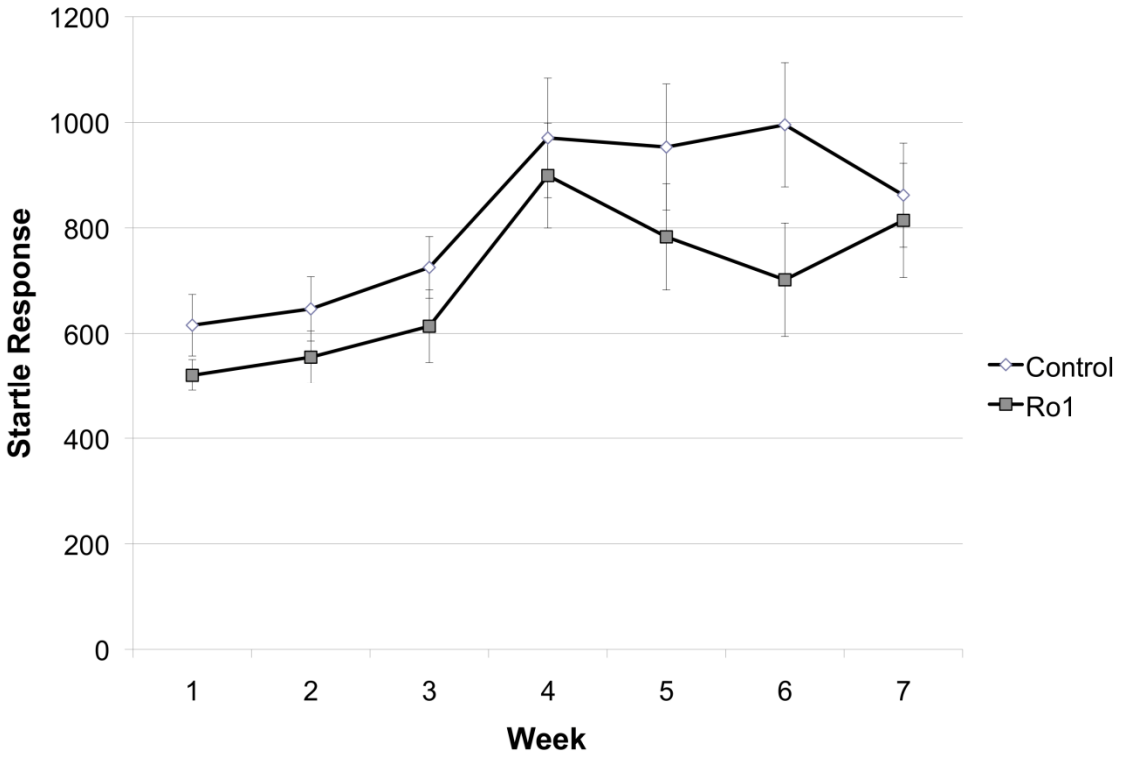

Figure 21. There are no differences in the startle response between Ro1 mice and littermate controls up to seven weeks following the removal of dox. Startle responses to a 120 dB acoustic stimulus were measured every week for seven weeks. p = 0.23. Control, n = 11; Ro1, n = 10.

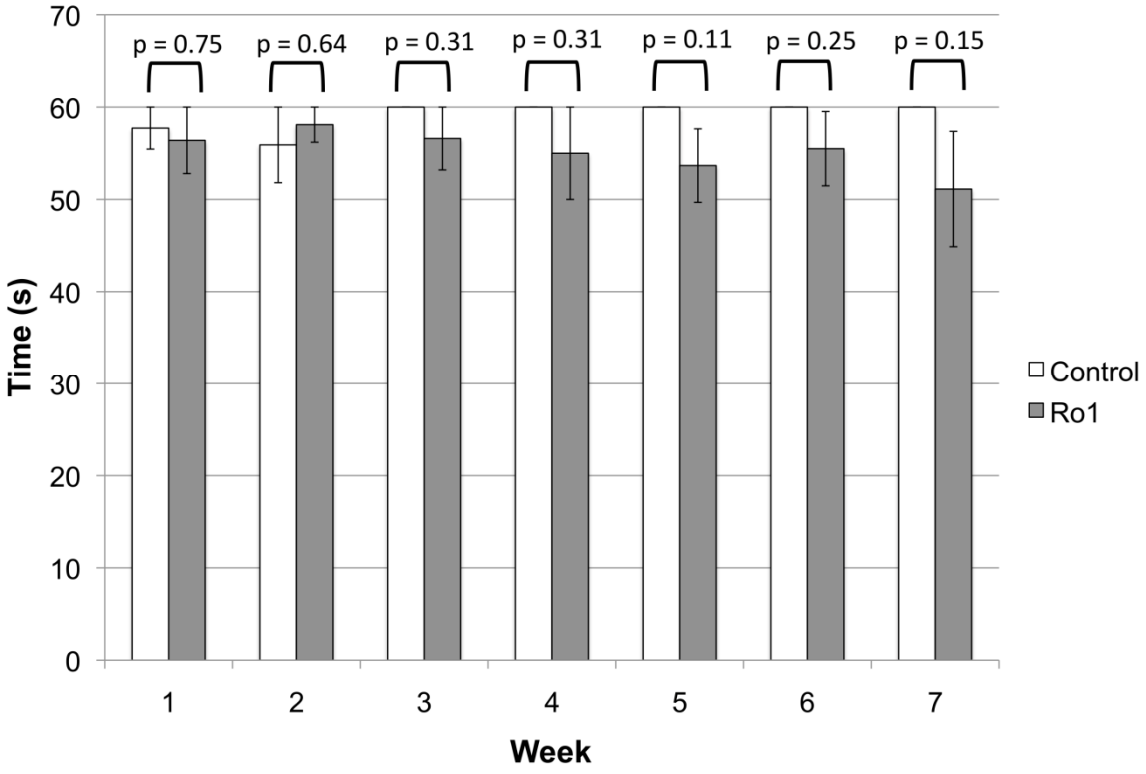

Figure 22. There are no differences in grip strength, as measured by the wire hang test, between Ro1 mice and littermate controls up to seven weeks following the removal of dox. The latency to fall off of a wire grid, with a maximum cut-off time of 60 seconds, was measured weekly for seven weeks. Control, n = 11; Ro1, n = 10.

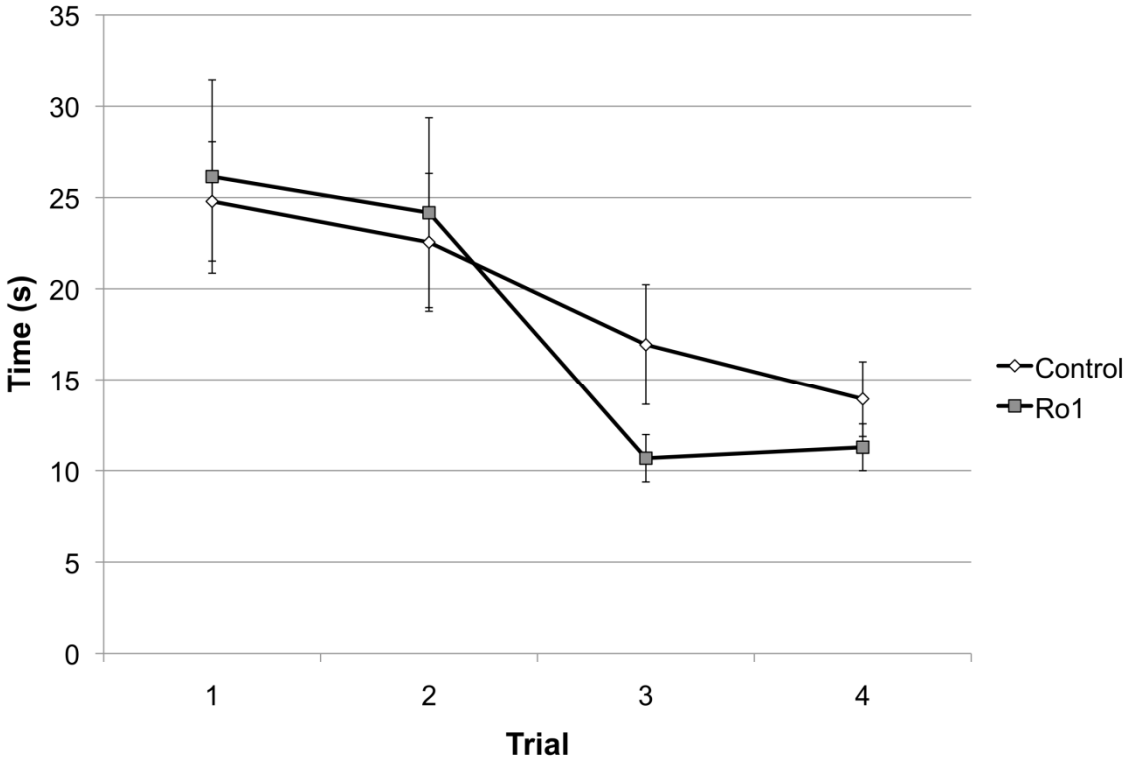

Figure 23. There are no differences in the latency to find the hidden platform in the Morris water maze test between Ro1 mice and littermate controls at 15 – 19 days off dox. The latency to find a hidden platform was tested over four consecutive days until the mice, as a group, reached the platform in less than 15 seconds. $p = 0.60$. Control, $n = 11$; Ro1, $n = 10$.

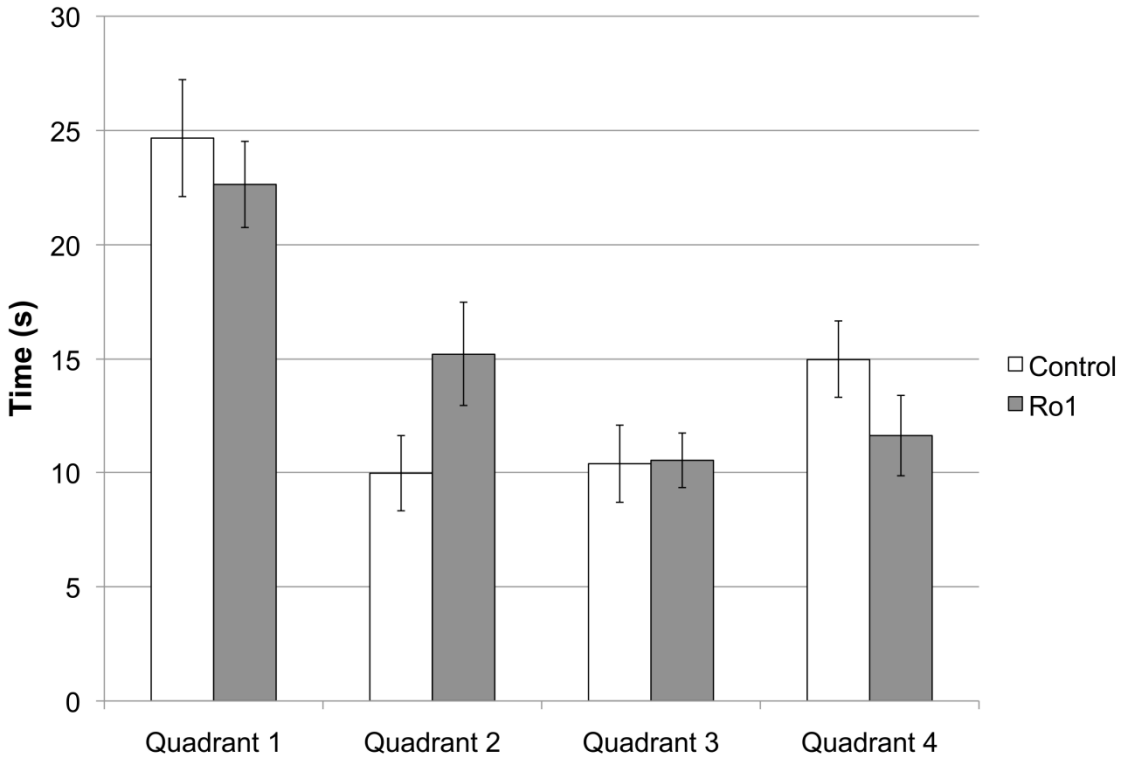

Figure 24. There are no differences in the hidden probe trial between Ro1 mice and littermate controls at 19 days off dox. The time spent in the quadrant where the escape platform had been previously located during the hidden acquisition trials was measured. p = 0.86. Control, n = 11; Ro1, n = 10.

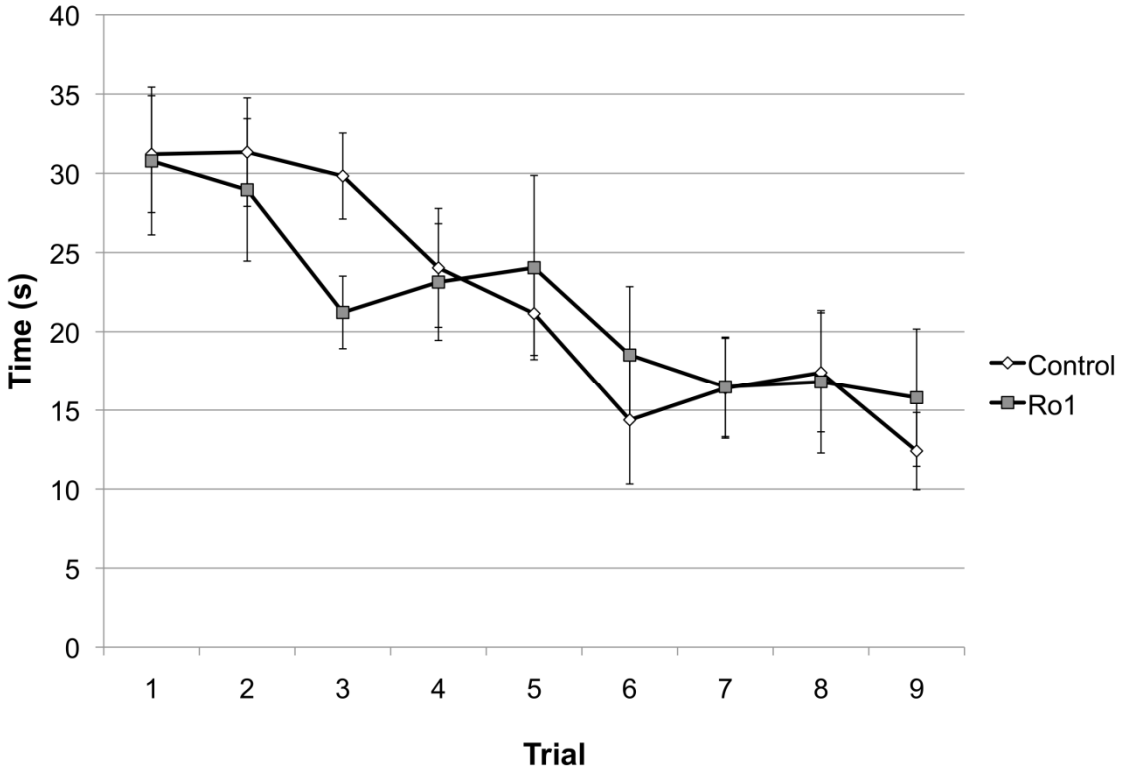

Figure 25. There are no differences in the latency to find the hidden platform during the reversal learning trials between Ro1 mice and littermate controls at 22 – 32 days off dox. The latency to find a hidden platform was tested over nine consecutive days until the mice, as a group, reached the platform in less than 15 seconds. $p = 0.93$. Control, $n = 11$; Ro1, $n = 10$.

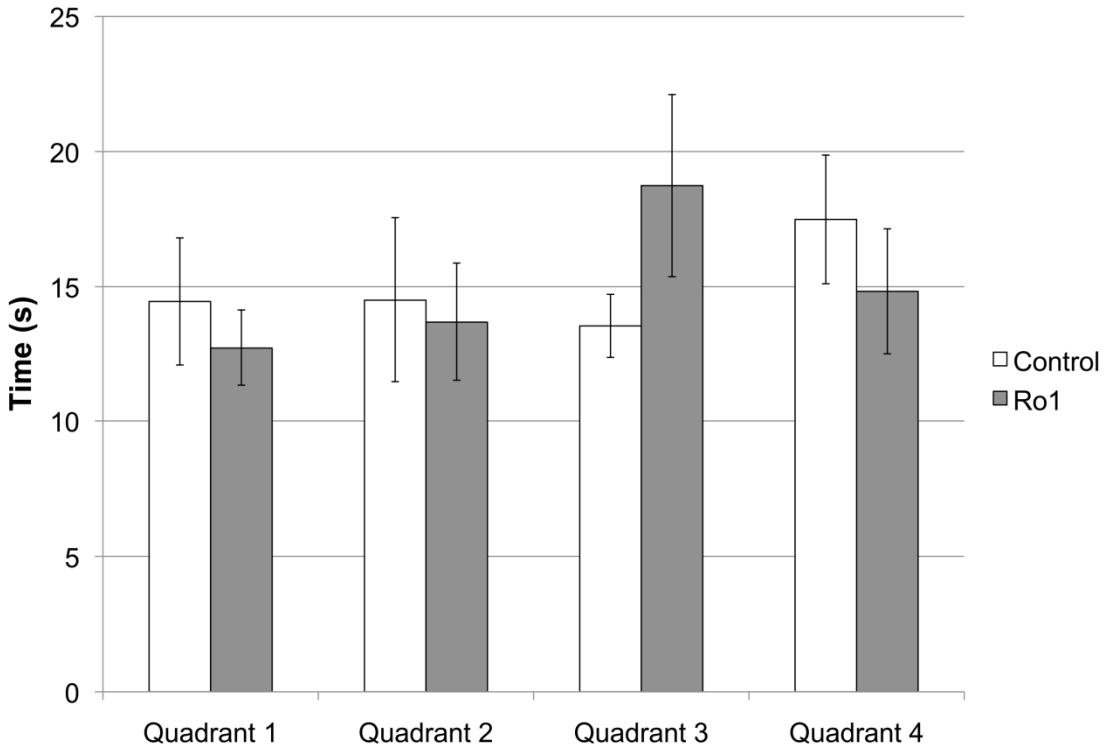

Figure 26. There are no differences in the reversal probe trial between Ro1 mice and littermate controls at 32 days off dox. The time spent in the quadrant where the escape platform had been previously located during the reversal learning trials was measured. $p = 0.17$. Control, $n = 11$; Ro1, $n = 10$.

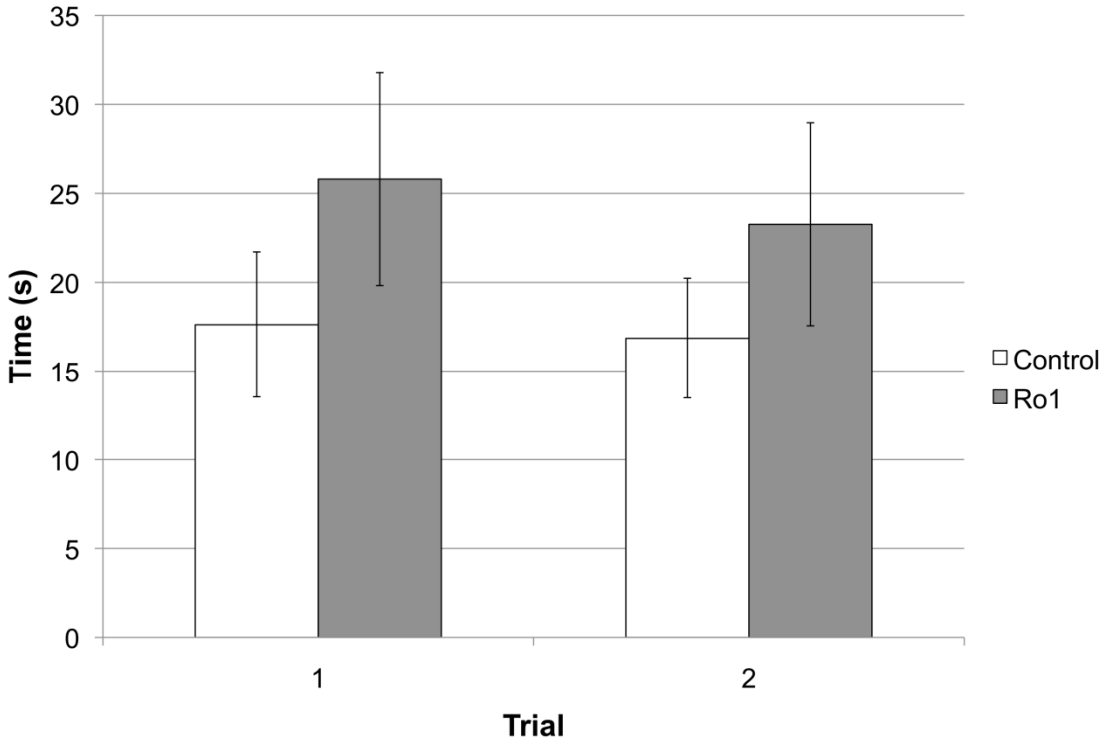

Figure 27. There are no significant differences in memory retention between Ro1 mice and littermate controls at 46 – 47 days off dox. After two weeks spent in their home cages, the mice were returned to the pool, and their latency to reach the hidden platform was recorded. The platform's location was the same as in the reversal learning trials. $p = 0.26$. Control, $n = 11$; Ro1, $n = 10$.

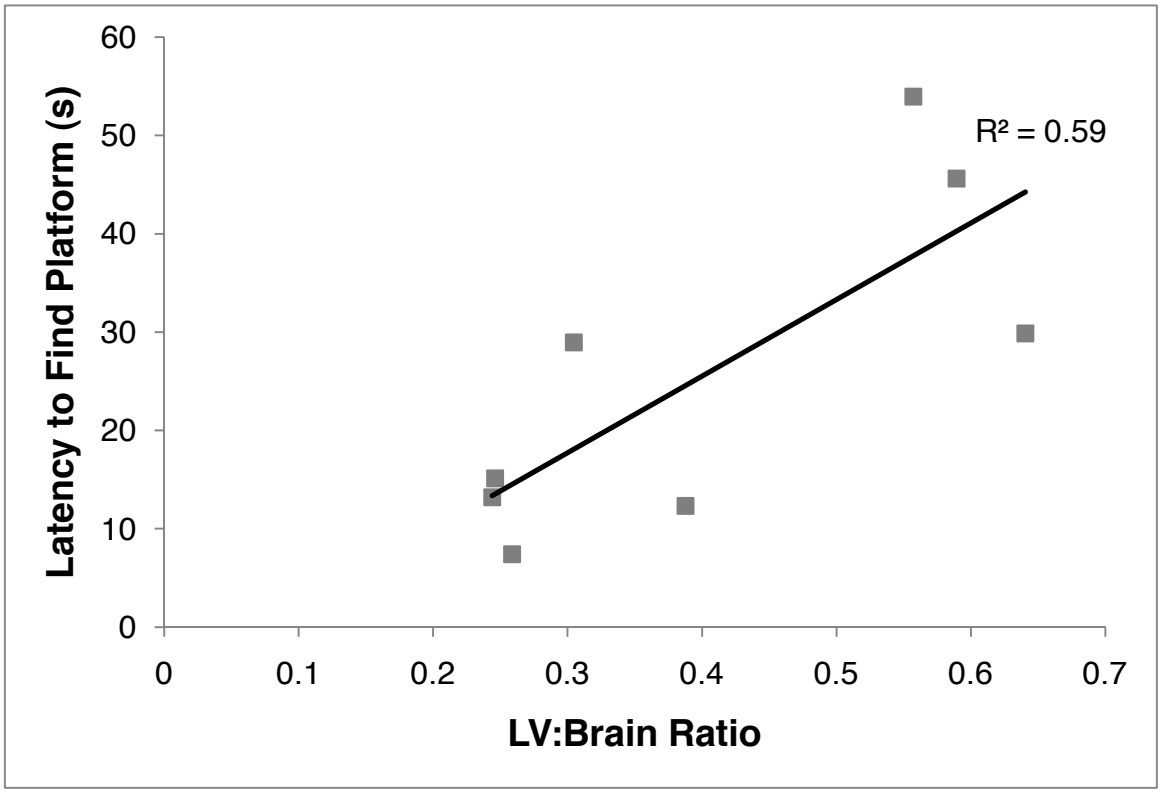

Figure 28. Lateral ventricle size is correlated to latency to find the hidden platform at 46 days off dox. Testing for memory retention of the location of the hidden platform was performed two weeks following the reversal probe trial. There was a moderate, but significant, correlation between the lateral ventricle to brain ratio and the latency to find the hidden platform at 46 days off dox (retention, trial 1), suggesting reduced memory in Ro1 mice ($r^2 = 0.59$; $p = 0.026$).

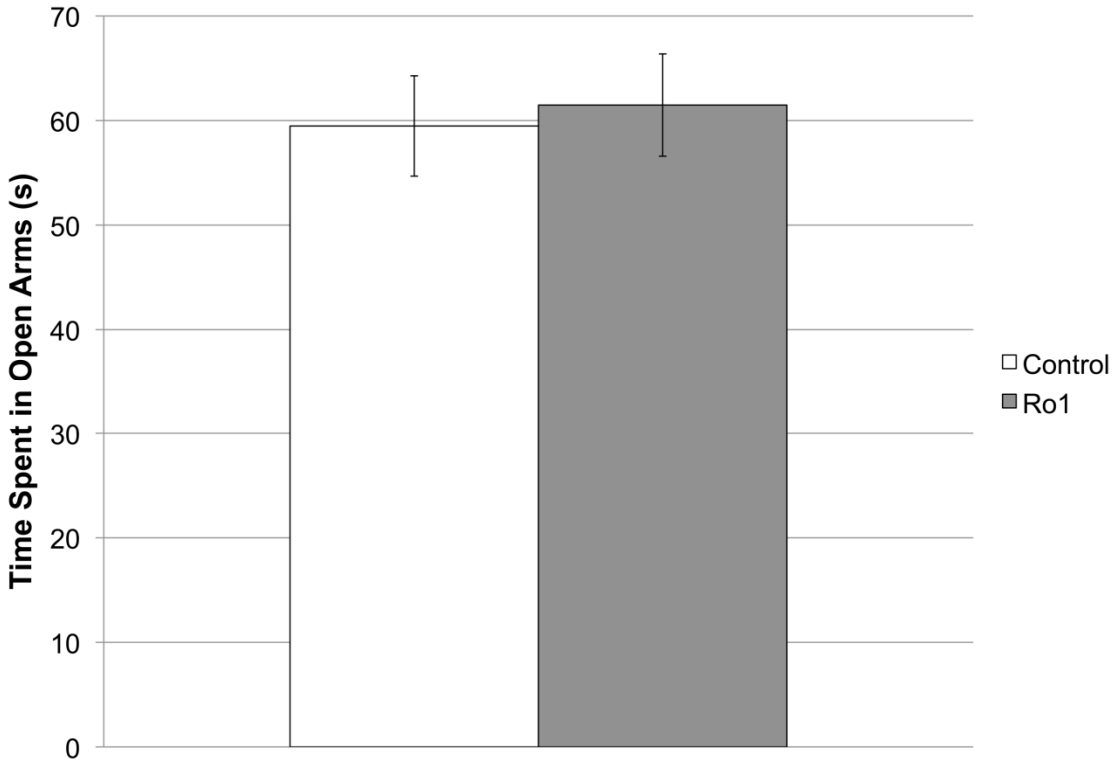

Figure 29. There are no differences between Ro1 mice and littermate controls in the elevated plus maze at 24 days off dox. Time spent in the open arms was recorded during a 5-min period on the elevated plus maze. $p = 0.78$. Control, $n = 17$; Ro1, $n = 13$.

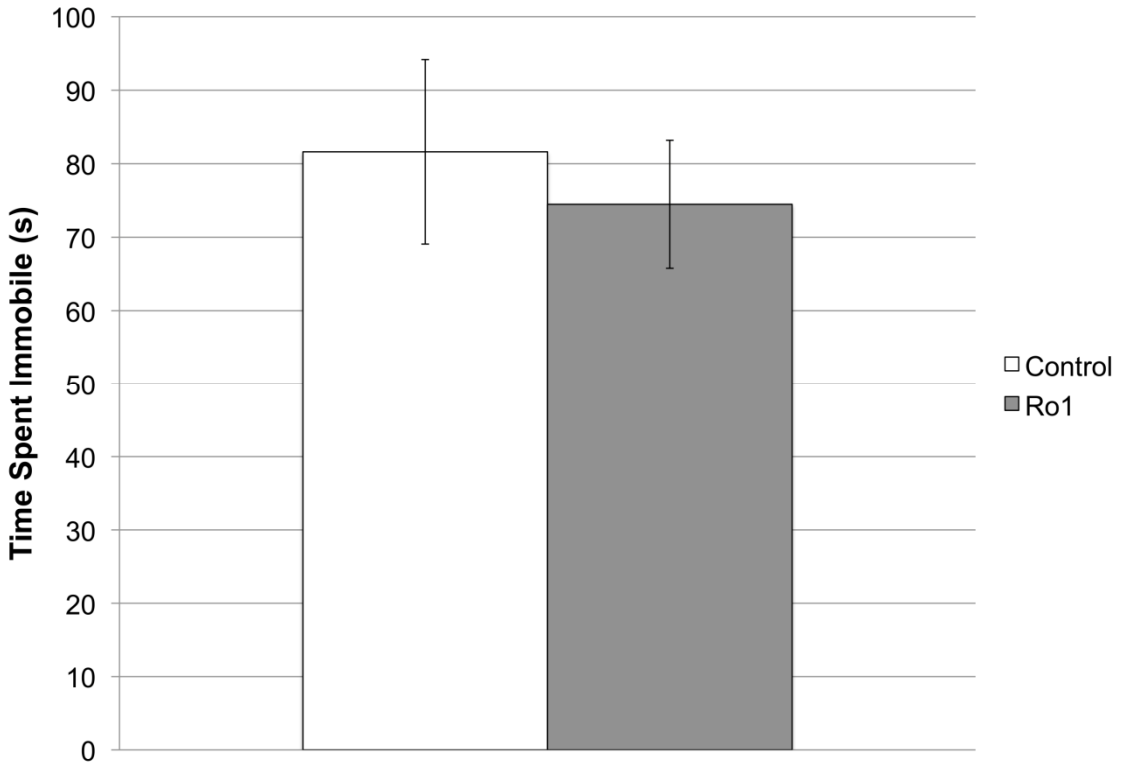

Figure 30. There are no differences between Ro1 mice and littermate controls in the forced swim test at 25 days off dox. Time spent immobile during a 6-min period was recorded. p = 0.66. Control, n = 17; Ro1, n = 13.

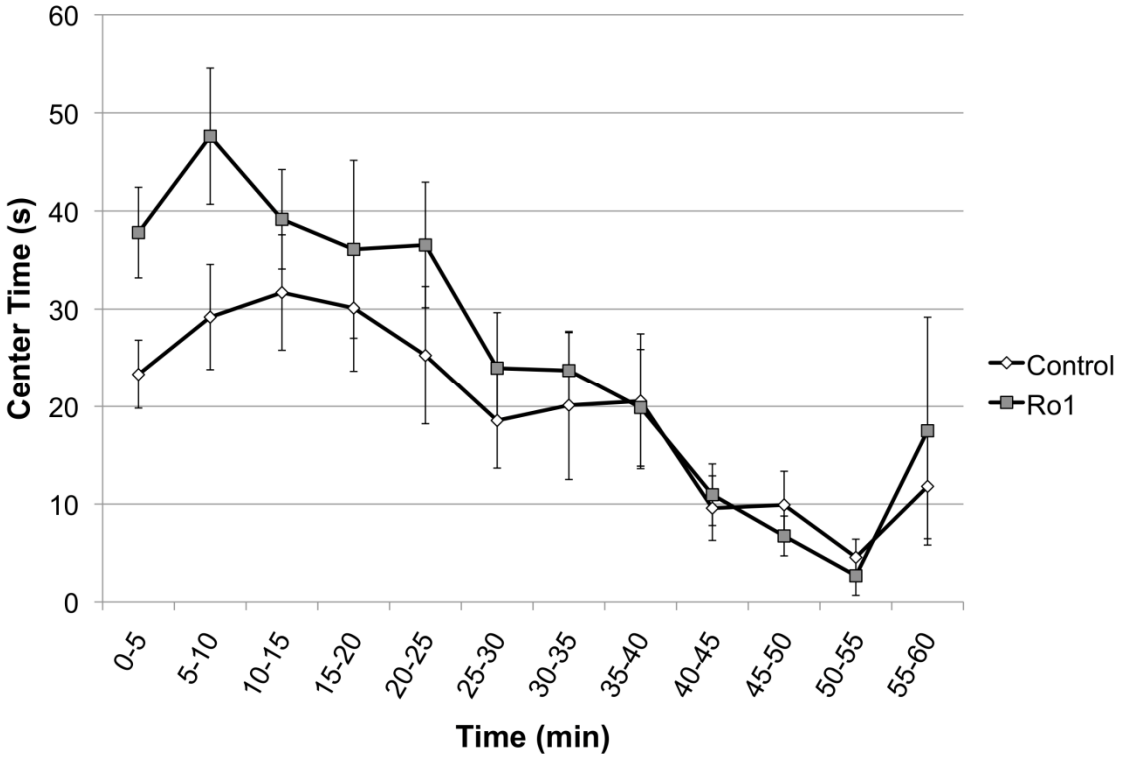

Figure 31. There are no differences between Ro1 mice and littermate controls in the time spent in the center of an open field at 31 days off dox. Center time was measured in 5-min bins over a 60 min period. $p = 0.33$. Control, $n = 17$; Ro1, $n = 13$.

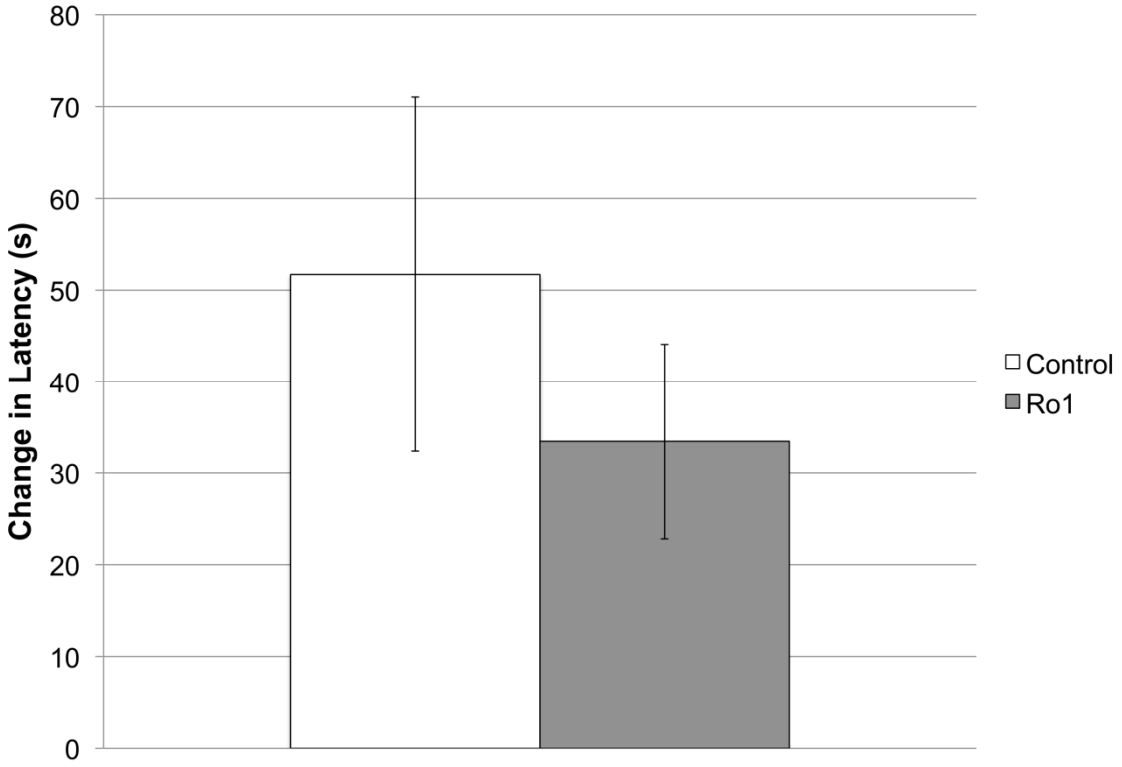

Figure 32. There are no differences in passive avoidance between Ro1 mice and littermate controls at 33 days off dox. On the first day of testing, mice learned to associate a mild footshock with the dark chamber. The change in latency to enter the dark chamber between the two days was recorded. $p = 0.45$. Control, $n = 17$; Ro1, $n = 13$.

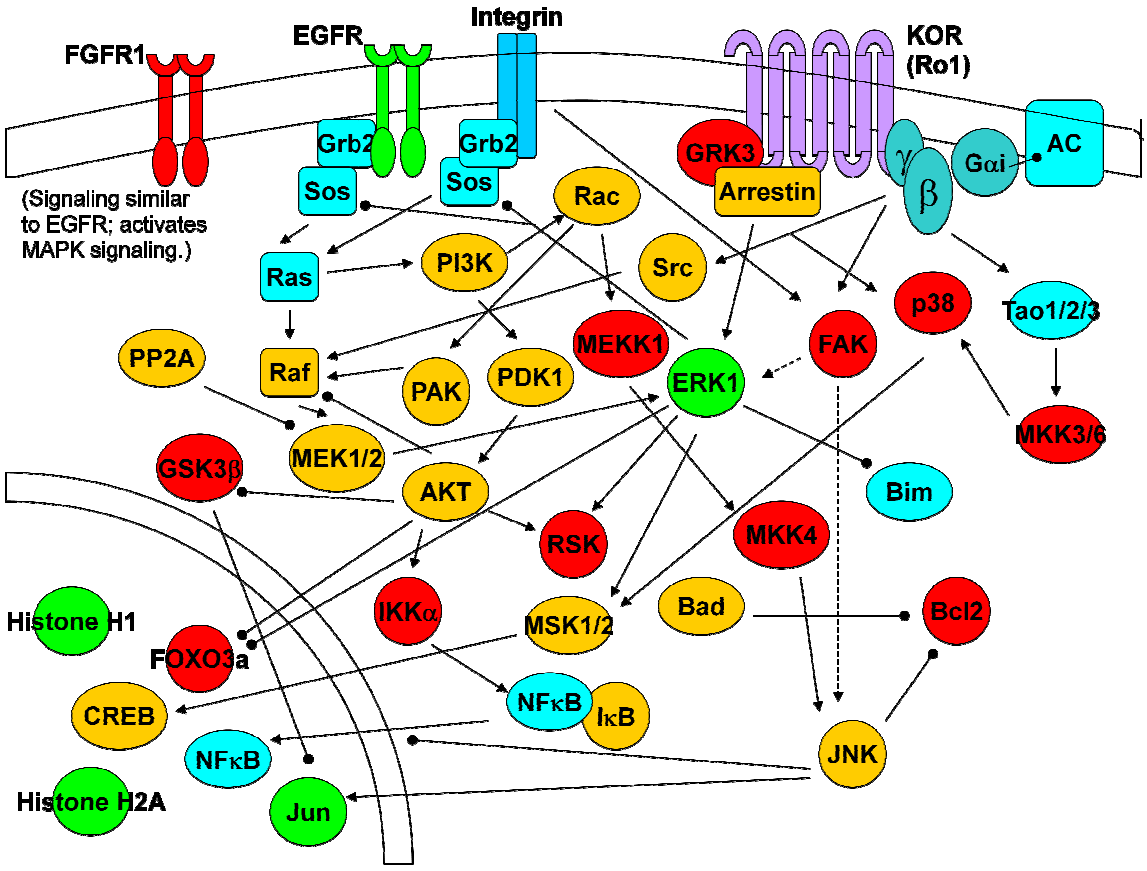

Figure 33. Signaling pathways altered in the Ro1 model of hydrocephalus. "Hits" generated from the Kinexus antibody microarray analysis were entered into literature mining tools (Chilibot, chilibot.net) to create a signaling pathway diagram to better visualize pathways altered in the Ro1 model of hydrocephalus. Pointed arrows represent protein "activation", while circle-headed arrows represent "inhibition." Lime green represents proteins upregulated in Ro1 mice, red represents proteins downregulated in Ro1 mice, and blue signifies that this protein was not present on the array. Yellow represents proteins present on the array that were not changed or for which quality of the spot on the array was highly suspect.

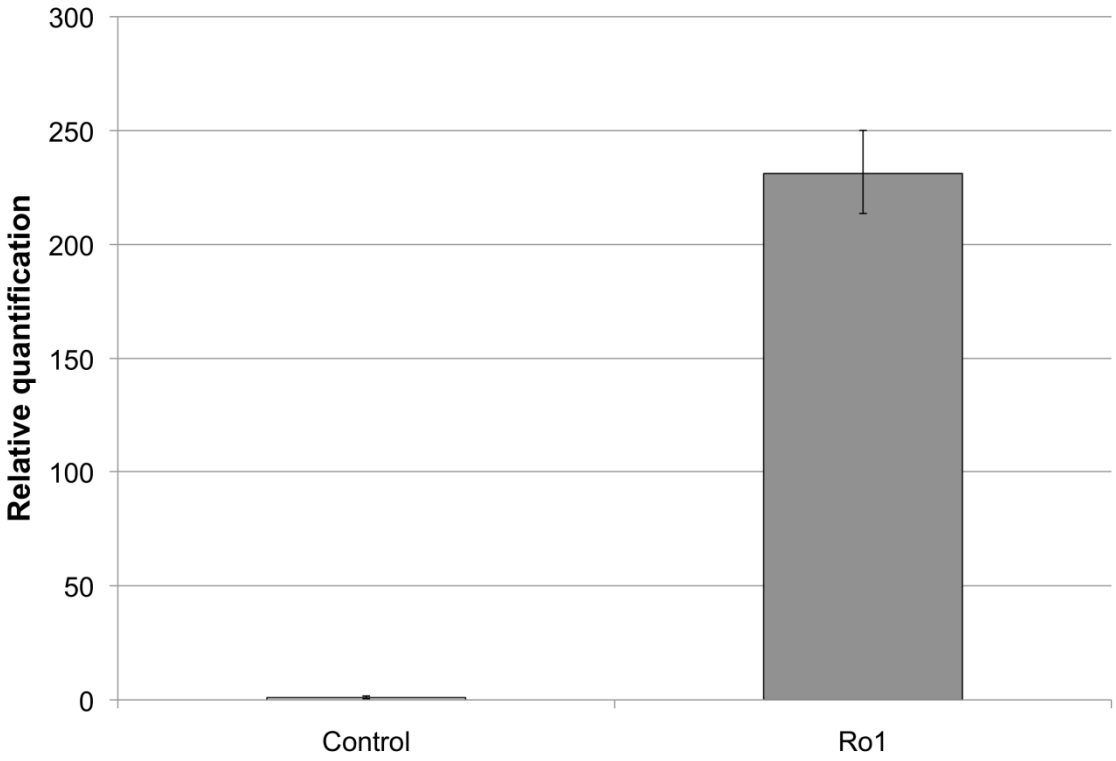

Figure 34. Ro1 receptor mRNA is highly expressed in primary astrocyte cultures from Ro1 pups maintained off dox, but not in cultures from littermate controls. Real-time PCR was used to measure Ro1 receptor mRNA expression levels using human KOR primers in lysates isolated from primary astrocyte cultures.

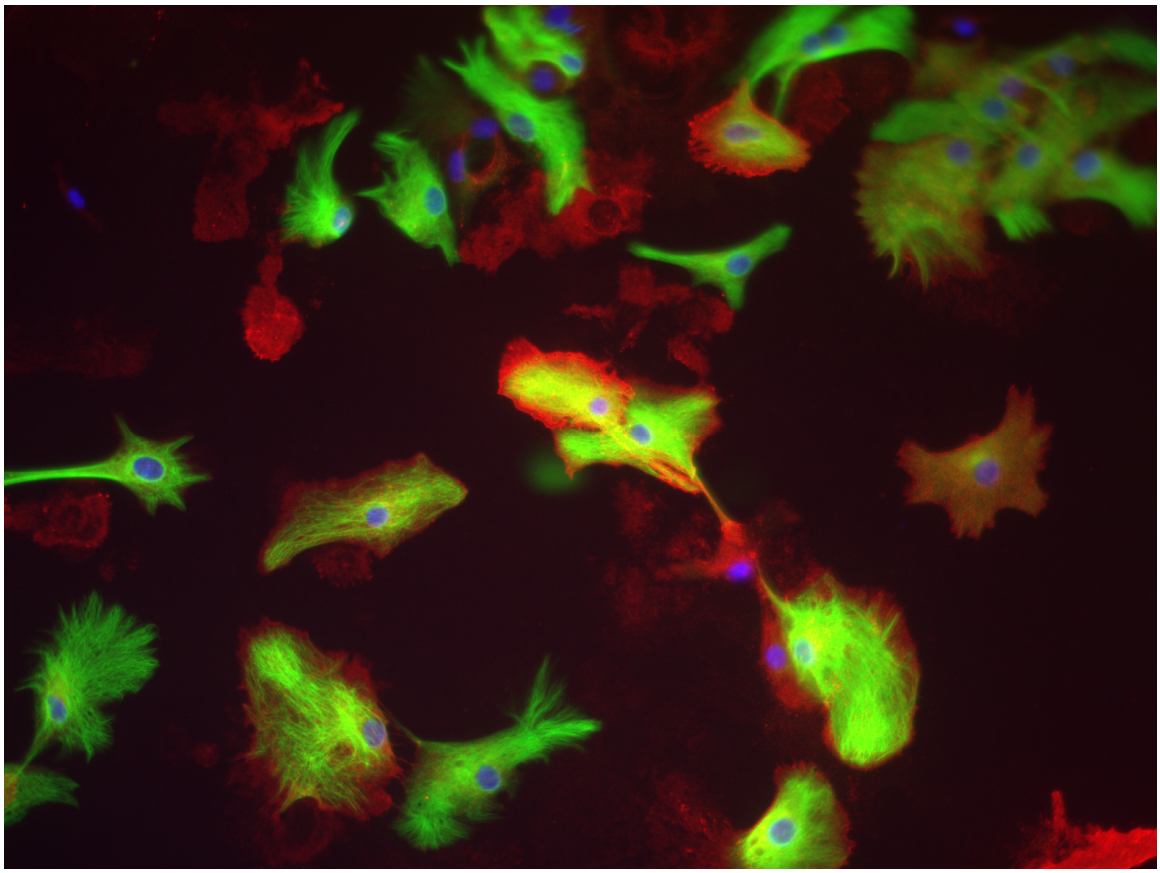

Figure 35. Cultured primary astrocytes express the Ro1 receptor. Staining for GFAP-positive cultured astrocytes (green) showed colocalization with the FLAG-tagged Ro1 receptor (red).

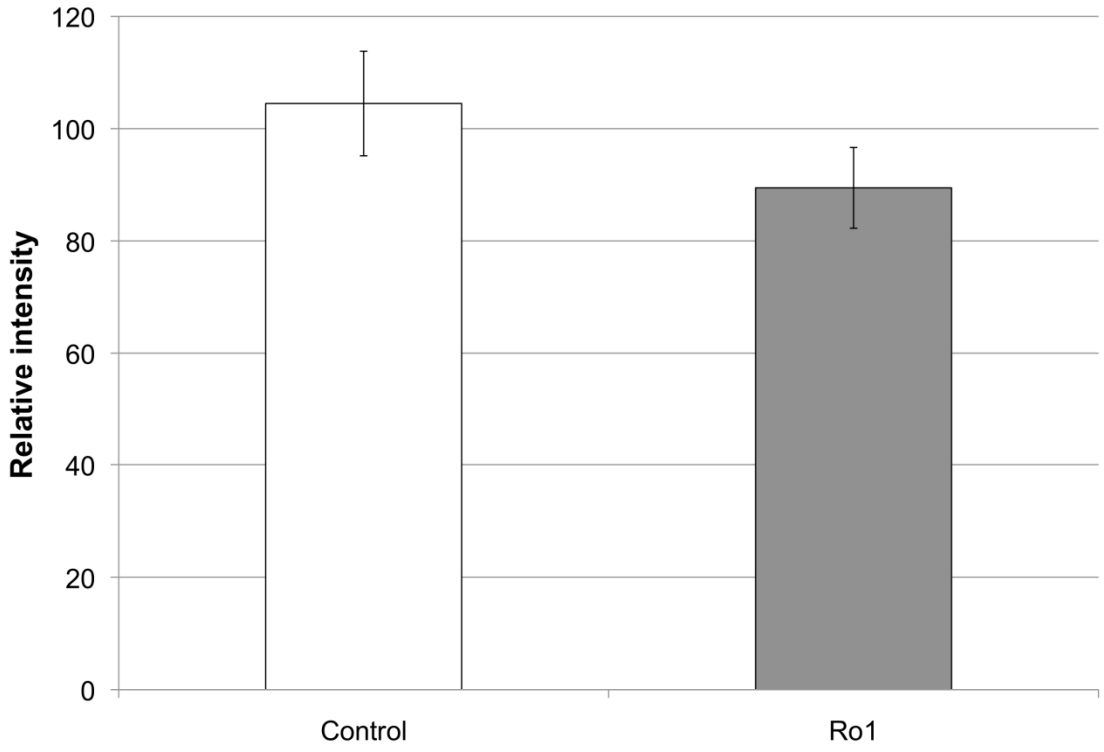

Figure 36. Aquaporin 4 levels show a decreasing trend in Ro1 mice as compared to littermate controls at 18 d off dox. Immunohistochemistry for aquaporin 4 was quantified in the ependymal and subependymal regions using MatLab software to analyze staining intensity over background. $p = 0.21$, $n = 12$.

References

Albeck, M.J., Skak, C., Nielsen, P.R., Olsen, K.S., Borgesen, S.E., Gjerris, F., 1998. Age dependency of resistance to cerebrospinal fluid outflow. J. Neurosurg. 89, 275-278.

Alcolado, R., Weller, R.O., Parrish, E.P., Garrod, D., 1988. The cranial arachnoid and pia mater in man: anatomical and ultrastructural observations. Neuropathol. Appl. Neurobiol. 14, 1-17.

al-Shroof, M., Karnik, A.M., Karnik, A.A., Longshore, J., Sliman, N.A., Khan, F.A., 2001. Ciliary dyskinesia associated with hydrocephalus and mental retardation in a Jordanian family. Mayo Clin. Proc. 76, 1219-1224.

Ambrosino, M.M., Hernanz-Schulman, M., Genieser, N.B., Wisoff, J., Epstein, F., 1988. Brain tumors in infants less than a year of age. Pediatr. Radiol. 19, 6-8.

Anton, E.S., Ghashghaei, H.T., Weber, J.L., McCann, C., Fischer, T.M., Cheung, I.D., Gassmann, M., Messing, A., Klein, R., Schwab, M.H., Lloyd, K.C., Lai, C., 2004. Receptor tyrosine kinase ErbB4 modulates neuroblast migration and placement in the adult forebrain. Nat. Neurosci. 7, 1319-1328.

Ashwell, J.D., 2006. The many paths to p38 mitogen-activated protein kinase activation in the immune system. Nat. Rev. Immunol. 6, 532-540.

Bakar, E.E., Bakar, B., 2010. Neuropsychological assessment of adult patients with shunted hydrocephalus. J. Korean Neurosurg. Soc. 47, 191-198.

Balasubramaniam, J., Del Bigio, M.R., 2002. Analysis of age-dependant alteration in the brain gene expression profile following induction of hydrocephalus in rats. Exp. Neurol. 173, 105-113.

Banizs, B., Pike, M.M., Millican, C.L., Ferguson, W.B., Komlosi, P., Sheetz, J., Bell, P.D., Schwiebert, E.M., Yoder, B.K., 2005. Dysfunctional cilia lead to altered ependyma and choroid plexus function, and result in the formation of hydrocephalus. Development. 132, 5329-5339.

Bannister, C.M., Mundy, J.E., 1979. Some scanning electron microscopic observations of the ependymal surface of the ventricles of hydrocephalic Hy3 mice and a human infant. Acta Neurochir. (Wien). 46, 159-168.

Bateman, G.A., 2000. Vascular compliance in normal pressure hydrocephalus. AJNR Am. J. Neuroradiol. 21, 1574-1585.

Bech, R.A., Juhler, M., Waldemar, G., Klinken, L., Gjerris, F., 1997. Frontal brain and leptomeningeal biopsy specimens correlated with cerebrospinal fluid outflow resistance and B-wave activity in patients suspected of normal-pressure hydrocephalus. Neurosurgery. 40, 497-502.

Becker, L.E., 1992. Infections of the developing brain. AJNR Am. J. Neuroradiol. 13, 537-549.

Bell, W.E., 1992. Bacterial meningitis in children. Selected aspects. Pediatr. Clin. North Am. 39, 651-668.

Bellur, S.N., Chandra, V., McDonald, L.W., 1980. Arachnoidal cell hyperplasia. Its relationship to aging and chronic renal failure. Arch. Pathol. Lab. Med. 104, 414-416.

Beni-Adani, L., Biani, N., Ben-Sirah, L., Constantini, S., 2006. The occurrence of obstructive vs absorptive hydrocephalus in newborns and infants: relevance to treatment choices. Childs Nerv. Syst. 22, 1543-1563.

Bergsneider, M., 2001. Evolving concepts of cerebrospinal fluid physiology. Neurosurg. Clin. N. Am. 12, 631-8, vii.

Blackshear, P.J., Graves, J.P., Stumpo, D.J., Cobos, I., Rubenstein, J.L., Zeldin, D.C., 2003. Graded phenotypic response to partial and complete deficiency of a brain-specific transcript variant of the winged helix transcription factor RFX4. Development. 130, 4539-4552.

Bloch, O., Auguste, K.I., Manley, G.T., Verkman, A.S., 2006. Accelerated progression of kaolin-induced hydrocephalus in aquaporin-4-deficient mice. J. Cereb. Blood Flow Metab. 26, 1527-1537.

Boassa, D., Yool, A.J., 2005. Physiological roles of aquaporins in the choroid plexus. Curr. Top. Dev. Biol. 67, 181-206.

Boesch, C., Issakainen, J., Kewitz, G., Kikinis, R., Martin, E., Boltshauser, E., 1989. Magnetic resonance imaging of the brain in congenital cytomegalovirus infection. Pediatr. Radiol. 19, 91-93.

Boillat, C.A., Jones, H.C., Kaiser, G.L., 1999. Aqueduct stenosis in hydrocephalus: ultrastructural investigation in neonatal H-Tx rat brain. Eur. J. Pediatr. Surg. 9 Suppl 1, 44-46.

Bondurant, C.P., Jimenez, D.F., 1995. Epidemiology of cerebrospinal fluid shunting. Pediatr. Neurosurg. 23, 254-8; discussion 259.

Bradley, W.G.,Jr, 2001. Diagnostic tools in hydrocephalus. Neurosurg. Clin. N. Am. 12, 661-84, viii.

Bret, P., Chazal, J., 1995. Chronic ("normal pressure") hydrocephalus in childhood and adolescence. A review of 16 cases and reappraisal of the syndrome. Childs Nerv. Syst. 11, 687-691.

Brightman, M.W., Reese, T.S., 1969. Junctions between intimately apposed cell membranes in the vertebrate brain. J. Cell Biol. 40, 648-677.

Brodbelt, A., Stoodley, M., 2007. CSF pathways: a review. Br. J. Neurosurg. 21, 510-520.
Bruchas, M.R., Chavkin, C., 2010. Kinase cascades and ligand-directed signaling at the kappa opioid receptor. Psychopharmacology (Berl). 210, 137-147.

Bruchas, M.R., Xu, M., Chavkin, C., 2008. Repeated swim stress induces kappa opioid-mediated activation of extracellular signal-regulated kinase 1/2. Neuroreport. 19, 1417-1422.

Bruchas, M.R., Land, B.B., Aita, M., Xu, M., Barot, S.K., Li, S., Chavkin, C., 2007a. Stress-induced p38 mitogen-activated protein kinase activation mediates kappa-opioid-dependent dysphoria. J. Neurosci. 27, 11614-11623.

Bruchas, M.R., Yang, T., Schreiber, S., Defino, M., Kwan, S.C., Li, S., Chavkin, C., 2007b. Long-acting kappa opioid antagonists disrupt receptor signaling and produce noncompetitive effects by activating c-Jun N-terminal kinase. J. Biol. Chem. 282, 29803-29811.

Bruchas, M.R., Macey, T.A., Lowe, J.D., Chavkin, C., 2006. Kappa opioid receptor activation of p38 MAPK is GRK3- and arrestin-dependent in neurons and astrocytes. J. Biol. Chem. 281, 18081-18089.

Bruni, J.E., 1998. Ependymal development, proliferation, and functions: a review. Microsc. Res. Tech. 41, 2-13.

Bruni, J.E., Reddy, K., 1987. Ependyma of the central canal of the rat spinal cord: a light and transmission electron microscopic study. J. Anat. 152, 55-70.

Bruni, J.E., Del Bigio, M.R., Clattenburg, R.E., 1985. Ependyma: normal and pathological. A review of the literature. Brain Res. 356, 1-19.

Bundgaard, M., 1986. Pathways across the vertebrate blood-brain barrier: morphological viewpoints. Ann. N. Y. Acad. Sci. 481, 7-19.

Bush, A., 2000. Primary ciliary dyskinesia. Acta Otorhinolaryngol. Belg. 54, 317-324.

Cahoy, J.D., Emery, B., Kaushal, A., Foo, L.C., Zamanian, J.L., Christopherson, K.S., Xing, Y., Lubischer, J.L., Krieg, P.A., Krupenko, S.A., Thompson, W.J., Barres, B.A., 2008. A transcriptome database for astrocytes, neurons, and oligodendrocytes: a new resource for understanding brain development and function. J. Neurosci. 28, 264-278.

Card, J.P., Rafols, J.A., 1978. Tanycytes of the third ventricle of the neonatal rat: a Golgi study. Am. J. Anat. 151, 173-189.

Cardinali, D.P., Vacas, M.I., Gejman, P.V., 1981. The sympathetic superior cervical ganglia as peripheral neuroendocrine centers. J. Neural Transm. 52, 1-21.

Cherian, S., Whitelaw, A., Thoresen, M., Love, S., 2004. The pathogenesis of neonatal post-hemorrhagic hydrocephalus. Brain Pathol. 14, 305-311.

Chodobski, A., Szmydynger-Chodobska, J., 2001. Choroid plexus: target for polypeptides and site of their synthesis. Microsc. Res. Tech. 52, 65-82.

Clark, R.G., Milhorat, T.H., 1970. Experimental hydrocephalus. 3. Light microscopic findings in acute and subacute obstructive hydrocephalus in the monkey. J. Neurosurg. 32, 400-413.

Clayton, C.C., Xu, M., Chavkin, C., 2009. Tyrosine phosphorylation of Kir3 following kappa-opioid receptor activation of p38 MAPK causes heterologous desensitization. J. Biol. Chem. 284, 31872-31881.

Coates, T.L., Hinshaw, D.B.,Jr, Peckman, N., Thompson, J.R., Hasso, A.N., Holshouser, B.A., Knierim, D.S., 1989. Pediatric choroid plexus neoplasms: MR, CT, and pathologic correlation. Radiology. 173, 81-88.

Conover, J.C., Doetsch, F., Garcia-Verdugo, J.M., Gale, N.W., Yancopoulos, G.D., Alvarez-Buylla, A., 2000. Disruption of Eph/ephrin signaling affects migration and proliferation in the adult subventricular zone. Nat. Neurosci. 3, 1091-1097.

Coward, P., Wada, H.G., Falk, M.S., Chan, S.D., Meng, F., Akil, H., Conklin, B.R., 1998a. Controlling signaling with a specifically designed Gi-coupled receptor. Proc. Natl. Acad. Sci. U. S. A. 95, 352-357.

Coward, P., Wada, H.G., Falk, M.S., Chan, S.D., Meng, F., Akil, H., Conklin, B.R., 1998b. Controlling signaling with a specifically designed Gi-coupled receptor. Proc. Natl. Acad. Sci. U. S. A. 95, 352-357.

da Silva Lopes, L., Slobodian, I., Del Bigio, M.R., 2009. Characterization of juvenile and young adult mice following induction of hydrocephalus with kaolin. Exp. Neurol.

Dahme, M., Bartsch, U., Martini, R., Anliker, B., Schachner, M., Mantei, N., 1997. Disruption of the mouse L1 gene leads to malformations of the nervous system. Nat. Genet. 17, 346-349.

Dandy, W.E., 1919. Experimental Hydrocephalus. Ann. Surg. 70, 129-142.

Danilov, A.I., Gomes-Leal, W., Ahlenius, H., Kokaia, Z., Carlemalm, E., Lindvall, O., 2009. Ultrastructural and antigenic properties of neural stem cells and their progeny in adult rat subventricular zone. Glia. 57, 136-152.

DaSilva, M.C., 2004. Pathophysiology of Hydrocephalus. In: Cinalli, G., Maixner, W.J., Sainte-Rose, C. (Eds.), Pediatric Hydrocephalus. Springer-Verlag, New York, pp. 65.

Davis, S.L., Tooley, W.H., Hunt, J.V., 1987. Developmental outcome following posthemorrhagic hydrocephalus in preterm infants. Comparison of twins discordant for hydrocephalus. Am. J. Dis. Child. 141, 1170-1174.

Davson, H., Oldendorf, W.H., 1967. Symposium on membrane transport. Transport in the central nervous system. Proc. R. Soc. Med. 60, 326-329.

Davy, B.E., Robinson, M.L., 2003. Congenital hydrocephalus in hy3 mice is caused by a frameshift mutation in Hydin, a large novel gene. Hum. Mol. Genet. 12, 1163-1170.

Dawe, H.R., Shaw, M.K., Farr, H., Gull, K., 2007. The hydrocephalus inducing gene product, Hydin, positions axonemal central pair microtubules. BMC Biol. 5, 33.

De Santi, M.M., Magni, A., Valletta, E.A., Gardi, C., Lungarella, G., 1990. Hydrocephalus, bronchiectasis, and ciliary aplasia. Arch. Dis. Child. 65, 543-544.

DE, S.N., 1950. A study of the changes in the brain in experimental internal hydrocephalus. J. Pathol. Bacteriol. 62, 197-208.

Del Bigio, M.R., 2004. Cellular damage and prevention in childhood hydrocephalus. Brain Pathol. 14, 317-324.

Del Bigio, M.R., Wilson, M.J., Enno, T., 2003. Chronic hydrocephalus in rats and humans: white matter loss and behavior changes. Ann. Neurol. 53, 337-346.

Del Bigio, M.R., Wang, X., Wilson, M.J., 2002. Sodium channel-blocking agents are not of benefit to rats with kaolin-induced hydrocephalus. Neurosurgery. 51, 460-6; discussion 466-7.

Del Bigio, M.R., 2001. Pathophysiologic consequences of hydrocephalus. Neurosurg. Clin. N. Am. 12, 639-49, vii.

Del Bigio, M.R., Massicotte, E.M., 2001. Protective effect of nimodipine on behavior and white matter of rats with hydrocephalus. J. Neurosurg. 94, 788-794.

Del Bigio, M.R., Zhang, Y.W., 1998. Cell death, axonal damage, and cell birth in the immature rat brain following induction of hydrocephalus. Exp. Neurol. 154, 157-169.

Del Bigio, M.R., Crook, C.R., Buist, R., 1997. Magnetic resonance imaging and behavioral analysis of immature rats with kaolin-induced hydrocephalus: pre- and postshunting observations. Exp. Neurol. 148, 256-264.

Del Bigio, M.R., da Silva, M.C., Drake, J.M., Tuor, U.I., 1994. Acute and chronic cerebral white matter damage in neonatal hydrocephalus. Can. J. Neurol. Sci. 21, 299-305.

Del Bigio, M.R., 1993. Neuropathological changes caused by hydrocephalus. Acta Neuropathol. 85, 573-585.

Del Bigio, M.R., Bruni, J.E., 1991. Silicone oil-induced hydrocephalus in the rabbit. Childs Nerv. Syst. 7, 79-84.

Del Bigio, M.R., Bruni, J.E., 1988. Changes in periventricular vasculature of rabbit brain following induction of hydrocephalus and after shunting. J. Neurosurg. 69, 115-120.

Del Bigio, M.R., Bruni, J.E., Fewer, H.D., 1985. Human neonatal hydrocephalus. An electron microscopic study of the periventricular tissue. J. Neurosurg. 63, 56-63.

di Rocco, C., Caldarelli, M., di Trapani, G., 1981. Infratentorial arachnoid cysts in children. Childs Brain. 8, 119-133.

Di Rocco, C., Di Trapani, G., Pettorossi, V.E., Caldarelli, M., 1979. On the pathology of experimental hydrocephalus induced by artificial increase in endoventricular CSF pulse pressure. Childs Brain. 5, 81-95.

Di Rocco, C., Di Trapani, G., Maira, G., Bentivoglio, M., Macchi, G., Rossi, G.F., 1977. Anatomo-clinical correlations in normotensive hydrocephalus. Reports on three cases. J. Neurol. Sci. 33, 437-452.

Di Terlizzi, R., Platt, S., 2006. The function, composition and analysis of cerebrospinal fluid in companion animals: part I - function and composition. Vet. J. 172, 422-431.

Doetsch, F., Caille, I., Lim, D.A., Garcia-Verdugo, J.M., Alvarez-Buylla, A., 1999a. Subventricular zone astrocytes are neural stem cells in the adult mammalian brain. Cell. 97, 703-716.

Doetsch, F., Caille, I., Lim, D.A., Garcia-Verdugo, J.M., Alvarez-Buylla, A., 1999b. Subventricular zone astrocytes are neural stem cells in the adult mammalian brain. Cell. 97, 703-716.

Doetsch, F., Garcia-Verdugo, J.M., Alvarez-Buylla, A., 1997. Cellular composition and three-dimensional organization of the subventricular germinal zone in the adult mammalian brain. J. Neurosci. 17, 5046-5061.

Dohrmann, G.J., 1971. The choroid plexus in experimental hydrocephalus. A light and electron microscopic study in normal, hydrocephalic, and shunted hydrocephalic dogs. J. Neurosurg. 34, 56-69.

Dominguez-Pinos, M.D., Paez, P., Jimenez, A.J., Weil, B., Arraez, M.A., Perez-Figares, J.M., Rodriguez, E.M., 2005. Ependymal denudation and alterations of the subventricular zone occur in human fetuses with a moderate communicating hydrocephalus. J. Neuropathol. Exp. Neurol. 64, 595-604.

Drake, J.M., Kestle, J.R., Tuli, S., 2000. CSF shunts 50 years on--past, present and future. Childs Nerv. Syst. 16, 800-804.

Drake, J.M., Potts, D.G., Lemaire, C., 1989. Magnetic resonance imaging of silastic-induced canine hydrocephalus. Surg. Neurol. 31, 28-40.

Edwards, R.J., Dombrowski, S.M., Luciano, M.G., Pople, I.K., 2004. Chronic hydrocephalus in adults. Brain Pathol. 14, 325-336.

Egnor, M., Zheng, L., Rosiello, A., Gutman, F., Davis, R., 2002. A model of pulsations in communicating hydrocephalus. Pediatr. Neurosurg. 36, 281-303.

Elvidge, A.R., Branch, C.L., Thompson, G.B., 1957. Observations in a case of hydrocephalus treated with diamox. J. Neurosurg. 14, 628-38; discussion 638-9.

Erler, T., Klaber, H.G., 2001. Treatment of posthemorrhagic hydrocephalus with intraventricular administration of recombinant plasminogen activator (rt-PA) and dexamethasone--possible prevention of permanent shunt implantation?. Z. Geburtshilfe Neonatol. 205, 27-32.

Estanol, B.V., 1981. Gait apraxia in communicating hydrocephalus. J. Neurol. Neurosurg. Psychiatry. 44, 305-308.

Faraci, F.M., Mayhan, W.G., Heistad, D.D., 1990. Effect of vasopressin on production of cerebrospinal fluid: possible role of vasopressin (V1)-receptors. Am. J. Physiol. 258, R94-8.

Feigin, I.H., 1983. White matter myelinolysis after brain edema. Bull. Soc. Belge Ophtalmol. 208 Pt 1, 481-482.

Fishman, R.A., Greer, M., 1963. Experimental obstructive hydrocephalus. Changes in the cerebrum. Arch. Neurol. 8, 156-161.

Fletcher, J.M., McCauley, S.R., Brandt, M.E., Bohan, T.P., Kramer, L.A., Francis, D.J., Thorstad, K., Brookshire, B.L., 1996. Regional brain tissue composition in children with hydrocephalus. Relationships with cognitive development. Arch. Neurol. 53, 549-557.

Flood, C., Akinwunmi, J., Lagord, C., Daniel, M., Berry, M., Jackowski, A., Logan, A., 2001. Transforming growth factor-beta1 in the cerebrospinal fluid of patients with subarachnoid hemorrhage: titers derived from exogenous and endogenous sources. J. Cereb. Blood Flow Metab. 21, 157-162.

Foundas, A.L., Zipin, D., Browning, C.A., 1998. Age-related changes of the insular cortex and lateral ventricles: conventional MRI volumetric measures. J. Neuroimaging. 8, 216-221.

Fransen, E., D'Hooge, R., Van Camp, G., Verhoye, M., Sijbers, J., Reyniers, E., Soriano, P., Kamiguchi, H., Willemsen, R., Koekkoek, S.K., De Zeeuw, C.I., De Deyn, P.P., Van der Linden, A., Lemmon, V., Kooy, R.F., Willems, P.J., 1998. L1 knockout mice show dilated ventricles, vermis hypoplasia and impaired exploration patterns. Hum. Mol. Genet. 7, 999-1009.

Fransen, E., Lemmon, V., Van Camp, G., Vits, L., Coucke, P., Willems, P.J., 1995. CRASH syndrome: clinical spectrum of corpus callosum hypoplasia, retardation, adducted thumbs, spastic paraparesis and hydrocephalus due to mutations in one single gene, L1. Eur. J. Hum. Genet. 3, 273-284.

Frederickson, R.G., 1991. The subdural space interpreted as a cellular layer of meninges. Anat. Rec. 230, 38-51.

Frolkis, V.V., Kvitnitskaya-Ryzhova, T.Y., Dubiley, T.A., 1999. Vasopressin, hypothalamo-neurohypophyseal system and aging. Arch. Gerontol. Geriatr. 29, 193-214.

Fukumitsu, H., Ohmiya, M., Nitta, A., Furukawa, S., Mima, T., Mori, K., 2000. Aberrant expression of neurotrophic factors in the ventricular progenitor cells of infant congenitally hydrocephalic rats. Childs Nerv. Syst. 16, 516-521.

Gadsdon, D.R., Variend, S., Emery, J.L., 1979. Myelination of the corpus callosum. II. The effect of relief of hydrocephalus upon the processes of myelination. Z. Kinderchir. Grenzgeb. 28, 314-321.

Galbreath, E., Kim, S.J., Park, K., Brenner, M., Messing, A., 1995. Overexpression of TGF-beta 1 in the central nervous system of transgenic mice results in hydrocephalus. J. Neuropathol. Exp. Neurol. 54, 339-349.

Gammal, T.E., Allen, M.B.,Jr, Brooks, B.S., Mark, E.K., 1987. MR evaluation of hydrocephalus. AJR Am. J. Roentgenol. 149, 807-813.

Glees, P., Voth, D., 1988. Clinical and ultrastructural observations of maturing human frontal cortex. Part I (Biopsy material of hydrocephalic infants). Neurosurg. Rev. 11, 273-278.

Go, K.G., Stokroos, I., Blaauw, E.H., Zuiderveen, F., Molenaar, I., 1976. Changes of ventricular ependyma and choroid plexus in experimental hydrocephalus, as observed by scanning electron microscopy. Acta Neuropathol. 34, 55-64.

Goh, D., Minns, R.A., 1995. Intracranial pressure and cerebral arterial flow velocity indices in childhood hydrocephalus: current review. Childs Nerv. Syst. 11, 392-396.

Goodman, M., Meyer, W.J., 2001. Dementia reversal in post-shunt normal pressure hydrocephalus predicted by neuropsychological assessment. J. Am. Geriatr. Soc. 49, 685-686.

Gould, S.J., Howard, S., Papadaki, L., 1990. The development of ependyma in the human fetal brain: an immunohistological and electron microscopic study. Brain Res. Dev. Brain Res. 55, 255-267.

Greitz, D., 2004. Radiological assessment of hydrocephalus: new theories and implications for therapy. Neurosurg. Rev. 27, 145-65; discussion 166-7.

Grondona, J.M., Perez-Martin, M., Cifuentes, M., Perez, J., Jimenez, A.J., Perez-Figares, J.M., Fernandez-Llebrez, P., 1996. Ependymal denudation, aqueductal obliteration and hydrocephalus after a single injection of neuraminidase into the lateral ventricle of adult rats. J. Neuropathol. Exp. Neurol. 55, 999-1008.

Gunnarson, E., Zelenina, M., Aperia, A., 2004. Regulation of brain aquaporins. Neuroscience. 129, 947-955.

Gurwell, J.A., Duncan, M.J., Maderspach, K., Stiene-Martin, A., Elde, R.P., Hauser, K.F., 1996. kappa-opioid receptor expression defines a phenotypically distinct subpopulation of astroglia: relationship to Ca2+ mobilization, development, and the antiproliferative effect of opioids. Brain Res. 737, 175-187.

Haines, D.E., Harkey, H.L., al-Mefty, O., 1993. The "subdural" space: a new look at an outdated concept. Neurosurgery. 32, 111-120.

Hakim, S., Adams, R.D., 1965. The special clinical problem of symptomatic hydrocephalus with normal cerebrospinal fluid pressure. Observations on cerebrospinal fluid hydrodynamics. J. Neurol. Sci. 2, 307-327.

Hakvoort, A., Johanson, C.E., 2000. Growth factor modulation of CSF formation by isolated choroid plexus: FGF-2 vs. TGF-beta1. Eur. J. Pediatr. Surg. 10 Suppl 1, 44-46.

Hale, P.M., McAllister, J.P.,2nd, Katz, S.D., Wright, L.C., Lovely, T.J., Miller, D.W., Wolfson, B.J., Salotto, A.G., Shroff, D.V., 1992. Improvement of cortical morphology in infantile hydrocephalic animals after ventriculoperitoneal shunt placement. Neurosurgery. 31, 1085-96; discussion 1096.

Hanlo, P.W., Gooskens, R.J., van Schooneveld, M., Tulleken, C.A., van der Knaap, M.S., Faber, J.A., Willemse, J., 1997. The effect of intracranial pressure on myelination and the relationship with neurodevelopment in infantile hydrocephalus. Dev. Med. Child Neurol. 39, 286-291.

Hansen, A.R., Volpe, J.J., Goumnerova, L.C., Madsen, J.R., 1997. Intraventricular urokinase for the treatment of posthemorrhagic hydrocephalus. Pediatr. Neurol. 17, 213-217.

Harris, N.G., Plant, H.D., Inglis, B.A., Briggs, R.W., Jones, H.C., 1997. Neurochemical changes in the cerebral cortex of treated and untreated hydrocephalic rat pups quantified with in vitro 1H-NMR spectroscopy. J. Neurochem. 68, 305-312.

Hawkins, D., Bowers, T.M., Bannister, C.M., Miyan, J.A., 1997. The functional outcome of shunting H-Tx rat pups at different ages. Eur. J. Pediatr. Surg. 7 Suppl 1, 31-34.

Hayward, R., 2005. Venous hypertension and craniosynostosis. Childs Nerv. Syst. 21, 880-888.

Hermans, E., 2003. Biochemical and pharmacological control of the multiplicity of coupling at G-protein-coupled receptors. Pharmacol. Ther. 99, 25-44.

Higashi, K., Asahisa, H., Ueda, N., Kobayashi, K., Hara, K., Noda, Y., 1986. Cerebral blood flow and metabolism in experimental hydrocephalus. Neurol. Res. 8, 169-176.

Hill, A., Shackelford, G.D., Volpe, J.J., 1984. A potential mechanism of pathogenesis for early posthemorrhagic hydrocephalus in the premature newborn. Pediatrics. 73, 19-21.

Hill, A., Volpe, J.J., 1982. Decrease in pulsatile flow in the anterior cerebral arteries in infantile hydrocephalus. Pediatrics. 69, 4-7.

Hiratsuka, H., Tabata, H., Tsuruoka, S., Aoyagi, M., Okada, K., Inaba, Y., 1982. Evaluation of periventricular hypodensity in experimental hydrocephalus by metrizamide CT ventriculography. J. Neurosurg. 56, 235-240.

Hong, H.K., Chakravarti, A., Takahashi, J.S., 2004. The gene for soluble N-ethylmaleimide sensitive factor attachment protein alpha is mutated in hydrocephaly with hop gait (hyh) mice. Proc. Natl. Acad. Sci. U. S. A. 101, 1748-1753.

Hoon, A.H.,Jr, Melhem, E.R., 2000. Neuroimaging: applications in disorders of early brain development. J. Dev. Behav. Pediatr. 21, 291-302.

Hutchings, M., Weller, R.O., 1986. Anatomical relationships of the pia mater to cerebral blood vessels in man. J. Neurosurg. 65, 316-325.

Ibanez-Tallon, I., Pagenstecher, A., Fliegauf, M., Olbrich, H., Kispert, A., Ketelsen, U.P., North, A., Heintz, N., Omran, H., 2004. Dysfunction of axonemal dynein heavy chain Mdnah5 inhibits ependymal flow and reveals a novel mechanism for hydrocephalus formation. Hum. Mol. Genet. 13, 2133-2141.

Jarvis, C.R., Andrew, R.D., 1988. Correlated electrophysiology and morphology of the ependyma in rat hypothalamus. J. Neurosci. 8, 3691-3702.

Jensen, F., 1979. Acquired hydrocephalus. III. A pathophysiological study correlated with neuropathological findings and clinical manifestations. Acta Neurochir. (Wien). 47, 91-104.

Jensen, F., Jensen, F.T., 1979. Acquired hydrocephalus. I. A clinical analysis of 160 patients studied for hydrocephalus. Acta Neurochir. (Wien). 46, 119-133.

Jimenez, A.J., Garcia-Verdugo, J.M., Gonzalez, C.A., Batiz, L.F., Rodriguez-Perez, L.M., Paez, P., Soriano-Navarro, M., Roales-Bujan, R., Rivera, P., Rodriguez, S., Rodriguez, E.M., Perez-Figares, J.M., 2009. Disruption of the neurogenic niche in the subventricular zone of postnatal hydrocephalic hyh mice. J. Neuropathol. Exp. Neurol. 68, 1006-1020.

Jimenez, A.J., Tome, M., Paez, P., Wagner, C., Rodriguez, S., Fernandez-Llebrez, P., Rodriguez, E.M., Perez-Figares, J.M., 2001. A programmed ependymal denudation precedes congenital hydrocephalus in the hyh mutant mouse. J. Neuropathol. Exp. Neurol. 60, 1105-1119.

Johanson, C.E., Duncan, J.A.,3rd, Klinge, P.M., Brinker, T., Stopa, E.G., Silverberg, G.D., 2008. Multiplicity of cerebrospinal fluid functions: New challenges in health and disease. Cerebrospinal Fluid Res. 5, 10.

Johanson, C.E., 2003. The choroid plexus-CSF nexus: Gateway to the brain. In: Conn, M.P. (Ed.), Neuroscience in Medicine. Humana Press Inc., Totowa, NJ, pp. 165.

Johanson, C.E., Szmydynger-Chodobska, J., Chodobski, A., Baird, A., McMillan, P., Stopa, E.G., 1999. Altered formation and bulk absorption of cerebrospinal fluid in FGF-2-induced hydrocephalus. Am. J. Physiol. 277, R263-71.

Jones, H.C., Lopman, B.A., Jones, T.W., Carter, B.J., Depelteau, J.S., Morel, L., 2000a. The expression of inherited hydrocephalus in H-Tx rats. Childs Nerv. Syst. 16, 578-584.

Jones, H.C., Rivera, K.M., Coleman, J.E., 1996. Spatial learning and visual discrimination tests in hydrocephalic rat pups performed using the Morris water maze. Eur. J. Pediatr. Surg. 6 Suppl 1, 37.

Jones, H.C., Bucknall, R.M., Harris, N.G., 1991. The cerebral cortex in congenital hydrocephalus in the H-Tx rat: a quantitative light microscopy study. Acta Neuropathol. 82, 217-224.

Jones, H.C., Bucknall, R.M., 1988. Inherited prenatal hydrocephalus in the H-Tx rat: a morphological study. Neuropathol. Appl. Neurobiol. 14, 263-274.

Kam, A.Y., Chan, A.S., Wong, Y.H., 2004. Phosphatidylinositol-3 kinase is distinctively required for mu-, but not kappa-opioid receptor-induced activation of c-Jun N-terminal kinase. J. Neurochem. 89, 391-402.

Karahalios, D.G., Rekate, H.L., Khayata, M.H., Apostolides, P.J., 1996. Elevated intracranial venous pressure as a universal mechanism in pseudotumor cerebri of varying etiologies. Neurology. 46, 198-202.

Kazan, S., Gura, A., Ucar, T., Korkmaz, E., Ongun, H., Akyuz, M., 2005. Hydrocephalus after intraventricular hemorrhage in preterm and low-birth weight infants: analysis of associated risk factors for ventriculoperitoneal shunting. Surg. Neurol. 64 Suppl 2, S77-81; discussion S81.

Khan, O.H., McPhee, L.C., Moddemann, L.N., Del Bigio, M.R., 2007. Calcium antagonism in neonatal rats with kaolin-induced hydrocephalus. J. Child Neurol. 22, 1161-1166.

Khan, O.H., Enno, T.L., Del Bigio, M.R., 2006. Brain damage in neonatal rats following kaolin induction of hydrocephalus. Exp. Neurol. 200, 311-320.

Khan, O.H., Enno, T., Del Bigio, M.R., 2003a. Magnesium sulfate therapy is of mild benefit to young rats with kaolin-induced hydrocephalus. Pediatr. Res. 53, 970-976.

Khan, O.H., Enno, T., Del Bigio, M.R., 2003b. Tacrolimus and cyclosporine A are of no benefit to young rats with kaolin-induced hydrocephalus. Pediatr. Neurosurg. 39, 309-313.

Kiefer, M., Eymann, R., von Tiling, S., Muller, A., Steudel, W.I., Booz, K.H., 1998. The ependyma in chronic hydrocephalus. Childs Nerv. Syst. 14, 263-270.

Kimelberg, H.K., 2004. Water homeostasis in the brain: basic concepts. Neuroscience. 129, 851-860.

Klinge, P.M., Samii, A., Muhlendyck, A., Visnyei, K., Meyer, G.J., Walter, G.F., Silverberg, G.D., Brinker, T., 2003. Cerebral hypoperfusion and delayed hippocampal response after induction of adult kaolin hydrocephalus. Stroke. 34, 193-199.

Kobayashi, Y., Watanabe, M., Okada, Y., Sawa, H., Takai, H., Nakanishi, M., Kawase, Y., Suzuki, H., Nagashima, K., Ikeda, K., Motoyama, N., 2002. Hydrocephalus, situs inversus, chronic sinusitis, and male infertility in DNA polymerase lambda-deficient mice: possible implication for the pathogenesis of immotile cilia syndrome. Mol. Cell. Biol. 22, 2769-2776.

Kondziella, D., Sonnewald, U., Tullberg, M., Wikkelso, C., 2008. Brain metabolism in adult chronic hydrocephalus. J. Neurochem. 106, 1515-1524.

Kondziella, D., Qu, H., Ludemann, W., Brinker, T., Sletvold, O., Sonnewald, U., 2003. Astrocyte metabolism is disturbed in the early development of experimental hydrocephalus. J. Neurochem. 85, 274-281.

Krapivinsky, G., Krapivinsky, L., Wickman, K., Clapham, D.E., 1995. G beta gamma binds directly to the G protein-gated K+ channel, IKACh. J. Biol. Chem. 270, 29059-29062.

Krauss, J.K., Regel, J.P., Vach, W., Droste, D.W., Borremans, J.J., Mergner, T., 1996. Vascular risk factors and arteriosclerotic disease in idiopathic normal-pressure hydrocephalus of the elderly. Stroke. 27, 24-29.

Krebs, D.L., Metcalf, D., Merson, T.D., Voss, A.K., Thomas, T., Zhang, J.G., Rakar, S., O'bryan, M.K., Willson, T.A., Viney, E.M., Mielke, L.A., Nicola, N.A., Hilton, D.J., Alexander, W.S., 2004. Development of hydrocephalus in mice lacking SOCS7. Proc. Natl. Acad. Sci. U. S. A. 101, 15446-15451.

Kuban, K.C., 1998. White-matter disease of prematurity, periventricular leukomalacia, and ischemic lesions. Dev. Med. Child Neurol. 40, 571-573.

Kuchler, S., Graff, M.N., Gobaille, S., Vincendon, G., Roche, A.C., Delaunoy, J.P., Monsigny, M., Zanetta, J.P., 1994. Mannose dependent tightening of the rat ependymal cell barrier. In vivo and in vitro study using neoglycoproteins. Neurochem. Int. 24, 43-55.

Kumar, R., Singh, S., 2005. Childhood choroid plexus papillomas: operative complications. Childs Nerv. Syst. 21, 138-143.

Lang, B., Song, B., Davidson, W., MacKenzie, A., Smith, N., McCaig, C.D., Harmar, A.J., Shen, S., 2006. Expression of the human PAC1 receptor leads to dose-dependent hydrocephalus-related abnormalities in mice. J. Clin. Invest. 116, 1924-1934.

Larroche, J.C., 1972. Post-haemorrhagic hydrocephalus in infancy. Anatomical study. Biol. Neonate. 20, 287-299.

Larsson, A., Stephensen, H., Wikkelso, C., 1999. Adult patients with "asymptomatic" and "compensated" hydrocephalus benefit from surgery. Acta Neurol. Scand. 99, 81-90.

Laurence, K.M., Coats, S., 1962. The natural history of hydrocephalus. Detailed analysis of 182 unoperated cases. Arch. Dis. Child. 37, 345-362.

Lawson, R.F., Raimondi, A.J., 1973. Hydrocephalus-3, a murine mutant: I. Alterations in fine structure of choroid plexus and ependyma. Surg. Neurol. 1, 115-128.

Lazareff, J.A., Peacock, W., Holly, L., Ver Halen, J., Wong, A., Olmstead, C., 1998. Multiple shunt failures: an analysis of relevant factors. Childs Nerv. Syst. 14, 271-275.
LeMay, M., Hochberg, F.H., 1979. Ventricular differences between hydrostatic hydrocephalus and hydrocephalus ex vacuo by computed tomography. Neuroradiology. 17, 191-195.

Levine, D.N., 2008. Intracranial pressure and ventricular expansion in hydrocephalus: have we been asking the wrong question?. J. Neurol. Sci. 269, 1-11.

Li, X., Miyajima, M., Jiang, C., Arai, H., 2007. Expression of TGF-betas and TGF-beta type II receptor in cerebrospinal fluid of patients with idiopathic normal pressure hydrocephalus. Neurosci. Lett. 413, 141-144.

Li, X., Miyajima, M., Mineki, R., Taka, H., Murayama, K., Arai, H., 2005. Analysis of cerebellum proteomics in the hydrocephalic H-Tx rat. Neuroreport. 16, 571-574.

Lim, D.A., Alvarez-Buylla, A., 1999. Interaction between astrocytes and adult subventricular zone precursors stimulates neurogenesis. Proc. Natl. Acad. Sci. U. S. A. 96, 7526-7531.

Lindeman, G.J., Dagnino, L., Gaubatz, S., Xu, Y., Bronson, R.T., Warren, H.B., Livingston, D.M., 1998. A specific, nonproliferative role for E2F-5 in choroid plexus function revealed by gene targeting. Genes Dev. 12, 1092-1098.

Lindvall, M., Owman, C., 1981. Autonomic nerves in the mammalian choroid plexus and their influence on the formation of cerebrospinal fluid. J. Cereb. Blood Flow Metab. 1, 245-266.

Lois, C., Garcia-Verdugo, J.M., Alvarez-Buylla, A., 1996. Chain migration of neuronal precursors. Science. 271, 978-981.

Lois, C., Alvarez-Buylla, A., 1994. Long-distance neuronal migration in the adult mammalian brain. Science. 264, 1145-1148.

Long, D.M., 1985. Aging in the nervous system. Neurosurgery. 17, 348-354.

Lopes Lda, S., Slobodian, I., Del Bigio, M.R., 2009. Characterization of juvenile and young adult mice following induction of hydrocephalus with kaolin. Exp. Neurol. 219, 187-196.

Lorber, J., Salfield, S., Lonton, T., 1983. Isosorbide in the management of infantile hydrocephalus. Dev. Med. Child Neurol. 25, 502-511.

Lorber, J., 1975. Isosorbide in treatment of infantile hydrocephalus. Arch. Dis. Child. 50, 431-436.

Lui, K., Hellmann, J., Sprigg, A., Daneman, A., 1990. Cerebral blood-flow velocity patterns in post-hemorrhagic ventricular dilation. Childs Nerv. Syst. 6, 250-253.

Luskin, M.B., 1993. Restricted proliferation and migration of postnatally generated neurons derived from the forebrain subventricular zone. Neuron. 11, 173-189.

Madara, J.L., 1988. Tight junction dynamics: is paracellular transport regulated?. Cell. 53, 497-498.

Mangano, F.T., McAllister, J.P.,2nd, Jones, H.C., Johnson, M.J., Kriebel, R.M., 1998. The microglial response to progressive hydrocephalus in a model of inherited aqueductal stenosis. Neurol. Res. 20, 697-704.

Mao, X., Enno, T.L., Del Bigio, M.R., 2006. Aquaporin 4 changes in rat brain with severe hydrocephalus. Eur. J. Neurosci. 23, 2929-2936.

Martens, N., Uzan, G., Wery, M., Hooghe, R., Hooghe-Peters, E.L., Gertler, A., 2005. Suppressor of cytokine signaling 7 inhibits prolactin, growth hormone, and leptin signaling by interacting with STAT5 or STAT3 and attenuating their nuclear translocation. J. Biol. Chem. 280, 13817-13823.

Mashayekhi, F., Draper, C.E., Bannister, C.M., Pourghasem, M., Owen-Lynch, P.J., Miyan, J.A., 2002. Deficient cortical development in the hydrocephalic Texas (H-Tx) rat: a role for CSF. Brain. 125, 1859-1874.

Mason, H.A., Ito, S., Corfas, G., 2001. Extracellular signals that regulate the tangential migration of olfactory bulb neuronal precursors: inducers, inhibitors, and repellents. J. Neurosci. 21, 7654-7663.

Matsumae, M., Kikinis, R., Morocz, I.A., Lorenzo, A.V., Sandor, T., Albert, M.S., Black, P.M., Jolesz, F.A., 1996. Age-related changes in intracranial compartment volumes in normal adults assessed by magnetic resonance imaging. J. Neurosurg. 84, 982-991.

Matuoka, K., Miki, H., Takahashi, K., Takenawa, T., 1997. A novel ligand for an SH3 domain of the adaptor protein Nck bears an SH2 domain and nuclear signaling motifs. Biochem. Biophys. Res. Commun. 239, 488-492.

May, C., Kaye, J.A., Atack, J.R., Schapiro, M.B., Friedland, R.P., Rapoport, S.I., 1990. Cerebrospinal fluid production is reduced in healthy aging. Neurology. 40, 500-503.
McAllister, J.P.,2nd, Chovan, P., 1998. Neonatal hydrocephalus. Mechanisms and consequences. Neurosurg. Clin. N. Am. 9, 73-93.

McAllister, J.P.,2nd, Maugans, T.A., Shah, M.V., Truex, R.C.,Jr, 1985. Neuronal effects of experimentally induced hydrocephalus in newborn rats. J. Neurosurg. 63, 776-783.

McCullough, D.C., Balzer-Martin, L.A., 1982. Current prognosis in overt neonatal hydrocephalus. J. Neurosurg. 57, 378-383.

McDonald, P.H., Chow, C.W., Miller, W.E., Laporte, S.A., Field, M.E., Lin, F.T., Davis, R.J., Lefkowitz, R.J., 2000. Beta-arrestin 2: a receptor-regulated MAPK scaffold for the activation of JNK3. Science. 290, 1574-1577.

McLennan, G.P., Kiss, A., Miyatake, M., Belcheva, M.M., Chambers, K.T., Pozek, J.J., Mohabbat, Y., Moyer, R.A., Bohn, L.M., Coscia, C.J., 2008. Kappa opioids promote the proliferation of astrocytes via Gbetagamma and beta-arrestin 2-dependent MAPK-mediated pathways. J. Neurochem. 107, 1753-1765.

McLone, D.G., 2004. The anatomy of the ventricular system. Neurosurg. Clin. N. Am. 15, 33-38.

Miller, J.M., McAllister, J.P.,2nd, 2007. Reduction of astrogliosis and microgliosis by cerebrospinal fluid shunting in experimental hydrocephalus. Cerebrospinal Fluid Res. 4, 5.

Miller, J.M., Kumar, R., McAllister, J.P.,2nd, Krause, G.S., 2006. Gene expression analysis of the development of congenital hydrocephalus in the H-Tx rat. Brain Res. 1075, 36-47.

Mirzadeh, Z., Merkle, F.T., Soriano-Navarro, M., Garcia-Verdugo, J.M., Alvarez-Buylla, A., 2008. Neural stem cells confer unique pinwheel architecture to the ventricular surface in neurogenic regions of the adult brain. Cell. Stem Cell. 3, 265-278.

Miyan, J.A., Nabiyouni, M., Zendah, M., 2003. Development of the brain: a vital role for cerebrospinal fluid. Can. J. Physiol. Pharmacol. 81, 317-328.

Miyan, J.A., Mashayekhi, F., Bannister, C.M., 2001. Developmental abnormalities in early-onset hydrocephalus: clues to signalling. Symp. Soc. Exp. Biol. (53), 91-106.

Miyazawa, T., Sato, K., Ikeda, Y., Nakamura, N., Matsumoto, K., 1997. A rat model of spontaneously arrested hydrocephalus. A behavioural study. Childs Nerv. Syst. 13, 189-193.

Miyazawa, T., Sato, K., 1991. Learning disability and impairment of synaptogenesis in HTX-rats with arrested shunt-dependent hydrocephalus. Childs Nerv. Syst. 7, 121-128.

Morgan, F.W., Stewart, J.A., Smith, A.N., Tarnuzzer, R.W., 2005. Differential expression of stress response genes in the H-Tx rat model of congenital hydrocephalus. Brain Res. Mol. Brain Res. 138, 273-290.

Mori, K., 1995. Current concept of hydrocephalus: evolution of new classifications. Childs Nerv. Syst. 11, 523-31; discussion p 531-2.

Morrisey, R., Bannister, C.M., Street, K., Khan, M.I., Miyan, J., 1996. Preliminary investigation of the performance of normal hydrocephalic and treated hydrocephalic HTx and Lewis rats in an 8-arm radial maze. Eur. J. Pediatr. Surg. 6 Suppl 1, 37-39.

Moseley, M.E., Cohen, Y., Kucharczyk, J., Mintorovitch, J., Asgari, H.S., Wendland, M.F., Tsuruda, J., Norman, D., 1990. Diffusion-weighted MR imaging of anisotropic water diffusion in cat central nervous system. Radiology. 176, 439-445.

Murata, T., Handa, H., Mori, K., Nakano, Y., 1981. The significance of periventricular lucency on computed tomography: experimental study with canine hydrocephalus. Neuroradiology. 20, 221-227.

Murphy, B.P., Inder, T.E., Rooks, V., Taylor, G.A., Anderson, N.J., Mogridge, N., Horwood, L.J., Volpe, J.J., 2002. Posthaemorrhagic ventricular dilatation in the premature infant: natural history and predictors of outcome. Arch. Dis. Child. Fetal Neonatal Ed. 87, F37-41.

Nagib, M.G., O'Fallon, M.T., 2000. Lateral ventricle choroid plexus papilloma in childhood: management and complications. Surg. Neurol. 54, 366-372.

Nakada, J., Oka, N., Nagahori, T., Endo, S., Takaku, A., 1992. Changes in the cerebral vascular bed in experimental hydrocephalus: an angio-architectural and histological study. Acta Neurochir. (Wien). 114, 43-50.

Nakagawa, Y., Cervos-Navarro, J., Artigas, J., 1985. Tracer study on a paracellular route in experimental hydrocephalus. Acta Neuropathol. 65, 247-254.

Nakagawa, Y., Cervos-Navarro, J., Artigas, J., 1984. A possible paracellular route for the resolution of hydrocephalic edema. Acta Neuropathol. 64, 122-128.

Nakano, H., Bandoh, K., Miyaoka, M., Sato, K., 1996. Evaluation of hydrocephalic periventricular radiolucency by dynamic computed tomography and xenon-computed tomography. Neurosurgery. 39, 758-62; discussion 762-3.

Nicholson, C., 1988. Issues involved in the transmission of chemical signals through the brain extracellular space. Acta Morphol. Neerl. Scand. 26, 69-80.

Nilsson, C., Lindvall-Axelsson, M., Owman, C., 1992. Neuroendocrine regulatory mechanisms in the choroid plexus-cerebrospinal fluid system. Brain Res. Brain Res. Rev. 17, 109-138.

Nulsen, F.E., Spitz, E.B., 1951. Treatment of hydrocephalus by direct shunt from ventricle to jugular vain. Surg. Forum, 399-403.

Oi, S., Yamada, H., Sato, O., Matsumoto, S., 1996. Experimental models of congenital hydrocephalus and comparable clinical problems in the fetal and neonatal periods. Childs Nerv. Syst. 12, 292-302.

Okuyama, T., Hashi, K., Sasaki, S., Sudo, K., Kurokawa, Y., 1987. Changes in cerebral microvasculature in congenital hydrocephalus of the inbred rat LEW/Jms: light and electron microscopic examination. Surg. Neurol. 27, 338-342.

Owen-Lynch, P.J., Draper, C.E., Mashayekhi, F., Bannister, C.M., Miyan, J.A., 2003. Defective cell cycle control underlies abnormal cortical development in the hydrocephalic Texas rat. Brain. 126, 623-631.

Owler, B.K., Pitham, T., Wang, D., 2010. Aquaporins: relevance to cerebrospinal fluid physiology and therapeutic potential in hydrocephalus. Cerebrospinal Fluid Res. 7, 15.

Paez, P., Batiz, L.F., Roales-Bujan, R., Rodriguez-Perez, L.M., Rodriguez, S., Jimenez, A.J., Rodriguez, E.M., Perez-Figares, J.M., 2007. Patterned neuropathologic events occurring in hyh congenital hydrocephalic mutant mice. J. Neuropathol. Exp. Neurol. 66, 1082-1092.

Page, R.B., Rosenstein, J.M., Dovey, B.J., Leure-duPree, A.E., 1979. Ependymal changes in experimental hydrocephalus. Anat. Rec. 194, 83-103.

Page, R.B., 1975. Scanning electron microscopy of the ventricular system in normal and hydrocephalic rabbits. Preliminary report and atlas. J. Neurosurg. 42, 646-664.

Paneth, N., 1999. Classifying brain damage in preterm infants. J. Pediatr. 134, 527-529.

Panicker, A.K., Buhusi, M., Thelen, K., Maness, P.F., 2003. Cellular signalling mechanisms of neural cell adhesion molecules. Front. Biosci. 8, d900-11.

Papadopoulos, M.C., Verkman, A.S., 2007. Aquaporin-4 and brain edema. Pediatr. Nephrol. 22, 778-784.

Papaiconomou, C., Bozanovic-Sosic, R., Zakharov, A., Johnston, M., 2002. Does neonatal cerebrospinal fluid absorption occur via arachnoid projections or extracranial lymphatics?. Am. J. Physiol. Regul. Integr. Comp. Physiol. 283, R869-76.

Park, Y.S., Park, S.W., Suk, J.S., Nam, T.K., 2011. Development of an acute obstructive hydrocephalus model in rats using N-butyl cyanoacrylate. Childs Nerv. Syst. 27, 903-910.

Pascual-Castroviejo, I., Velez, A., Pascual-Pascual, S.I., Roche, M.C., Villarejo, F., 1991. Dandy-Walker malformation: analysis of 38 cases. Childs Nerv. Syst. 7, 88-97.

Patwardhan, R.V., Nanda, A., 2005. Implanted ventricular shunts in the United States: the billion-dollar-a-year cost of hydrocephalus treatment. Neurosurgery. 56, 139-44; discussion 144-5.

Pelech, S., Zhang, H., 2007. Antibody-Based Proteomics Analysis of Tumor Cell Signaling Pathways. In: Bronchud, M.H. (Ed.), Principles of Molecular Oncology. Humana Press Inc., Totowa, NJ.

Peng, J., Bencsik, M., Louie, A., Lu, W., Millard, S., Nguyen, P., Burghardt, A., Majumdar, S., Wronski, T.J., Halloran, B., Conklin, B.R., Nissenson, R.A., 2008. Conditional expression of a Gi-coupled receptor in osteoblasts results in trabecular osteopenia. Endocrinology. 149, 1329-1337.

Persson, E.K., Anderson, S., Wiklund, L.M., Uvebrant, P., 2007. Hydrocephalus in children born in 1999-2002: epidemiology, outcome and ophthalmological findings. Childs Nerv. Syst. 23, 1111-1118.

Peter, J.C., Fieggen, G., 1999. Congenital malformations of the brain--a neurosurgical perspective at the close of the twentieth century. Childs Nerv. Syst. 15, 635-645.

Piatt, J.H.,Jr, Carlson, C.V., 1993. A search for determinants of cerebrospinal fluid shunt survival: retrospective analysis of a 14-year institutional experience. Pediatr. Neurosurg. 19, 233-41; discussion 242.

Picco, P., Leveratto, L., Cama, A., Vigliarolo, M.A., Levato, G.L., Gattorno, M., Zammarchi, E., Donati, M.A., 1993. Immotile cilia syndrome associated with hydrocephalus and precocious puberty: a case report. Eur. J. Pediatr. Surg. 3 Suppl 1, 20-21.

Podell, M., Hadjiconstantinou, M., 1997. Cerebrospinal fluid gamma-aminobutyric acid and glutamate values in dogs with epilepsy. Am. J. Vet. Res. 58, 451-456.

Pradilla, G., Jallo, G., 2007. Arachnoid cysts: case series and review of the literature. Neurosurg. Focus. 22, E7.

Pratico, D., Yao, Y., Rokach, J., Mayo, M., Silverberg, G.G., McGuire, D., 2004. Reduction of brain lipid peroxidation by CSF drainage in Alzheimer's disease patients. J. Alzheimers Dis. 6, 385-9; discussion 443-9.

Preston, J.E., McMillan, P.N., Stopa, E.G., Nashold, J.R., Duncan, J.A., Johanson, C.E., 2003. Atrial natriuretic peptide induction of dark epithelial cells in choroid plexus: consistency with the model of CSF downregulation in hydrocephalus. Eur. J. Pediatr. Surg. 13 Suppl 1, S40-2.

Preston, J.E., 2001. Ageing choroid plexus-cerebrospinal fluid system. Microsc. Res. Tech. 52, 31-37.

Purves, D., Augustine, G.J., Fitzpatrick, D., 2001. Neuroscience. Sinauer Associates, Sunderland, MA.

Rahme, R., Bojanowski, M.W., 2010. Internal hydrocephalus, external hydrocephalus, and the syndrome of intracerebral cerebrospinal fluid entrapment: a challenge to current theories on the pathophysiology of communicating hydrocephalus. Med. Hypotheses. 74, 95-98.

Raimondi, A.J., 1994. A unifying theory for the definition and classification of hydrocephalus. Childs Nerv. Syst. 10, 2-12.

Raimondi, A.J., Clark, S.J., McLone, D.G., 1976. Pathogenesis of aqueductal occlusion in congenital murine hydrocephalus. J. Neurosurg. 45, 66-77.

Rakic, P., Sidman, R.L., 1968. Subcommissural organ and adjacent ependyma: autoradiographic study of their origin in the mouse brain. Am. J. Anat. 122, 317-335.

Redfern, C.H., Degtyarev, M.Y., Kwa, A.T., Salomonis, N., Cotte, N., Nanevicz, T., Fidelman, N., Desai, K., Vranizan, K., Lee, E.K., Coward, P., Shah, N., Warrington, J.A., Fishman, G.I., Bernstein, D., Baker, A.J., Conklin, B.R., 2000. Conditional expression of a Gi-coupled receptor causes ventricular conduction delay and a lethal cardiomyopathy. Proc. Natl. Acad. Sci. U. S. A. 97, 4826-4831.

Redfern, C.H., Coward, P., Degtyarev, M.Y., Lee, E.K., Kwa, A.T., Hennighausen, L., Bujard, H., Fishman, G.I., Conklin, B.R., 1999. Conditional expression and signaling of a specifically designed Gi-coupled receptor in transgenic mice. Nat. Biotechnol. 17, 165-169.

Redzic, Z.B., Segal, M.B., 2004. The structure of the choroid plexus and the physiology of the choroid plexus epithelium. Adv. Drug Deliv. Rev. 56, 1695-1716.

Rolf, B., Kutsche, M., Bartsch, U., 2001. Severe hydrocephalus in L1-deficient mice. Brain Res. 891, 247-252.

Roth, Y., Kimhi, Y., Edery, H., Aharonson, E., Priel, Z., 1985. Ciliary motility in brain ventricular system and trachea of hamsters. Brain Res. 330, 291-297.

Rubenstein, E., 1998. Relationship of senescence of cerebrospinal fluid circulatory system to dementias of the aged. Lancet. 351, 283-285.

Sadja, R., Alagem, N., Reuveny, E., 2003. Gating of GIRK channels: details of an intricate, membrane-delimited signaling complex. Neuron. 39, 9-12.

Sainte-Rose, C., Piatt, J.H., Renier, D., Pierre-Kahn, A., Hirsch, J.F., Hoffman, H.J., Humphreys, R.P., Hendrick, E.B., 1991. Mechanical complications in shunts. Pediatr. Neurosurg. 17, 2-9.

Sakakibara, S., Nakamura, Y., Yoshida, T., Shibata, S., Koike, M., Takano, H., Ueda, S., Uchiyama, Y., Noda, T., Okano, H., 2002. RNA-binding protein Musashi family: roles for CNS stem cells and a subpopulation of ependymal cells revealed by targeted disruption and antisense ablation. Proc. Natl. Acad. Sci. U. S. A. 99, 15194-15199.

Sarnat, H.B., 1995. Ependymal reactions to injury. A review. J. Neuropathol. Exp. Neurol. 54, 1-15.

Sarnat, H.B., 1992. Role of human fetal ependyma. Pediatr. Neurol. 8, 163-178.

Sawamoto, K., Wichterle, H., Gonzalez-Perez, O., Cholfin, J.A., Yamada, M., Spassky, N., Murcia, N.S., Garcia-Verdugo, J.M., Marin, O., Rubenstein, J.L., Tessier-Lavigne, M., Okano, H., Alvarez-Buylla, A., 2006. New neurons follow the flow of cerebrospinal fluid in the adult brain. Science. 311, 629-632.

Scearce-Levie, K., Lieberman, M.D., Elliott, H.H., Conklin, B.R., 2005. Engineered G protein coupled receptors reveal independent regulation of internalization, desensitization and acute signaling. BMC Biol. 3, 3.

Scearce-Levie, K., Coward, P., Redfern, C.H., Conklin, B.R., 2001a. Engineering receptors activated solely by synthetic ligands (RASSLs). Trends Pharmacol. Sci. 22, 414-420.

Schoeman, J., Donald, P., van Zyl, L., Keet, M., Wait, J., 1991. Tuberculous hydrocephalus: comparison of different treatments with regard to ICP, ventricular size and clinical outcome. Dev. Med. Child Neurol. 33, 396-405.

Schrander-Stumpel, C., Fryns, J.P., 1998. Congenital hydrocephalus: nosology and guidelines for clinical approach and genetic counselling. Eur. J. Pediatr. 157, 355-362.

Shen, X.Q., Miyajima, M., Ogino, I., Arai, H., 2006. Expression of the water-channel protein aquaporin 4 in the H-Tx rat: possible compensatory role in spontaneously arrested hydrocephalus. J. Neurosurg. 105, 459-464.

Shih, W.J., Tasdemiroglu, E., 1995. Reversible hypoperfusion of the cerebral cortex in normal-pressure hydrocephalus on technetium-99m-HMPAO brain SPECT images after shunt operation. J. Nucl. Med. 36, 470-473.

Shinnar, S., Gammon, K., Bergman, E.W.,Jr, Epstein, M., Freeman, J.M., 1985. Management of hydrocephalus in infancy: use of acetazolamide and furosemide to avoid cerebrospinal fluid shunts. J. Pediatr. 107, 31-37.

Shprecher, D., Schwalb, J., Kurlan, R., 2008. Normal pressure hydrocephalus: diagnosis and treatment. Curr. Neurol. Neurosci. Rep. 8, 371-376.

Shuman, R.M., 1995. The Chiari malformations: a constellation of anomalies. Semin. Pediatr. Neurol. 2, 220-226.

Silverberg, G.D., 2004. Normal pressure hydrocephalus (NPH): ischaemia, CSF stagnation or both. Brain. 127, 947-948.

Silverberg, G.D., Mayo, M., Saul, T., Rubenstein, E., McGuire, D., 2003. Alzheimer's disease, normal-pressure hydrocephalus, and senescent changes in CSF circulatory physiology: a hypothesis. Lancet Neurol. 2, 506-511.

Silverberg, G.D., Huhn, S., Jaffe, R.A., Chang, S.D., Saul, T., Heit, G., Von Essen, A., Rubenstein, E., 2002. Downregulation of cerebrospinal fluid production in patients with chronic hydrocephalus. J. Neurosurg. 97, 1271-1275.

Siraj, S., 2011. An overview of normal pressure hydrocephalus and its importance: how much do we really know?. J. Am. Med. Dir. Assoc. 12, 19-21.

Sjaastad, O., Skalpe, I.O., Engeset, A., 1969. The width of the temporal horn in the differential diagnosis between pressure hydrocephalus and hydrocephalus ex vacuo. Neurology. 19, 1087-1093.

Song, X., Coffa, S., Fu, H., Gurevich, V.V., 2009. How does arrestin assemble MAPKs into a signaling complex?. J. Biol. Chem. 284, 685-695.

Spassky, N., Merkle, F.T., Flames, N., Tramontin, A.D., Garcia-Verdugo, J.M., Alvarez-Buylla, A., 2005. Adult ependymal cells are postmitotic and are derived from radial glial cells during embryogenesis. J. Neurosci. 25, 10-18.

Speake, T., Whitwell, C., Kajita, H., Majid, A., Brown, P.D., 2001. Mechanisms of CSF secretion by the choroid plexus. Microsc. Res. Tech. 52, 49-59.

Spencer, R.J., Jin, W., Thayer, S.A., Chakrabarti, S., Law, P.Y., Loh, H.H., 1997. Mobilization of Ca2+ from intracellular stores in transfected neuro2a cells by activation of multiple opioid receptor subtypes. Biochem. Pharmacol. 54, 809-818.

Stevenson, K.L., 2004. Chiari Type II malformation: past, present, and future. Neurosurg. Focus. 16, E5.

Stiene-Martin, A., Mattson, M.P., Hauser, K.F., 1993. Opiates selectively increase intracellular calcium in developing type-1 astrocytes: role of calcium in morphine-induced morphologic differentiation. Brain Res. Dev. Brain Res. 76, 189-196.

Sutton, L.N., Wood, J.H., Brooks, B.R., Barrer, S.J., Kline, M., Cohen, S.R., 1983. Cerebrospinal fluid myelin basic protein in hydrocephalus. J. Neurosurg. 59, 467-470.
Sweger, E.J., McCarthy, K.D., 2009. Expression of the Gi-coupled RASSL Ro1 in GFAP-positive cells: a novel model of hydrocephalus.

Sweger, E.J., Casper, K.B., Scearce-Levie, K., Conklin, B.R., McCarthy, K.D., 2007. Development of hydrocephalus in mice expressing the G(i)-coupled GPCR Ro1 RASSL receptor in astrocytes. J. Neurosci. 27, 2309-2317.

Sztriha, L., Frossard, P., Hofstra, R.M., Verlind, E., Nork, M., 2000. Novel missense mutation in the L1 gene in a child with corpus callosum agenesis, retardation, adducted thumbs, spastic paraparesis, and hydrocephalus. J. Child Neurol. 15, 239-243.

Tada, T., Kanaji, M., Kobayashi, S., 1994. Induction of communicating hydrocephalus in mice by intrathecal injection of human recombinant transforming growth factor-beta 1. J. Neuroimmunol. 50, 153-158.

Takano, T., Becker, L.E., 1997. Overexpression of nestin and vimentin in the ependyma of spinal cords from hydrocephalic infants. Neuropathol. Appl. Neurobiol. 23, 3-15.

Takei, F., Sato, O., 1995. Morphological analysis of progressive hydrocephalus and shunt-dependent arrested hydrocephalus. An experimental study. Pediatr. Neurosurg. 23, 246-253.

Takei, F., Shapiro, K., Kohn, I., 1987. Influence of the rate of ventricular enlargement on the white matter water content in progressive feline hydrocephalus. J. Neurosurg. 66, 577-583.

Tarazi, R.A., Zabel, T.A., Mahone, E.M., 2008. Age-related differences in executive function among children with spina bifida/hydrocephalus based on parent behavior ratings. Clin. Neuropsychol. 22, 585-602.

Tarkowski, E., Tullberg, M., Fredman, P., Wikkelso, C., 2003. Normal pressure hydrocephalus triggers intrathecal production of TNF-alpha. Neurobiol. Aging. 24, 707-714.

Tashiro, Y., Drake, J.M., 1998. Reversibility of functionally injured neurotransmitter systems with shunt placement in hydrocephalic rats: implications for intellectual impairment in hydrocephalus. J. Neurosurg. 88, 709-717.

Tashiro, Y., Chakrabortty, S., Drake, J.M., Hattori, T., 1997a. Progressive loss of glutamic acid decarboxylase, parvalbumin, and calbindin D28K immunoreactive neurons in the cerebral cortex and hippocampus of adult rat with experimental hydrocephalus. J. Neurosurg. 86, 263-271.

Tashiro, Y., Drake, J.M., Chakrabortty, S., Hattori, T., 1997b. Functional injury of cholinergic, GABAergic and dopaminergic systems in the basal ganglia of adult rat with kaolin-induced hydrocephalus. Brain Res. 770, 45-52.

Tripathi, B.J., Tripathi, R.C., 1974. Vacuolar transcellular channels as a drainage pathway for cerebrospinal fluid. J. Physiol. 239, 195-206.

Tsubokawa, T., Katayama, Y., Kawamata, T., 1988. Impaired hippocampal plasticity in experimental chronic hydrocephalus. Brain Inj. 2, 19-30.

Turgut, M., Alabaz, D., Erbey, F., Kocabas, E., Erman, T., Alhan, E., Aksaray, N., 2005. Cerebrospinal fluid shunt infections in children. Pediatr. Neurosurg. 41, 131-136.

Ulfig, N., Bohl, J., Neudorfer, F., Rezaie, P., 2004. Brain macrophages and microglia in human fetal hydrocephalus. Brain Dev. 26, 307-315.

Vale, F.A., Miranda, S.J., 2002. Clinical and demographic features of patients with dementia attended in a tertiary outpatient clinic. Arq. Neuropsiquiatr. 60, 548-552.

Vandenabeele, F., Creemers, J., Lambrichts, I., 1996. Ultrastructure of the human spinal arachnoid mater and dura mater. J. Anat. 189 (Pt 2), 417-430.

Vaughn, D.M., Coleman, E., Simpson, S.T., Satjawatcharaphong, C., 1988. Analysis of neurotransmitter metabolite concentrations in canine cerebrospinal fluid. Am. J. Vet. Res. 49, 1302-1306.

Verkman, A.S., Binder, D.K., Bloch, O., Auguste, K., Papadopoulos, M.C., 2006. Three distinct roles of aquaporin-4 in brain function revealed by knockout mice. Biochim. Biophys. Acta. 1758, 1085-1093.

Vertinsky, A.T., Barnes, P.D., 2007. Macrocephaly, increased intracranial pressure, and hydrocephalus in the infant and young child. Top. Magn. Reson. Imaging. 18, 31-51.

Vetsika, E.K., Bannister, C.M., Buckle, A.M., Miyan, J.A., 1999. The effects of CSF blockage in early-onset hydrocephalus on the activity of the germinal epithelium. Eur. J. Pediatr. Surg. 9 Suppl 1, 43-44.

Vintzileos, A.M., Ingardia, C.J., Nochimson, D.J., 1983. Congenital hydrocephalus: a review and protocol for perinatal management. Obstet. Gynecol. 62, 539-549.

Wada, M., 1988. Congenital hydrocephalus in HTX-rats: incidence, pathophysiology, and developmental impairment. Neurol. Med. Chir. (Tokyo). 28, 955-964.

Wagner, C., Batiz, L.F., Rodriguez, S., Jimenez, A.J., Paez, P., Tome, M., Perez-Figares, J.M., Rodriguez, E.M., 2003. Cellular mechanisms involved in the stenosis and obliteration of the cerebral aqueduct of hyh mutant mice developing congenital hydrocephalus. J. Neuropathol. Exp. Neurol. 62, 1019-1040.

Wahlund, L.O., Almkvist, O., Basun, H., Julin, P., 1996. MRI in successful aging, a 5-year follow-up study from the eighth to ninth decade of life. Magn. Reson. Imaging. 14, 601-608.

Weed, L.H., 1914. Studies on Cerebro-Spinal Fluid. No. III : The pathways of escape from the Subarachnoid Spaces with particular reference to the Arachnoid Villi. J. Med. Res. 31, 51-91.

Weller, R.O., Wisniewski, H., Shulman, K., Terry, R.D., 1971. Experimental hydrocephalus in young dogs: histological and ultrastructural study of the brain tissue damage. J. Neuropathol. Exp. Neurol. 30, 613-626.

Whitelaw, A., Christie, S., Pople, I., 1999. Transforming growth factor-beta1: a possible signal molecule for posthemorrhagic hydrocephalus?. Pediatr. Res. 46, 576-580.

Wickman, K.D., Clapham, D.E., 1995. G-protein regulation of ion channels. Curr. Opin. Neurobiol. 5, 278-285.

Wilkinson, H.A., Wilson, R.B., Patel, P.P., Esmaili, M., 1974. Corticosteroid therapy of experimental hydrocephalus after intraventricular-subarachnoid haemorrhage. J. Neurol. Neurosurg. Psychiatry. 37, 224-229.

Williams, M.A., McAllister, J.P., Walker, M.L., Kranz, D.A., Bergsneider, M., Del Bigio, M.R., Fleming, L., Frim, D.M., Gwinn, K., Kestle, J.R., Luciano, M.G., Madsen, J.R., Oster-Granite, M.L., Spinella, G., 2007. Priorities for hydrocephalus research: report from a National Institutes of Health-sponsored workshop. J. Neurosurg. 107, 345-357.

Wittkowski, W., 1998. Tanycytes and pituicytes: morphological and functional aspects of neuroglial interaction. Microsc. Res. Tech. 41, 29-42.

Wright, L.C., McAllister, J.P.,2nd, Katz, S.D., Miller, D.W., Lovely, T.J., Salotto, A.G., Wolfson, B.J., 1990. Cytological and cytoarchitectural changes in the feline cerebral cortex during experimental infantile hydrocephalus. Pediatr. Neurosurg. 16, 139-155.

Wyss-Coray, T., Feng, L., Masliah, E., Ruppe, M.D., Lee, H.S., Toggas, S.M., Rockenstein, E.M., Mucke, L., 1995. Increased central nervous system production of extracellular matrix components and development of hydrocephalus in transgenic mice overexpressing transforming growth factor-beta 1. Am. J. Pathol. 147, 53-67.

Yamada, H., Oi, S., Tamaki, N., Matsumoto, S., Sudo, K., 1992. Histological changes in the midbrain around the aqueduct in congenital hydrocephalic rat LEW/Jms. Childs Nerv. Syst. 8, 394-398.

Yamasaki, M., Thompson, P., Lemmon, V., 1997. CRASH syndrome: mutations in L1CAM correlate with severity of the disease. Neuropediatrics. 28, 175-178.

Yapicioglu, H., Narli, N., Satar, M., Soyupak, S., Altunbasak, S., 2003. Intraventricular streptokinase for the treatment of posthaemorrhagic hydrocephalus of preterm. J. Clin. Neurosci. 10, 297-299.

Yashon, D., 1963. Prognosis in Infantile Hydrocephalus: Past and Present. J. Neurosurg. 20, 105-111.

Yeates, K.O., Loss, N., Colvin, A.N., Enrile, B.G., 2003. Do children with myelomeningocele and hydrocephalus display nonverbal learning disabilities? An empirical approach to classification. J. Int. Neuropsychol. Soc. 9, 653-662.

Yoshida, Y., Koya, G., Tamayama, K., Kumanishi, T., Abe, S., 1990. Development of GFAP-positive cells and reactive changes associated with cystic lesions in HTX rat brain. Neurol. Med. Chir. (Tokyo). 30, 445-450.

Zemack, G., Romner, B., 2002. Adjustable valves in normal-pressure hydrocephalus: a retrospective study of 218 patients. Neurosurgery. 51, 1392-400; discussion 1400-2.

Zhang, D., Zeldin, D.C., Blackshear, P.J., 2007. Regulatory factor X4 variant 3: a transcription factor involved in brain development and disease. J. Neurosci. Res. 85, 3515-3522.

Zhang, J., Williams, M.A., Rigamonti, D., 2006a. Genetics of human hydrocephalus. J. Neurol. 253, 1255-1266.

Zimmerman, R.A., Bilaniuk, L.T., Rebsamen, S., 1992. Magnetic resonance imaging of pediatric posterior fossa tumors. Pediatr. Neurosurg. 18, 58-64.